Mass Spectrum and Form Factors for Heavy Baryons and a Study of Stochastic Gauge Fixing in Lattice QCD

Orlando Olavo Aragão Aleixo Neves de Oliveira

Doctor of Philosophy

The University of Edinburgh

1996

À Tila, Claudia, João Pedro e Ana Luisa.

Abstract

In this thesis we study two aspects of the lattice formulation of Quantum Chromodynamics (QCD).

We first describe the study of baryons with one heavy and two light quarks. We compute the full spectrum for the ground state of the channels with quantum numbers $J^P = \frac{1}{2}^+, \frac{3}{2}^+$, isospin $I = 0, 1$ and strangeness $S = 0, -1, -2$.

For the channel with quantum numbers $J^P = \frac{1}{2}^+$ we discuss the form factors for semileptonic decays of heavy baryons, compute the Isgur-Wise function and study its dependence on the light quark mass. Then, we make predictions for the partial decay rates of $\Lambda_b \to \Lambda_c \, l \, \overline{\nu}_l$ and $\Xi_b \to \Xi_c \, l \, \overline{\nu}_l$ decays.

In the second part of this thesis, we report the numerical results of a first study of a one-parameter family of covariant, non-perturbative gauge-fixing conditions. The gauge dependence of the gluon propagator is discussed.

Declaration

This thesis has been composed wholly by me and contains my own work carried out as a member of the UKQCD Collaboration.

The analysis described in Chapters 4 and 5 was performed in collaboration with Nicoletta Stella. The final chapter of this thesis is the result of a collaboration with Sinead Ryan, Claudio Parrinello and David Henty.

The results in Chapter 4 are in agreement with the numbers published in

- K. C. Bowler *et al.* (UKQCD Collaboration), Phys. Rev. **D54** (1996) 3619.

An article with the results in Chapter 5 is in preparation,

- K.C. Bowler *et. al.* (UKQCD Collaboration), *First Lattice Study of Semileptonic Decays of* Λ_b *and* Ξ_b *Baryons.*

The results of chapter 6 have just been accepted for publication in Phys. Rev. **D** and are available as a hep-lat preprint

- D. Henty, O. Oliveira, C. Parrinello, S. Ryan, hep-lat 9607014.

Orlando Oliveira

Acknowledgements

First of all I would like to thank Augusto Barroso for the suggestion of Edinburgh and José Urbano for making Edinburgh possible to me. I am also grateful to Ken Bowler, Richard Kenway and Brian Pendleton for their guidance in my first lattice steps. A special thanks goes to Ken Bowler for the careful reading of this thesis. I am also grateful to Claudio Parrinello for the careful reading of the last chapter of this thesis. I thanks Claudio Parrinello, David Henty, Nick Hazel and David Richards for many invaluable discussions.

A very special thank goes to Sinead Ryan, Harry Newton and Nick Hazel for making my 3 years at Edinburgh such a memorable time. For all of you I wish the very best from life.

At last but not at least, I would like to thank my latino-america-iberia friends who were able to make me return to my latin origins. Among them I cannot thank enough Victor and Olga for the very nice moments together. Sorte para todos vocês e fico a espera da vossa visita.

Finally, I would like to acknowledge JNICT for the financial support through grant BD/2714/93.

Contents

Chapter 1

Introduction and Motivation

Gauge theories [1] play a very important role in particle physics today. Their importance increased after it was realized that all fundamental interactions can be described by this type of renormalisable vector field theory[1]. The final boost came with the discovery of the electroweak bosons Z^0, W^+ and W^- in the early eighties, establishing the Standard Model as the theory for particle physics. Despite the enormous activity searching for extensions, it is generally accepted that the Standard Model is the right theoretical framework to describe particle physics at presently attainable experimental energies.

The Standard Model (SM) [2] is a gauge theory based on the group $SU(3) \otimes SU(2) \otimes U(1)$. It is usual to consider two separate sectors.

The electroweak sector [5, 6, 7] associated with the group $SU(2) \otimes U(1)$ accounts for all the electromagnetic and weak phenomena. Perturbation theory is the preferred computational scheme for understanding such phenomena. However, when the electromagnetic and weak processes involve hadrons, nonperturbative techniques are required for computing the hadronic matrix elements[2]. The study of semileptonic decays of heavy baryons presented in this thesis can be used to test different aspects of the SM in the heavy quark sector. Despite its motivation, our work is not about electroweak phenomenology and a detailed description of the electroweak theory will not be given here.

The part of the SM associated with the group $SU(3)$, Quantum Chromodynamics (QCD) [8], describes the dynamics of quark and gluon interactions. While QCD is

[1] Gravity is the only exception. Gravity can be formulated as a gauge theory but is not renormalisable.

[2] Also, the understanding of the scalar sector of the SM, depending on the value of the Higgs mass, may have to rely on nonperturbative techniques.

supposed to explain all characteristics of hadrons, from their spectrum to matrix elements, the electroweak sector of the Standard Model describes the electroweak interactions of leptons and of hadrons at the quark level. Quarks are believed to be the fundamental building blocks of hadronic matter. Yet, they cannot be observed isolated. A theory for strong interactions should be able to explain this observation. In QCD, the fundamental fields are the quark and gluon fields. Studies of heavy quark interactions, the gluon propagator, and the evolution of the effective coupling between quarks as a function of momentum transfer consistently support the confinement hypothesis; quarks are permanently bound inside hadrons. However, a definitive proof for confinement is still lacking in QCD. If Quantum Chromodynamics is a confining theory, its explanation clearly stays outside perturbation theory, i.e. it is necessary to use nonperturbative techniques for a full understanding of QCD . The formulation of QCD on a lattice [9], provides us with a computational tool capable of fulfilling this goal.

The idea behind field theory on a lattice is to introduce a regulator, making the quantum theory finite. The calculation of physical quantities requires taking the appropriate continuum limit. The lattice regulator combined with imaginary time formalism shapes Lattice Field Theory as Classical Statistical Mechanics in four dimensions. Then, the standard techniques of Statistical Physics, mean field techniques, high and low temperature expansions, Monte Carlo simulations, etc., can be used in particle physics. In Lattice QCD, the Green's functions are computed using MC simulations, a model-independent first principles calculation. Unfortunately, this approach has its drawback; even simple computations require the most powerful computers available and simplifications are usually needed. This is true especially for QCD, where most of present day calculations use the so-called quenched or valence approximation. It is mainly computer technology which seriously limits the type of studies we are able to perform. The good news is that, despite these limitations, Lattice QCD is now reaching the state of providing estimates for a number of observables of experimental relevance, such as hadron masses, hadronic form factors, strong coupling constant, etc.

Although, QCD requires nonperturbative computational techniques, most of our knowledge about quarks and gluons comes from perturbative calculations. The

property which justifies the use of perturbation theory in certain regimes is asymptotic freedom [14, 15]. In an asymptotically free theory[3], the effective coupling depends on the energy scale of the interaction in such a way that it decreases with increasing transferred energy. Another way of saying it is that the interaction becomes weaker when quarks become closer. In addition to suggesting quark confinement, asymptotic freedom allows perturbative QCD to make predictions for processes where the typical energy scale is sufficiently high, i.e. where the effective coupling is small enough, to allow the use of perturbative techniques. Deep inelastic scattering, Drell-Yan processes and hadronic jet production in e^+e^- annihilation are typical situations where perturbative QCD is a reliable tool. In the low energy regime, i.e. when long distance effects are dominant, perturbation theory is of little or no use. It is the overall picture emerging from studies in perturbative QCD and lattice techniques that supports QCD as the correct theory for describing hadronic physics.

1.1 The Heavy Baryon Spectrum

In 1970, Glashow, Iliopoulos and Maiani [17] to explain the suppression of weak transitions where the strangeness changes by one or two units, $|\Delta S| = 1, 2$ and total baryonic electric charge is conserved, $\Delta Q = 0$, introduced an extra quark, the charm (c) quark, in the formulation of $SU(2)' \otimes U(1)$ gauge theory of electroweak interactions. The analysis of various weak transitions suggested that if the new quark existed it had to be considerable heavier than the quarks known at the time, u, d, s. In 1974, the charm quark was observed [18, 19] with the properties as predicted by Glashow, Iliopoulos and Maiani. The discovery of the charm quark, together with the detection of yet another heavy quark , the b quark, in 1977 [20] initiated the study of heavy hadrons. Since then, many particles with heavy flavours have been found and their properties investigated both from the theoretical point of view and experimentally.

The area of heavy flavoured hadrons has seen an enormous activity. However, most of the collected information about heavy hadrons is related to mesons. The first candidate charm baryon states were detected in 1975 [21]. However, the first

[3]Coleman and Gross [16] have shown that only non-Abelian gauge theories are asymptotically free in 4 dimensions.

complete reconstruction of a charm baryon event only happened in 1979 [22]. For b-baryons, the first observations were reported as early as 1981 [23] but reliable determinations of the Λ_b mass [24] and mean life [25] had to wait for a decade.

A look at the new Particle Data Group (PDG) book [26] shows that currently all ground-state $J^P = 1/2^+$ charm baryons[4] have been observed[5]. For b-baryons, only the mass of one particle, Λ_b, is reported there. Recently, there have been claims of observations of the Σ_c^* [27], Ξ_c^{*0} [28] and Ξ_c^{*+} [29] $J^P = 3/2^+$ charm baryons and Ξ_b [30], Σ_b and Σ_b^* [31] $J^P = 1/2^+, 3/2^+$ b-baryons. All the major experimental facilities have ongoing experiments focusing on heavy flavour physics. Therefore, new particles and more data on heavy baryons spectroscopy and their decays is expected in the years to come. The interpretation of these experiments requires a clear theoretical description of heavy flavour physics.

From the theoretical point of view, the study of new particles always starts by the explanation of their spectrum. Despite giving us further confidence in the theoretical description, the investigation of the particle spectrum is a pre-requisite to understand their decays. The study of c- and b-baryons are not exceptions to this rule.

In the past twenty years, the subject of heavy baryon spectroscopy has been widely discussed in the literature - for an early review see [32]. Typically, the heavy baryon spectrum has been investigated with quark potential models [33, 34, 35, 36, 37], Heavy Quark Effective Theory [38] or a combination of the latter with chiral perturbation theory [39]. The modelling of the quark dynamics requires assumptions about the interaction and/or quark wave functions. Despite the consistency of results given by these studies, it is important that model-independent predictions directly from QCD become available. At present, Lattice QCD calculations are the only way of performing non-perturbative, first principles, model-independent predictions.

On the lattice, only recently there were attempts to compute the mass of Λ_Q (one heavy quark and two light quarks) [40, 41, 43] and of Ξ_{QQ} (two heavy quarks and

[4]The classification of baryon states is discussed on chapter 4.

[5]Note that for all the heavy baryons reported by the PDG, their quantum numbers have not yet been confirmed experimentally.

one light quark) [42]. A first spectroscopy study of the lowest-lying baryons with one heavy quark (c or b) was done by us, within the UKQCD collaboration [44]. In chapter 5 of this thesis, we give a detailed description of this investigation.

1.2 Semileptonic Decays of Heavy Baryons

In the phenomenology of weak interactions, the semileptonic and leptonic decays of hadrons are good laboratories for studying strong interactions, and testing the couplings between electroweak gauge bosons and matter fields.

For the experimentalist, because the final state involves only a single charged lepton, both the semileptonic and leptonic decays are among the easiests to identify and study - for a review of experimental situation see [45]. On the other hand, the theoretical analysis of these decays is simplified considerably by the factorisation of the decay amplitude into a leptonic part and a hadronic part. It is the combination of the above features which make the leptonic and semileptonic decays of hadrons play such an important role in particle physics.

In the Standard Model, the leptonic amplitude is well described by perturbation theory, and no big theoretical uncertainties are associated with it. The hadronic amplitude is understood in terms of quark transitions, and a bridge between the quark picture and the hadron picture has to be build. This requires nonperturbative techniques. Typically, that means modelling the quark behaviour. By doing so, one introduces ambiguities which are the dominant theoretical uncertainty in the description of the decays. Once more, Lattice QCD can play here a very important role in reducing this uncertainty. To see how this can be achieved, let us have a closer look at the theoretical description of semileptonic and leptonic decays.

The semileptonic and leptonic decays of hadrons are explained via the couplings of the electroweak gauge bosons Z^0, W^+ and W^- to the matter fields. For transitions involving the charged bosons, the interaction with quarks and leptons is described

by the following Lagrangian

$$\mathcal{L} = -\frac{g}{\sqrt{2}}\{(\,\overline{u}\;\;\overline{c}\;\;\overline{t}\,)\begin{pmatrix} V_{ud} & V_{us} & V_{ub} \\ V_{cd} & V_{cs} & V_{cb} \\ V_{td} & V_{ts} & V_{tb} \end{pmatrix}\gamma^{\mu}\frac{1}{2}(1-\gamma_5)\begin{pmatrix} d \\ s \\ b \end{pmatrix} + (\,\overline{\nu}_e\;\;\overline{\nu}_{\mu}\;\;\overline{\nu}_{\tau}\,)\gamma^{\mu}\frac{1}{2}(1-\gamma_5)\begin{pmatrix} e \\ \mu \\ \tau \end{pmatrix}\}W^{+}_{\mu} + \text{h.c.}\,, \tag{1.1}$$

where V_{ij} are the elements of an unitary matrix, the Cabibbo-Kobayashi-Maskawa (CKM) matrix, and g is the weak isospin coupling constant[6].

In order to be precise, let us consider the decay studied in chapter 5, $\Lambda_b \to \Lambda_c l\overline{\nu}$. If one discard the particles masses when compared with the W mass, to lowest order in g the decay amplitude is given by

$$\mathcal{M}(\Lambda_b \to \Lambda_c l\overline{\nu}) = -i\frac{G_F}{\sqrt{(2)}}V_{cb}H^{\mu}L_{\mu}\,, \tag{1.2}$$

where the hadronic matrix element, H^{μ}, and the leptonic matrix element, L_{μ}, are

$$H^{\mu} = \langle\Lambda_c|\,\overline{c}\,\gamma^{\mu}(1-\gamma_5)\,b\,|\Lambda_b\rangle\,, \tag{1.3}$$

$$L^{\mu} = \overline{u}_l\,\gamma^{\mu}(1-\gamma_5)\,u_{\nu}\,, \tag{1.4}$$

and u_j is the spinor for particle j. As defined, the L^{μ} involves only free particle Dirac spinors and gamma matrices, therefore its computation is not a problem. On the other hand, the evaluation of the matrix element of the hadronic current requires the knowledge of the quark wave functions inside the hadrons. This information is not available and H^{μ} cannot be computed. The usual procedure is to subsume all our ignorance about quark wave functions into functions of the momentum transfer, the form factors, and try to measure these functions. Then, the task of the theoretical physicist is to explain and/or predict the form factors.

The interest in computing the form factors goes beyond the understanding of

[6] g is related to the Fermi coupling constant by $G_F = \sqrt{2}g^2/8M_W^2$, where M_W is the W boson mass.

strong interactions. Once the form factors are known, a complete theoretical description of the decay is accessible, and a study of other facets of the Standard Model becomes possible. The partial decay rate for the semileptonic decay $\Lambda_b \rightarrow \Lambda_c l\overline{\nu}$ can be predicted, the polarisation of the $W-b$ coupling can be measured [46, 47], the angular distribution of the daughter particles can be described and an independent measure of V_{cb} can be made. All this features provide important tests of the Standard Model of electroweak interactions in the heavy quark sector.

For this particular transition, the form factors have been computed using either quark models - see references in [85] - or QCD sum rules [48]. Our calculation of the semileptonic form factors [112], see chapter 5, is the first Lattice QCD study.

1.3 Stochastic Gauge Fixing

In particle physics, the majority of the studies involving gauge theories use perturbative methods. Within perturbation theory, the problem of the quantisation of gauge theories was solved long ago by Feynman [49], DeWitt [50] and Faddeev and Popov [51]. Their quantisation method requires a choice of a gauge condition, uniquely satisfied in each gauge orbit, in order to define the generating functional for the Green functions. For small field amplitudes [7] the gauge condition is uniquely satisfied in each gauge orbit. However, if large field amplitudes are involved, the gauge condition has multiple solutions in each gauge orbit [52]. Gribov's results mean that the nonperturbative quantization of Yang-Mills theories can not be described by the usual methods of perturbation theory. Singer [53] generalised Gribov's results by proving that it is impossible to find a local continuous and unambiguous gauge fixing condition for any $SU(N)$ gauge theory defined on the manifold S_4. Singer's theorem was extended to the the four-torus by Killingback [54].

A correct nonperturbative gauge-fixing condition for Yang-Mills theories was obtained only in the beginning of the current decade. In 1990, Zwanziger [55] and, simultaneously, Parrinello and Jona-Lasinio [56] proposed a path integral formulation for Yang-Mills theories, containing a global gauge fixing term, which solved the problem of Gribov copies. The Gribov ambiguity is solved by introducing a

[7] Such is the case considered in perturbation theory.

normalised probability distribution over each gauge orbit and doing a weighted sum over the gauge orbits. In this way, instead of trying to single out one configuration from each gauge orbit, all the configurations are taken properly into account. This gauge fixing method is suitable to describe both the weak coupling and the strong coupling regimes of a gauge theory. Therefore, he is a natural candidate to introduce gauge fixing in Lattice QCD.

The quantisation of gauge theories on the lattice does not requires gauge fixing. Then, why do we want to gauge fix in Lattice QCD? It is well known (Elitzur's theorem) that correlation functions of local operators which are gauge dependent vanish on the lattice. Examples of local operators which are not gauge invariant are the quark and gluon fields themselves. Thus, the Green functions of individual quark and gluons have to be computed in a fixed gauge. These functions are interesting quantities to compute because they are the most fundamental computable quantities in QCD. For example, the quark and gluon propagators contain direct information about the mechanisms of confinement and chiral symmetry breaking. Furthermore, the quark-gluon vertex allows a first principles determination of the running QCD coupling [57, 58] and may be relevant for understanding the physics of pomeron exchange from the point of view of QCD [59]. In addition, by choosing a gauge one can compute renormalisation constants for composite operators by sandwiching the operators between quark states [60].

All the above applications require choosing a gauge. After fixing a gauge, it is important to disentangle the gauge independent properties of the Green functions from the gauge dependent ones. Therefore, it is crucial to be able to compute the different Green functions in different gauges.

In chapter 6 we describe a numerical study of the stochastic gauge fixing method of Zwanziger-Parrinello-Jona-Lasinio as adapted to Lattice QCD by Fachin and Parrinello [123]. Apart from avoiding the problem of the Gribov copies, with our choice for the probability distribution, a whole family of nonperturbative gauge conditions can be investigated by varying one gauge parameter. In this exploratory investigation, we focus on the gluon propagator and study its dependence on the gauge parameter.

Chapter 2

Lattice QCD

The work described in this thesis uses the lattice formulation of QCD. All Green's functions were computed with Monte Carlo sampling techniques.

In this chapter we will try to give a general overview of what Lattice QCD is and how computations are done within this framework. In section 1 the Lagrangian for classical QCD is presented. As a preamble for the lattice formulation of QCD, section 2 discusses the path ordered formulation of gauge theories. In section 3 we formulate QCD on a lattice and quantise it. Section 4 discusses the continuum limit. Finally, section 5 gives a brief description of how to perform a MC simulation and explains the improvement program for Lattice QCD.

2.1 Gauge and Matter Fields in the Continuum

QCD is a gauge theory based on the group $SU(3)$. The classical QCD Lagrangian involves only quark and gluon fields. Quark fields are assumed to belong to the fundamental representation of $SU(3)$. To distinguish between the different types of quarks, a flavour index is introduced. Generally, a quark field is represented by

$$q^{Af}(x); \quad A = 1,2,3; \quad f = u,d,c,s,t,b,\cdots \tag{2.1}$$

We will adopt the convention that, for quark fields, capital Latin letters refer to colour and small Latin letters refer to quark flavour.

In addition to quarks, the theory involves eight gluon fields $A^a_\mu(x)$, $a = 1\ldots8$, the $SU(3)$ gauge particles, belonging to the adjoint representation of the gauge group.

The classical QCD Lagrangian reads

$$\mathcal{L}_{QCD} = -\frac{1}{4}\sum_a F^a_{\mu\nu}(x)F^{a\mu\nu}(x) + \sum_{A,B,f} \overline{q}^{Af}(x)\,(\,i\gamma^\mu[D_\mu]_{AB} - m_f\delta_{AB}\,)\,q^{Bf}(x) \tag{2.2}$$

where the gluon field-strength tensor, $F^a_{\mu\nu}$, and the covariant derivative, D^μ, are defined by

$$[D^\mu]_{AB} = \delta_{AB}\partial^\mu + ig[T^a]_{AB}A^{a\mu}(x) \qquad igT^aF^a_{\mu\nu}(x) = [D_\mu, D_\nu]\,; \tag{2.3}$$

a sum over the colour index a is implied. The colour matrices T^a represent the $SU(3)$ generators. We choose their normalisation in the conventional way

$$\mathrm{Tr}(\,T^aT^b\,) = \frac{1}{2}\delta^{ab} \tag{2.4}$$

As defined, QCD is invariant under the local gauge transformation

$$q(x) \to \quad q'(x) \;= G(x)\,q(x) \tag{2.5}$$

$$A_\mu(x) \to \quad A'_\mu(x) \;= G(x)\,(\,A_\mu(x) - \frac{i}{g}\partial_\mu\,)\,G^\dagger(x) \tag{2.6}$$

where $A_\mu(x) = \sum_a T^aA^a_\mu(x)$ and $G(x)$ is a $SU(3)$ matrix.

The form of the quark-gluon interaction is restricted by gauge invariance. The classical Lagrangian (2.2) is fixed by requiring both gauge invariance and the minimal coupling prescription[1]. Since the dynamics is given by the gauge principle, preferred quantum formulations of QCD are those where gauge symmetry is preserved exactly. The lattice formulation of QCD belongs to this class.

On the lattice, derivatives are replaced by finite differences. The action for Lattice QCD is going to involve products of quark fields at different space-time points. To build a gauge invariant quantity from the product of quark fields at different space-time points, we need to discuss the path representation of gauge groups.

[1]Gauge invariance allows other types of interaction. However, in the quantum theory, (2.2) is the only Lagrangian compatible both with gauge invariance and renormalizability.

2.2 Path Representation of the Gauge Group

In this section gauge theories are described using path representations. This approach to gauge theories has an underlying geometric structure which we are not going to explore in great detail[2]. Our motivation for the path representation of gauge theories comes from providing a natural language to build gauge-invariant operators on the lattice.

Consider a theory with a global symmetry associated with the unitary group[3] $SU(N)$. At each space-time point matter fields have values in a linear space which is the tensor product of Lorentz representations and group representations. The linear space associated with the group index is referred to as charge space or internal space. A field is given by

$$\psi(x) = \sum_{\alpha} \psi^{\alpha}(x)\,\omega_{\alpha} \ , \tag{2.7}$$

where $\{\omega_{\alpha}\}$ define a basis on the charge space. The theory being invariant under the action of the group $SU(N)$ means that

$$\psi(x) \quad \text{and} \quad \psi'(x) = G\,\psi(x) \quad , G \in SU(N) \tag{2.8}$$

represent the same physics. In geometrical language, the action of the group on a particle field can be viewed as a rotation in the internal space. Global invariance is equivalent to freedom of choosing globally the axes orientation[4] in the charge space.

In a theory with a local symmetry (gauge symmetry), the fields related by a gauge transformation

$$\psi(x) \quad \text{and} \quad \psi'(x) = G(x)\,\psi(x) \quad , G(x) \in SU(N) \tag{2.9}$$

describe the same physical situation. The geometric interpretation for gauge invariance is freedom to choose the axes in the charge space, independently, at

[2]For the geometric structure of gauge theories see, for example, [61].

[3]The extension to other groups is straightforward.

[4]We are adopting a passive view. When discussing the total change of the field between two neighbour points we will switch to the active description.

each space-time point. For a gauge theory, the field associated with a particle is represented by

$$\psi(x) = \sum_{\alpha} \psi^{\alpha}(x)\,\omega_{\alpha}(x) \ , \tag{2.10}$$

where $\{\omega(x)_{\alpha}\}$ are a basis on the internal space at space-time point x. A gauge transformation on the field is equivalent to a local change of basis

$$\psi'(x) = G(x)\psi(x) = \sum_{\alpha} \psi^{\alpha}(x)\,\omega'_{\alpha}(x) \ , \tag{2.11}$$

with the new basis defined by

$$\omega'_{\alpha}(x) = G(x)\,\omega_{\alpha}(x) \ . \tag{2.12}$$

Consider now a gauge theory and lets try to describe how the field changes between different space-time points. The total change on the corresponding field is twofold. There is a contribution coming from the space-time dependence of the field and a contribution from the change in orientation of the internal space axes between the space-time points. For simplicity lets look at two infinitesimally close space-time points, x and $x + dx$. The change of the field due to dependence on space-time is represented by the operator $P(x, x + dx) = \exp(-idx^{\mu}P_{\mu})$, where P_{μ} is to be identified with the momentum operator associated with the particle described by the field. The change in the internal space is an infinitesimal rotation of the field. In an active description, one can write this rotation in terms of real vector fields $A^{a}_{\mu}(x)$,

$$\Omega(x, x + dx) = \exp(igdx^{\mu}A^{a}_{\mu}(x)T^{a}) \simeq 1 + igdx^{\mu}A^{a}_{\mu}(x)T^{a} \ , \tag{2.13}$$

where T^{a} are the group generators for the given representation. The translation into the passive point of view, means the following relation between the basis of the charge space at the different space-time points

$$\omega_{\alpha}(x + dx) = \Omega^{\dagger}(x, x + dx)\,\omega_{\alpha}(x) \ . \tag{2.14}$$

A gauge transformation changes the basis in the internal space at each space-time point. Therefore, a gauge transformation changes $\Omega(x, x + dx)$, i.e. the set of real

fields $A^a_\mu(x)$ must transform non-trivially under a group rotation. Denoting the gauge transformed objects by

$$\begin{aligned} \Omega'(x, x+dx) &= \exp\left(igdx^\mu A'^a_\mu(x)T^a\right) \simeq 1 + igdx^\mu A'^a_\mu(x)T^a \quad (2.15) \\ \omega'_\alpha(x+dx) &= \Omega'^\dagger(x, x+dx)\ \omega'_\alpha(x) \quad (2.16) \\ \omega'_\alpha(x) &= G(x)\ \omega_\alpha(x) \quad (2.17) \end{aligned}$$

under a gauge transformation

$$\Omega(x, x+dx) \to \Omega'(x, x+dx) = G(x)\,\Omega(x, x+dx)\,G^\dagger(x+dx)\ . \quad (2.18)$$

In terms of the set of real fields defined in equation (2.13), the above transformation reads

$$A_\mu(x) \to A'_\mu(x) = G(x)\,A_\mu(x)G^\dagger(x) + \frac{i}{g}\,\partial_\mu G(x)\,G^\dagger(x)\ , \quad (2.19)$$

i.e. the vector fields $A^a_\mu(x)$ have the usual transformation properties associated with the gauge fields. Further support to identify $A^a_\mu(x)$ with the gauge fields is given by the total change of the field

$$dx^\mu\,D_\mu\,\psi(x) = dx^\mu\,(\,\partial_\mu + igA_\mu(x)\,)\,\psi(x)\ , \quad (2.20)$$

and its transformation under the action of the gauge group

$$D_\mu\,\psi(x) \to D'_\mu\,\psi'(x) = G(x)D_\mu\,\psi(x)\ . \quad (2.21)$$

Once $A^a_\mu(x)$ have been identified with the gauge fields, we want to compute the difference in orientation in the internal space between space-time points separated by a finite interval. To achieve this goal, one divides the particle path connecting the two points, Γ, into infinitesimal paths and compute the total change by summing the differences along the infinitesimal paths, see figure 2.1,

$$\Omega_\Gamma(x, y) = \prod_z \exp\left(igA_\mu(z)dz^\mu\right) = \mathcal{P}\,\exp\left(ig\int_x^y A_\mu(z)dz^\mu\right); \quad (2.22)$$

where $\mathcal{P}$ stands for path ordered. The operator $\Omega_\Gamma(x, y)$ is path dependent and

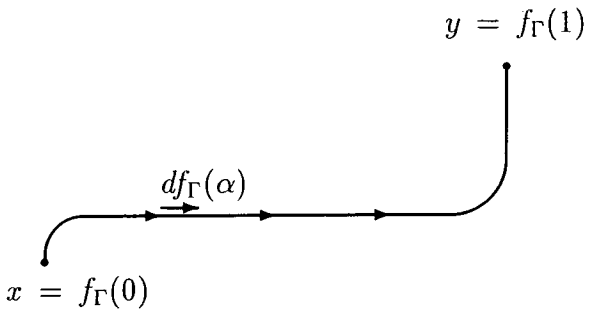

Figure 2.1: For a space-time points connect by the path $f_\Gamma(\alpha)$, $\alpha \in [0,1]$, with $x = f_\Gamma(0)$ and $y = f_\Gamma(1)$, the charge space basis at y is rotated from the charge space basis at x by $\omega_\alpha(y) = \Omega^\dagger(y - df_\Gamma(1), y) \times \cdots \times \Omega^\dagger(x, x + df_\Gamma(0))\,\omega_\alpha(x)$.

under a gauge transformation transforms according to

$$\Omega_\Gamma(x,y) \to G(x)\,\Omega_\Gamma(x,y)\,G^\dagger(y). \tag{2.23}$$

For the infinitesimal closed path shown in figure 2.2

$$\begin{aligned} \Omega_{d\Gamma}(x,x) &= 1 + ig \oint A_\mu(z) dz^\mu \\ &= 1 + igF_{\mu\nu}(x) dx^\mu dy^\nu \end{aligned} \tag{2.24}$$

where $F_{\mu\nu}(x)$ is the field-strength tensor.

The operator Ω_Γ depends only on the gauge fields, for a given path. If Ω_Γ is known for all paths one can recover the gauge fields, i.e the gauge theory can be formulated only in terms of Ω_Γ [62]. It can be shown that it is sufficient to consider Ω_Γ over all closed loops [63].

A product of fields at different space-time points becomes a gauge-invariant expression only after the insertion of the operator Ω_Γ, i.e. $\overline{\psi}(x)\,\Omega_\Gamma(x,y)\,\psi(y)$, with Γ representing any path connecting the two points, is gauge invariant. To keep gauge invariance, the lattice formulation of gauge theories uses $\Omega_\Gamma(x,y)$ instead of the gauge fields $A^a_\mu(x)$.

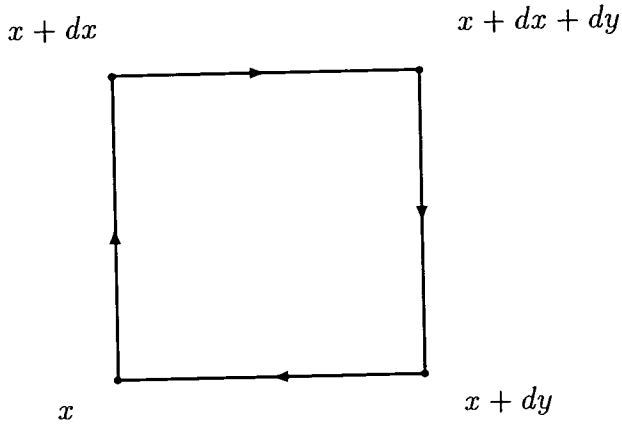

Figure 2.2: Infinitesimal closed path, $d\Gamma$. The integral of the gauge fields around a closed path defines the field-strength-tensor flux through the area enclosed by the path, $\oint_{d\Gamma} A_\mu(z)dz^\mu = F_{\mu\nu}(x)dx^\mu dy^\nu$.

2.3 Lattice Formulation of QCD

In the previous sections, the classical formulation of gauge theories was discussed. Now, we want to formulate quantum gauge field theories.

For quantum theories [64], the Green's functions summarize the theory. In a Quantum Field Theory (QFT), where classical fields, $\phi_j(x)$, are replaced by operators, $\hat{\phi}_j(x)$, acting in the Hilbert space of the states of the theory, the Green's functions are defined as expectation values, on the vacuum state, of product of field operators time-ordered,

$$G^{(n)}_{j_1\cdots j_n}(x_1,\cdots,x_n) = < 0|\,\mathcal{T}\,(\,\hat{\phi}_{j_1}(x_1)\cdots\hat{\phi}_{j_n}(x_n)\,)\,|0> \ . \tag{2.25}$$

In the path integral formulation, (2.25) are functional integrals over classical fields

$$G^{(n)}_{j_1\cdots j_n}(x_1,\cdots,x_n) = \frac{1}{Z[\phi]}\int \prod_k \mathcal{D}\phi_k\,\phi_{j_1}(x_1)\cdots\phi_{j_n}(x_n)\,\exp\left(iS[\phi]\right)\ , \tag{2.26}$$

where the vacuum functional is given by

$$Z[\phi] = \int \prod_k \mathcal{D}\phi_k\,\exp\left(iS[\phi]\right) \tag{2.27}$$

and $S[\phi]$ is the action for the theory.

The imaginary time formalism estabilishes a formal connection between QFT and Classical Statistical Mechanics. Performing a Wick rotation, were time, t, is replaced by Euclidean time, $t = -ix_4$ ($x_4 \in R$), Green's function are analytically continued into imaginary time and the path integral for the quantum theory becames identical to a partition function of a statistical mechanics problem,

$$Z[\phi] = \int \prod_k \mathcal{D}\phi_k \exp\left(iS[\phi]\right) \longrightarrow Z^{(E)}[\phi] = \int \prod_k \mathcal{D}\phi_k \exp\left(-S^{(E)}[\phi]\right) ; \quad (2.28)$$

$S^{(E)}[\phi(x)]$ is the so called Euclidean action. Lattice Field Theory explores this connection with Statistical Physics.

To perform calculations within the quantum theory, as an intermediate step, a regulator is needed to make the theory mathematically well defined [5]. For the study of nonperturbative aspects of Field Theory, the preferred regulator is to introduce a finite lattice, Lattice Field Theory (LFT).

In Lattice Field Theory, continuum space-time is replaced by a finite set of discrete points, typically at the vertices of an hypercube. Fields have meaning only on the sites of the lattice. Then, the integrals (2.26), (2.27) and (2.28) become integrals over a finite number of degrees of freedom, opening the possibility for exact calculations of the Euclidean formulation of the theory via numerical methods (Monte Carlo integration). Euclidean Lattice Field Theory computes exactly, via the Monte Carlo method, the Green's functions. In our work we adopt Euclidean Lattice Field Theory as the theoretical framework to perform calculations within QCD. Therefore, from now on when we refer to Lattice Field Theory it should be understood as Euclidean Lattice Field Theory.

In LFT derivatives are replaced by finite differences. To make contact with continuum physics, it is required that the lattice action reproduce the continuum action in the limit of zero lattice spacing and as many as possible of the continuum symmetries should be kept in the discrete version of the theory. Adopting these guide lines to construct Lattice Field Theories, they do not fix completely the lattice action. The freedom left can be used in reducing the lattice artifacts.

[5] Physical results are independent of the regularization used.

This leads to the improvement program, to be discussed later for QCD.

The lattice action involves products of the fermionic fields at different space-time points. As discussed in the previous section, to write the action in a gauge-invariant way, the operator $\Omega_\Gamma(x, x+\Delta x)$ should be inserted in between the Dirac spinors, $\overline{\psi}(x)\psi(x+\Delta x)$. The lattice action uses group variables, $\Omega_\Gamma(x, x+\Delta x)$, instead of algebra variables, $A^a_\mu(x)$. The relation between gauge fields and group variables was established already in section 2.2.

2.3.1 The Lattice Action For Gauge Fields

Consider an hypercubic lattice[6], with lattice spacing a in all directions. For an $SU(N)$ gauge symmetry define

$$\begin{aligned} U_\mu(x) &= \Omega_\Gamma(x, x+a\hat{\mu}) \\ &= \exp\left(ig_0 a A_\mu(x+\tfrac{a}{2}\hat{\mu})\right) \\ U^\dagger_\mu(x) &= \Omega(x+a\hat{\mu}, x) \end{aligned} \tag{2.29}$$

where $\hat{\mu}$ is the unit vector along the positive direction of the μ axis, g_0 is the bare coupling constant and Γ is the line connecting the point x and $x+a\hat{\mu}$. The relation between the gauge fields and $U_\mu(x)$, (2.29), is only valid for small lattice spacing.

A gauge-invariant quantity can be built from the operator $\Omega_\Gamma(x,x)$ by taking its trace. On the lattice, the simplest closed loop is a plaquette

$$\begin{aligned} P_{\mu\nu}(x) &= U_\mu(x)\, U_\nu(x+a\hat{\mu})\, U^\dagger_\mu(x+a\hat{\nu})\, U^\dagger_\nu(x) \\ &\cong \exp\left(i\, g_0\, a^2\, F_{\mu\nu}(x)\right) . \end{aligned} \tag{2.30}$$

Using $P_{\mu\nu}(x)$, the action for the gauge fields [65] is given by

$$S_W = -\beta \sum_x \sum_{\mu>\nu} \left(1 - \frac{1}{N} \Re\left(Tr[\, P_{\mu\nu}(x)\,]\right)\right) \tag{2.31}$$

[6]All the work presented in this thesis uses hypercubic lattices. The extension for other geometries is straightforward.

with $\beta = 2N/g_0^2$. In the limit of zero lattice spacing, S_W reduces to the usual continuum gauge action

$$S_W = \int d^4x \frac{1}{4} \sum_{a,\mu,\nu} (F^a_{\mu\nu})^2 + \mathcal{O}(a^2) . \tag{2.32}$$

The quantum theory for the Wilson gauge action is defined through the generating functional

$$Z[U] = \int \mathcal{D}U \exp(-S_W) . \tag{2.33}$$

For finite lattices, boundary conditions at the edges of the lattice have to be supplied. In our work, for gauge fields we used periodic boundary conditions in all lattice directions.

The generating functional for the quantum theory (2.33) is a well-defined mathematical expression which does not requires additional input. For example, on the lattice it is not necessary to choose a gauge. However, in special cases gauge fixing is a useful step in extracting physical information. A discussion of gauge fixing on the lattice is given in the last chapter of this thesis.

2.3.2 The Lattice Action For Fermions

To formulate the matter field on the lattice we start with the continuum free field Lagrangian in Euclidean time[7],

$$\mathcal{L} = \overline{\psi}(x)(\gamma_\mu \partial_\mu + m)\psi(x) \tag{2.34}$$

and replace the derivative by finite differences

$$\mathcal{L} = \frac{1}{2a} \overline{\psi}(x) \gamma_\mu [\psi(x + a\hat{\mu}) - \psi(x - a\hat{\mu})] + m_0 \overline{\psi}(x)\psi(x) ; \tag{2.35}$$

m_0 stands for the bare mass. The Lagrangian (2.35) is not a good candidate for defining fermion fields on the lattice because its continuum limit describes 2^4 degenerate fermions instead of a single fermion, the species doubling problem. One way of identifying the extra degrees of freedom is to look for poles in the free

[7] For the definition of the gamma matrices and their properties, see appendix A.

propagator,

$$G(p) = \frac{am_0 - i\sum_\mu \gamma_\mu \sin(ap_\mu)}{(am_0)^2 + \sum_\mu \sin^2(ap_\mu)} . \tag{2.36}$$

The poles occurs at

$$0 = \sum_\mu \sin^2(ap_\mu) + (am_0)^2 . \tag{2.37}$$

For fermions, the boundary conditions used are periodic in spatial directions and anti-periodic in time direction. Then, the allowed values for Euclidean momenta follow in the intervals

$$\begin{aligned} p_j &\in [-\tfrac{\pi}{a}, \tfrac{\pi}{a}] \qquad\qquad j = 1 \cdots 3 \\ p_4 &\in [\tfrac{\pi}{aT}(1-T), \tfrac{\pi}{aT}(1+T)] \end{aligned} \tag{2.38}$$

with T being the lattice extension in the time direction. Equation (2.37) does not distinguish momenta separated by $\frac{\pi}{a}$. For each lattice direction (2.37) has two solutions corresponding to momenta separated by $\frac{\pi}{a}$, i.e. (2.35) describes 2^4 fermions with the same mass, species doubling problem. This is a feature which holds independently of the value of the quark mass.

The species doubling is connected to the problem of defining a good regulator for chiral fermions [66]. The translation of the Nielsen and Ninomiya no-go theorem for the lattice regularisation is that, as long as chiral invariance is not explicitly broken for massless fermions, it is not possible to avoid the extra fermionic degrees of freedom.

Despite the negative result of Nielsen and Ninomiya, there are two approaches which, in practice, get around the problem of species doubling on the lattice. Both rely on the identification of the extra degrees of freedom with momenta at the edges of the first Brillouin zone. In the staggered fermion [67] "solution", a Dirac spinor is distributed over the lattice. The Brillouin zone is reduced or, equivalently, the lattice spacing is doubled, avoiding in this way the higher momenta of the Brillouin zone. The advantage of staggered fermions is that they are computationally less expensive and chiral symmetry is always preserved. The big disadvantage is that flavour and translational invariance are mixed, making the writing of the operators and the identification of physical observables more

involved. This approach was not adopted in our work and we won't discuss it anymore.

The other "solution" to the doubling problem is known as Wilson fermions [68]. In the Wilson fermion approach, a mass proportional to the cut-off is given to the extra degrees of freedom. In the continuum limit, these states became infinitely heavy and decouple from the theory. The action describing Wilson fermions is obtained from the naive action by adding a second derivative-like term

$$S^{(WF)} = a^4 \sum_x \overline{\psi}(x) [\frac{1}{2a} \sum_\mu \gamma_\mu (\psi(x + a\hat{\mu}) - \psi(x - a\hat{\mu})) + m_0 \psi(x) - \frac{r}{2a} \sum_\mu (\psi(x + a\hat{\mu}) + \psi(x - a\hat{\mu}) - 2\psi(x))] \quad (2.39)$$

r is a new parameter of the theory which, in principle, can take any value. For small lattice spacing, $S^{(WF)}$ approaches the usual continuum action with the corrections of $\mathcal{O}(a)$. Following the same procedure as for naive fermions, the conclusion is that the $\vec{p} = 0$ state has mass am_0 while the mass for the states at the edges of the Brillouin is proportional to r/a, as required.

The Wilson approach to fermions on the lattice, by explicitly breaking chiral symmetry, does not fall into the category of actions studied by Nielsen and Ninomiya. The question of recovering chiral symmetry in the continuum limit needs to be checked. Bochicchio et al [69] were able to prove that, for Wilson fermions, chiral symmetry can be recovered in the continuum limit. Simulations on the lattice seems to confirm this trend of the Wilson formulation - see for example [70, 71].

It is usual to write the fermionic action in terms of dimensionless quantities. Define

$$\kappa = 1/2(am_0 + 4r) \quad (2.40)$$

$$\psi(x) = \sqrt{2\kappa}\, a^{-\frac{3}{2}}\, \psi^{(phys)}(x) \quad (2.41)$$

were κ is the hopping parameter and $\psi^{(phys)}(x)$ is the dimensionful spinor. To write a gauge invariant fermionic action, the operator $U_\mu(x)$ has to be inserted

where appropriate. The gauge-invariant Wilson fermion action is given by

$$S^{WF} = \sum_x \overline{\psi}(x)\psi(x) - \kappa \sum_{x,\mu} \overline{\psi}(x)\left[(r-\gamma_\mu)\,U_\mu(x)\,\psi(x+\hat{\mu}) + (r+\gamma_\mu)\,U_\mu^\dagger(x-\hat{\mu})\,\psi(x-\hat{\mu})\right] . \quad (2.42)$$

2.4 Continuum Limit Of Lattice Theories

By formulating a field theory on a finite lattice, a regulator is introduced limiting the range of momentum values, the cut-off being $\Lambda \sim 1/a$ where a is the lattice spacing. Approaching the continuum means taking the limit $a \to 0$, i.e. removing the cut-off. To recover continuum field theory the limit $a \to 0$ has to be taken with physical (renormalised) quantities fixed. This requires taking the limit of zero lattice spacing and, simultaneously, tuning the bare parameters of the action to keep renormalised quantities fixed. Then, close to continuum theory, the lattice spacing and the bare parameters are no longer independent variables.

For Lattice QCD, because of asymptotic freedom, the continuum limit is given by

$$\lim_{a\to 0} g_0(a) = 0 \quad \text{such that} \quad \lim_{a\to 0} (\, a\,\xi(g_0(a))\,)^{-1} = m \ , \quad (2.43)$$

with $\xi(g_0(a))$ standing for a correlation length and m the corresponding physical mass. For small lattice spacing, $g_0(a)$ is small and perturbation theory comes to help. Combining perturbative calculations with renormalisation group techniques it is possible to compute the function $g_0(a)$. The two-loop result for $SU(N)$ theories with n_f light quark flavours is

$$a = \frac{1}{\Lambda_{LAT}} \left(\frac{1}{\beta_0 g_0^2}\right)^{-\frac{\beta_1}{2\beta_0^2}} \exp\left(-\frac{1}{2\beta_0 g_0^2}\right)\left[1 + \mathcal{O}(g_0^2)\right] \quad (2.44)$$

$$\beta_0 = \frac{1}{16\pi^2}\left(\frac{11}{3}N - \frac{2}{3}n_f\right) \quad (2.45)$$

$$\beta_1 = \left(\frac{1}{16\pi^2}\right)^2 \left(\frac{34}{3}N^2 - \frac{10}{3}N\,n_f - \frac{N^2-1}{N}\right) \quad (2.46)$$

where Λ_{LAT} is a cut-off independent, renormalisation-group-invariant mass parameter describing the strength of the strong interaction.

On the lattice, only dimensionless quantities are measured, i.e. given an observ-

able, $\mathcal{F}$, of mass dimension f the lattice computes $a^{-f}\mathcal{F}$. To get $\mathcal{F}$ one should proceed as follows

1. compute $\mathcal{F}$ in lattice units at several g_0;
2. observe $a^{-f}\mathcal{F}$ scaling according to (2.44) as g_0 is varied (asymptotic scaling);
3. use one dimensionful parameter to set the overall scale and predict all other dimensionful quantities.

In practice, not all calculations use this recipe. Typically, the bare coupling constant is set to a value corresponding to small a and the dependence on the lattice spacing is reduced by using the improvement program.

2.5 Computing with Lattice Field Theory

To finish this chapter, we now give a description of how Lattice Field Theory is used in actual calculations. The next subsection explains how a MC simulation is performed and why we use the quenched approximation. We end by describing the improvement program in Lattice QCD. The relation between the operators and physical information is discussed in appendix B.

In Field Theory, the primary quantities to be computed are the Green's functions. In our study of QCD, we considered two types of Green's functions

- quark Green's functions

$$G^{(2n)}_{\alpha_1\cdots\alpha_n,\beta_1\cdots\beta_n}(x_1,\cdots,x_n,y_1,\cdots,y_n) =$$

$$= \int \mathcal{D}U\,\mathcal{D}\psi\,\mathcal{D}\overline{\psi}\;\psi^{A_1}_{\alpha_1}(x_1)\,\overline{\psi}^{B_1}_{\beta_1}(y_1)\cdots\psi^{A_n}_{\alpha_n}(x_n)\,\overline{\psi}^{B_n}_{\beta_n}(y_n) \qquad (2.47)$$

$$\exp\left(-S_W[U] - S^{(WF)}[\overline{\psi},\psi,U]\right) .$$

In this class of Green's functions. the quark propagators

$$G^{AB}_{\alpha\beta}(x,y) = \int \mathcal{D}U\, \mathcal{D}\psi\, \mathcal{D}\overline{\psi}\, \psi^{A}_{\alpha}(x)\overline{\psi}^{B}_{\beta}(y)$$

$$\exp\left(-S_W[U] - S^{(WF)}[\overline{\psi},\psi,U]\right) \qquad (2.48)$$

$$= \int \mathcal{D}U\ \det(M[U])\,(M^{-1})^{AB}_{\alpha\beta}(x,y)\ \exp\left(-S_W[U]\right)$$

where the matrix $M[U]$ is defined by $S^{(WF)} = \sum_{xy}\overline{\psi}(x)M(x,y)\psi(y)$, are of special importance because any $(2n)$-point Green's function can be written as combinations of these 2-point functions.

- Gluon Green's functions, related to

$$\int \mathcal{D}U\, \mathcal{D}\psi\, \mathcal{D}\overline{\psi}\, U_{\mu_1}(x_1)\cdots U_{\mu_n}(x_n)\, \exp\left(-S_W[U] - S^{(WF)}[\overline{\psi},\psi,U]\right)\ . \quad (2.49)$$

In Lattice Field Theory, these integrals are defined as integrals in a space of high dimension[8]. The only numerical method capable of handling such high dimensional integrals is Monte Carlo integration.

2.5.1 The Monte Carlo Technique and the Quenched Approximation

In a MC simulation, an estimate of the mean value of a function $\mathcal{F}(\phi)$, with ϕ distributed according to the probability measure $P(\phi)$,

$$\langle\mathcal{F}\rangle = \int \mathcal{D}\phi\, \mathcal{F}(\phi)\, P(\phi)\ , \qquad (2.50)$$

is achieved by generating a long sequence $\phi^{(1)},\cdots,\phi^{(n)}$ of random samples from $P(\phi)$ and then using the sample mean

$$\langle\mathcal{F}\rangle = \langle\mathcal{F}\rangle_{(n)} + \mathcal{O}(\frac{1}{\sqrt{n}})\ , \qquad (2.51)$$

where

$$\langle\mathcal{F}\rangle_{(n)} = \frac{1}{n}\sum_{i=1}^{n}\mathcal{F}(\phi^{(i)})\ . \qquad (2.52)$$

[8]For example, for a $24^3 \times 48$ lattice the number of space-time points is 663 552.

The configurations $\phi^{(1)}, \cdots, \phi^{(n)}$ are generated by a Markov process. A transition probability, $T(\phi \to \phi')$, satisfying the following properties

1. $T(\phi \to \phi') > 0$;
2. $\int \mathcal{D}\phi' T(\phi \to \phi') = \int \mathcal{D}\phi T(\phi \to \phi') = 1$;
3. $T(\phi \to \phi') P(\phi) d\phi = T(\phi' \to \phi) P(\phi') d\phi'$;

is defined and used in generating a sequence of configurations $\tilde{\phi}^{(j)}$, $j = 1 \cdots N$. For a transition probability satisfying the above relations, it is possible to prove that any sequence of configurations generated with $T(\phi \to \phi')$ converges, in the large N limit, to the distribution $P(\phi)$. If the configurations $\tilde{\phi}^{(j)}$, $j = m \cdots N$ are distributed according to $P(\phi)$, then the Markov chain is said to be thermalized. The set $\phi^{(1)}, \cdots, \phi^{(n)}$ is chosen from the configurations $\tilde{\phi}^{(j)}$ after thermalisation has been achieved.

It can be shown that $\langle \mathcal{F} \rangle_{(n)}$ converges to $\langle \mathcal{F} \rangle$ with probability one and fluctuations of size $n^{-1/2}$. The different MC methods are distinguished by different transition amplitudes [72].

In Lattice QCD, the integration over the fermionic variables can be done exactly. The remaining integrations are integrations over the link variables, $U_\mu(x)$. The integration over the link variables is done by the MC method. The probability distribution of the links variables is

$$P(U) = \det(M[U]) \exp(-S_W[U]) . \tag{2.53}$$

In principle, one should use (2.53) when performing MC simulations. However, the calculation of the fermionic determinant, $\det(M[U])$, is a substantial overhead and, because of that, present day simulations usually replace the determinant by a constant, Quenched Lattice QCD. If one uses the language of Feynman diagrams, ignoring the contribution from the fermionic determinant means that closed fermion loops are not taken into account. At least in perturbation theory, quark loops are proportional to inverse powers of the quark mass and, therefore, one expects the quenched approximation to give better results as we go towards

heavier quarks. The quenched approximation is a rather drastic approximation, in the sense that there is no way of systematically correcting for these loops. Simulations with full QCD is a task for the new generation of machines. All the work presented in this thesis refers to Quenched Lattice QCD.

2.5.2 Improvement In Lattice QCD

Ignoring problems from algorithms and their performance, any MC simulation on a finite lattice has systematics due both to finite lattice spacing and to finite volume. The finite volume effects can be reduced by choosing a large enough lattice for the physics to be addressed. Reducing the errors from finite lattice spacing, means making a (β) as small (big) as possible. In a practical situation, because of finite computer resources and/or algorithmic problems, one cannot fulfil both requirements and a balance between the two limits has to be achieved. The idea of the improvement program is to reduce the systematics from finite lattice spacing.

In Lattice QCD various ways of reducing the lattice spacing artifacts have been devised. In all improvement programs an expansion in a small parameter is involved, being it the lattice spacing [73, 74], a boosted coupling constant [75] or the bare coupling constant [76, 77].

In our study of the baryon spectrum and form factors we make use of the improvement program established in [76]. The approach relies in perturbation theory, as an expansion in the bare coupling constant, to reduce the dependence on the lattice spacing by modifying the action and operators. For fermions, we use the action proposed by Sheikholeslami and Wohlert [77],

$$S^{(F)} = S^{(WF)} - ig_0\kappa\frac{ar}{2}a^4\sum_{x,\mu,\nu}\overline{\psi}(x)\,\sigma_{\mu\nu}F_{\mu\nu}(x)\,\psi(x) \tag{2.54}$$

where

$$F_{\mu\nu}(x) = \frac{1}{4}\frac{1}{i2g_0a^2}\sum_{\square=1}^{4}\left(P_{\square\mu\nu} - P^{\dagger}_{\square\mu\nu}\right); \tag{2.55}$$

the sum being over all four plaquettes lying in the $\mu\nu$ plan.

For evaluating matrix elements between hadron states, $< H'|\,J_\Gamma\,|H >$, of a quark current, $J_\Gamma = \overline{q}'\,\Gamma\,q$, in the current the quark fields have to be rotated [76, 78].

This is equivalent to replacing J_Γ by the improved current

$$J_\Gamma(x) = \overline{q}'(x)\,[\,\Gamma + \frac{ar}{2}(z\gamma\cdot D^{(\leftarrow)} + (1-z)m_0)\,\Gamma \\ - \frac{ar}{2}\,\Gamma\,(z\gamma\cdot D^{(\rightarrow)} - (1-z)m_0)\,]\,q(x)\;, \qquad (2.56)$$

where z is a constant which can take any value. Using the action (2.54) together with the improved current (2.56), a perturbative analysis shows that on-shell matrix elements have their errors due to finite lattice spacing reduced from $\mathcal{O}(a)$ to $\mathcal{O}(\alpha_s a)$. The improvement program is of particular relevance in our baryonic study because $\xi \sim 1/a$, which makes the finite lattice spacing corrections important. When performing the simulations we use dimensionless fields and parameters as defined in (2.40) and take $z = r = 1$.

Chapter 3

Heavy Quark Field Theory

In the study of heavy baryons described in the next two chapters, only particles composed of a heavy quark, b or c, and light quarks, u, d and/or s, are considered. In the simulation we use a β value corresponding to an inverse lattice spacing of $2.9\,GeV$ and a spatial volume of $(1.6\,fm)^3$. The charm quark has a mass of $\sim 1.3\,GeV$, therefore it can be simulated in such a lattice. On the other hand, the simulation of the b quark requires a much finer grid. To avoid finite volume effects, i.e. for the same spatial volume, the number of lattice points must be substantially increased, resulting in a memory overhead which makes the direct simulation of b physics not feasible on present day machines. Studies of b flavoured hadrons have either to use effective theories, such as Heavy Quark Effective Theory or Non-Relativistic QCD, or to perform Lattice QCD simulations using a set of quark masses around the charm mass, and extrapolate the results to the b mass. In our study, to stay within Lattice QCD, we choose the latter approach. For extrapolating to the b mass we rely on Heavy Quark Effective Theory.

Heavy Quark Effective Theory (HQET) [79, 80, 81, 82] is a good approximation to QCD for systems with one heavy quark interacting with light quarks [83]. In this chapter, we describe HQET, emphasizing features relevant for our investigation.

3.1 HQET - the basic ingredients

The Standard Model requires at least six quarks to describe hadronic physics. Looking at the values of their masses, see table 3.1, one can differentiate two groups. A lighter group, which includes the u, d, s quarks, with masses smaller than the typical hadronic scale, $\sim 1GeV$, and a heavier group, the remaining quarks, composed of quarks with mass $\sim 1GeV$ or larger. In order to understand hadronic phenomena, it is useful to start from the limit $m_q \to 0$ when describing

$m_u = 2 - 8\,MeV$	$m_d = 5 - 15\,MeV$	$m_s = 100 - 300\,MeV$
$m_c = 1.0 - 1.6\,GeV$	$m_b = 4.1 - 4.5\,GeV$	$m_t = 180 \pm 12\,GeV$

Table 3.1: Quark Masses as defined in [26].

the light sector. Similarly, taking the limit $m_q \to \infty$ has been fruitful in describing heavy flavour physics. In both cases, QCD can be replaced by an equivalent effective theory which uses only the relevant degrees of freedom. The effective theory is, in principle, simpler to handle than QCD, and should allow the incorporation of deviations from the ideal limit in a systematic way.

For light quarks, the effective theory equivalent to QCD is Chiral Perturbation Theory (χPT). Deviations from the limit of zero quark mass are quantified in an expansion in the quark mass. For heavy quarks, QCD can be replaced by an effective theory where corrections to the infinite mass limit are proportional to inverse powers of the heavy quark mass.

The two types of effective theories just mentioned are related differently to QCD. In the zero mass limit, QCD is invariant under chiral rotations. χPT uses chiral symmetry, formulated in terms of hadron fields, as a guideline to build the effective theory. Despite using chiral symmetry, a derivation of χPT directly from the QCD Lagrangian is still to be done. For heavy quarks, expansions of the QCD Lagrangian and Green's functions in inverse powers of the heavy quark mass are known. Heavy Quark Effective Theory is an example of such an expansion.

Let us consider hadrons composed of a single heavy quark and one or more light quarks. In the limit of infinite quark mass, the velocity of the heavy quark and the hadron velocity, v, are the same. The interactions of the heavy quark with the light degrees of freedom continuously change its momentum by an amount of order Λ_{QCD}. The corresponding change in the velocity of the heavy quark, Λ_{QCD}/m_Q, where m_Q is the heavy quark mass, vanishes in the limit of infinite mass. If we write the heavy quark momentum as $P_Q = m_Q v + k$, then $k \sim \Lambda_{QCD}$ is much smaller than $m_Q v$. The dynamics of the heavy quark is associated with the residual momentum k, and $m_Q v$ is a pure kinematic factor[1]. In this case, it

[1]HQET can be used to describe any system where the above decomposition of the heavy

is appropriate to introduce the field $\tilde{Q}_v(x)$ whose dynamics is connected with the residual momentum k. The relation of the heavy quark field, $Q(x)$, to $\tilde{Q}_v(x)$ is defined by

$$Q(x) = \exp(-im_Q v \cdot x)\tilde{Q}_v(x) . \tag{3.1}$$

This definition does not restrict v in any way, and HQET is not a non-relativistic approximation. It should be clear from (3.1), that each value of the hadron velocity, v, requires a different field $\tilde{Q}_v(x)$.

The field $\tilde{Q}_v(x)$ describes quarks and antiquarks which are essentially at rest. It is convenient to introduce the "upper" and "lower" components

$$\tilde{Q}_v(x) = h_v^{(+)}(x) + h_v^{(-)}(x) , \tag{3.2}$$

defined by

$$P_\pm \, h_v^{(\pm)}(x) = \pm h_v^{(\pm)}(x) \tag{3.3}$$

where $P_\pm = (1 \pm \not{v})/2$ are the positive (+) and negative (-) energy projectors. In the quark rest frame, $h_v^{(+)}(x)$ has only upper components, whereas $h_v^{(-)}(x)$ has only lower components. The field $\exp(-im_Q v \cdot x)h_v^{(+)}(x)$ annihilates a quark with velocity v and $\exp(-im_Q v \cdot x)h_v^{(-)}(x)$ creates an antiquark with the same velocity. Making the substitution of $Q(x)$ for $h_v^{(+)}(x)$ and $h_v^{(-)}(x)$, the QCD Lagrangian becomes

$$\begin{aligned} \mathcal{L}_{QCD} &= \overline{Q}(x)(\not{D} - m_Q)Q(x) = \\ &= \overline{h}_v^{(+)}(x) iv \cdot D h_v^{(+)}(x) - \overline{h}_v^{(-)}(x)(iv \cdot D + 2m_Q)h_v^{(-)}(x) \\ &\quad + \overline{h}_v^{(+)}(x) i\not{D}_\perp h_v^{(-)}(x) + \overline{h}_v^{(-)}(x) i\not{D}_\perp h_v^{(+)}(x) , \end{aligned} \tag{3.4}$$

where $D_\perp^\mu = D^\mu - (v \cdot D)v^\mu$ and we used the following relations

$$\not{v} h_v^{(\pm)}(x) = \pm h_v^{(\pm)}(x) , \qquad P_\pm \gamma_\mu P_\pm = \pm v_\mu , \tag{3.5}$$

when writing $\mathcal{L}_{QCD}$. In (3.4), $h_v^{(+)}$ describes massless degrees of freedom, whereas $h_v^{(-)}$ is associated with states of mass $2m_Q$. In the infinite mass limit, the degrees

quark momentum is a sensible thing to do.

of freedom described by $h_v^{(-)}$ decouple from the theory, i.e. the degrees of freedom associated with $h_v^{(-)}$ are relevant only for the high-energy regime. To study the low-energy regime it should be sufficient to consider the field $h_v^{(+)}$. To achieve this goal, $h_v^{(-)}$ has to be integrated out from the generating functional. Since $\mathcal{L}_{QCD}$ is quadratic in $h_v^{(-)}$, the integration of $h_v^{(-)}$ can be done explicitly. After performing the integration, the resulting theory is non-local. For finite quark mass, the non-locality can be understood as a consequence of the propagation of the antiquarks, represented by $h_v^{(-)}$. Using the operator-product expansion, the non-local terms can be rewritten as an infinite series in $1/m_Q$ of local operators. The effective theory defined in this way is equivalent to low energy QCD.

Short-distance effects involve large virtual momenta and are not reproduced in the effective theory. For example, processes with closed fermion loops are absent from the effective theory, because their description has need of the field $h_v^{(-)}$. Nevertheless, the short-distance effects can be added perturbatively[2], by matching the effective theory to QCD. The effect of the matching procedure is a renormalisation of the coefficients of the local operators in the effective theory. Since short-distance effects manifest themselves as renormalisations of local operators, to understand the structure of HQET it is enough to consider the classical theory.

On the classical level, one can use the equations of motion to eliminate the field $h_v^{(-)}$. The classical equations of motion derived from (3.4) are

$$i \not{D}_\perp h_v^{(+)}(x) - (iv \cdot D + 2m_Q) h_v^{(-)}(x) = 0 \tag{3.6}$$

$$iv \cdot D\, h_v^{(+)}(x) + \not{D}_\perp h_v^{(-)}(x) = 0 \,. \tag{3.7}$$

Solving the first equation for $h_v^{(-)}$,

$$h_v^{(-)}(x) = \frac{i \not{D}_\perp}{iv \cdot D + 2m_Q} h_v^{(+)}(x) = \frac{i \not{D}_\perp}{2m_Q} h_v^{(+)}(x) + \mathcal{O}(1/m_Q^2) \,, \tag{3.8}$$

and inserting the result into the second equation, we get the equation of motion for $h_v^{(+)}$

$$[iv \cdot D + i \not{D}_\perp \frac{1}{iv \cdot D + 2m_Q} i \not{D}_\perp] h_v^{(+)}(x) = 0 \,. \tag{3.9}$$

[2]For heavy quarks, the energy scale involved is much larger than Λ_{QCD}, and perturbation theory can be used.

The Lagrangian corresponding to this equation of motion is

$$\begin{aligned}\mathcal{L} &= \bar{h}_v^{(+)}(x)\, iv\cdot D\, h_v^{(+)}(x) + \bar{h}_v^{(+)}(x) i\not{D}_\perp \tfrac{1}{iv\cdot D+2m_Q}\, i\not{D}_\perp\, h_v^{(+)}(x) = \\ &= \bar{h}_v^{(+)}(x)\, iv\cdot D\, h_v^{(+)}(x) + \tfrac{1}{2m_Q}\bar{h}_v^{(+)}(x)\,(i\not{D}_\perp)^2\, h_v^{(+)}(x) + \mathcal{O}(1/m_Q^2)\,.\end{aligned} \tag{3.10}$$

This is the Lagrangian that defines HQET. The relation between the QCD field $Q(x)$ and the heavy quark field $h_v^{(+)}(x)$ is given by

$$Q(x) = \exp(-im_Q v\cdot x)\,(1 + \frac{i\not{D}_\perp}{2m_Q} + \cdots)\, h_v^{(+)}(x)\,, \tag{3.11}$$

at tree level. Given an operator with one or more heavy quarks, (3.11) relates, at tree level, the QCD operator to the corresponding HQET operator.

The Lagrangian defining HQET does not have terms which connect heavy quark fields of different velocities. The velocity v, which matches the heavy quark velocity in the infinite mass limit, is not changed by strong interactions (velocity superselection rule). A change in v should be due to the action of an external (weak or electromagnetic) source mediating the transition.

3.2 HQET - the computational framework

HQET is a good approximation to QCD for systems with one heavy quark and one or more light quarks. The corrections to the leading order in the $1/m_Q$ expansion are expected to be of the order Λ_{QCD}/m_Q to some power. Taking $\Lambda_{QCD} \sim 200MeV$, $m_c \sim 1.3GeV$ and $m_b \sim 4.3GeV$, then $\Lambda_{QCD}/m_c \sim 0.15$ and $\Lambda_{QCD}/m_b \sim 0.05$. Therefore, for charm-physics we expect the corrections to be of the order 15%, whereas for b-physics they might be of order 5%. The corrections to the leading order in the $1/m_Q$ expansion are expected to be small, and are treated perturbatively.

In HQET, the calculations use the eigenstates of the leading term in (3.10),

$$\mathcal{L}_{HQET} = \bar{h}_v^{(+)}(x)\, iv\cdot D\, h_v^{(+)}(x) \tag{3.12}$$

and handle the power corrections in perturbation theory.

The Lagrangian (3.12) is not invariant under Lorentz transformations and does not describe different quark flavours. Since $\mathcal{L}_{HQET}$ does not depend on the mass of the heavy quark, to include other heavy flavours one just has to add similar terms for the corresponding fields. To recover Lorentz invariance, a sum over all possible velocities must be done. An effective Lagrangian which contains all possible flavours and velocities is

$$\mathcal{L} = \sum_{i=1}^{N_h} \sum_{v} \overline{h}_v^{(i)}(x)\, iv \cdot D\, h_v^{(i)}(x) \;, \tag{3.13}$$

where N_h stands for the number of heavy flavours - note that we dropped the superfix $(+)$.

3.3 The Spin-Flavour Symmetry

The theory defined by (3.13) has a new type of symmetry which is not manifest in the QCD Lagrangian: the spin-flavour symmetry. We now want to study the implications of spin-flavour symmetry in the description of heavy flavours.

In (3.13) there are no terms which connect quark fields associated with different velocities. Changes in v are due to weak or electromagnetic transitions. Then, for studying strong interactions it is sufficient to consider the simpler Lagrangian

$$\mathcal{L} = \overline{h}_v(x)\, iv \cdot D\, h_v(x) \;, \tag{3.14}$$

where

$$h_v(x) = \begin{pmatrix} h_v^{(1)}(x) \\ \vdots \\ h_v^{(N_h)}(x) \end{pmatrix} . \tag{3.15}$$

For situations involving heavy-quark-to-heavy-quark transitions, a term related to the final state quark, with velocity v_f, should be added to (3.14).

The Lagrangian (3.14) is invariant under the flavour transformation

$$h_v(x) \to h'_v(x) = U h_v(x) \;, \tag{3.16}$$

where U is an arbitrary $SU(N_h)$ matrix. The meaning of flavour symmetry is that

the mass of the light degrees of freedom,

$$\overline{\Lambda} = M_{H_Q} - m_Q \ , \tag{3.17}$$

is, for given quantum numbers, independent of the type of heavy quark - M_{H_Q} stands for the mass of the hadron with the heavy quark Q. Another way of stating flavour symmetry is that the hadronic spectrum for heavy flavours is independent of the heavy flavour, apart an overall shift due to the heavy quark mass. The validity of this prediction can be checked, for example, by looking at mass differences of heavy mesons. The observed behaviour is in agreement with the flavour symmetry predictions - see for example [84]. The conserved current associated with flavour symmetry,

$$j^i_\mu = \overline{h}_v \, v_\mu \, T^i \, h_v \ , \tag{3.18}$$

with T^i representing the generator of $SU(N_h)$, relates amplitudes for processes involving different heavy flavours.

Another symmetry of (3.14) is the spin symmetry, i.e. (3.14) is invariant under rotations of the heavy quark spin,

$$h_v(x) \rightarrow h'_v(x) = \exp\left(i\vec{S}\cdot\hat{n}\theta\right) h_v(x) \ , \tag{3.19}$$

$\hat{n}$ and θ are respectively, the rotation axis and the rotation angle, and $\vec{S}$ is the spin operator for the heavy quark. Spin symmetry means that the light degrees of freedom are insensitive to the spin orientation of the heavy quark, i.e. the heavy quark spin and, therefore, the total angular momentum of the light degrees of freedom (light quarks and gluons altogether), j, are separately conserved by strong interactions. Spin symmetry predicts that, for fixed $j \neq 0$, there is a doublet of degenerate states with total spin $J = j \pm 1/2$. Similarly to the flavour symmetry, the conserved current associated to the spin symmetry can be used to relate amplitudes involving the two partners of such doublets.

The theory defined by the Lagrangian (3.14) is invariant under $SU(2N_h)$ spin-flavour transformations, (3.16) and (3.19). According to this symmetry, the hadron states with a heavy flavour can be classified by the quantum numbers (flavour, spin, parity, $\cdots$) of their light degrees of freedom.

3.4 The Isgur-Wise Function and the Weak Decay Form Factors

Spin-flavour symmetry relates various matrix elements involving heavy quark flavours, and fixes the absolute normalisation of some of them. Using this symmetry in the study of weak decay form factors leads to considerable simplifications. For semi-leptonic decays of heavy flavours, spin-flavour symmetry predicts that the form factors can be expressed in terms of a single function, the Isgur-Wise function, and gives its value at zero recoil.

In chapter 5 we describe the study of hadronic matrix elements involved in the electroweak decay $\Lambda_b \rightarrow \Lambda_c \, l \, \overline{\nu}$. Here, because the light degrees of freedom have the quantum numbers $j^P = 0^+$, the spin symmetry is very effective in reducing the number of independent form factors.

On the lattice we are not able to simulate the b quark. Therefore, instead of computing directly the matrix elements for the transition $\Lambda_b \rightarrow \Lambda_c$, we compute $\Lambda_{Q'} \rightarrow \Lambda_Q$ for a set of quark masses around the charm mass and use HQET to predict the $b \rightarrow c$ transition. For the electroweak transition $\Lambda_{Q'} \rightarrow \Lambda_Q \, l \, \overline{\nu}$, the baryonic matrix elements involve the vector current $V_\mu = \overline{Q}\gamma_\mu Q'$ and the axial current $A_\mu = \overline{Q}\gamma_\mu\gamma_5 Q'$. The baryonic matrix elements of the vector and axial vector currents are parametrised by six real form factors. We define them as

$$< \Lambda_Q(v) \,|\, V_\mu \,|\, \Lambda_{Q'}(v') > = \overline{u}_{\Lambda_Q}(v) \, [\, F_1(\omega)\gamma_\mu + F_2(\omega)v'_\mu + F_3(\omega)v_\mu \,] \, u_{\Lambda_{Q'}}(v') \quad , \tag{3.20}$$

$$< \Lambda_Q(v) \,|\, A_\mu \,|\, \Lambda_{Q'}(v') > = \overline{u}_{\Lambda_Q}(v) \, [\, G_1(\omega)\gamma_\mu + G_2(\omega)v'_\mu + G_3(\omega)v_\mu \,] \, \gamma_5 \, u_{\Lambda_{Q'}}(v') \, , \tag{3.21}$$

where $v_\mu = p_\mu / M_{\Lambda_Q}$ ($v'_\mu = p'_\mu / M_{\Lambda_{Q'}}$) is the velocity of the Λ_Q ($\Lambda_{Q'}$), $\omega = v \cdot v'$ is the velocity transfer and u_Λ stands for the Λ particle spinor. According to HQET, the hadronic form factors $F_i(\omega)$ and $G_i(\omega)$ can be expanded in powers of $1/m_Q$, and the coefficients of such an expansion can be related to universal, mass-independent functions of the velocity transfer, ω [86, 87, 88, 89]. Up to sub-leading order in the $1/m_Q$ expansion and next-to-leading order in the strong coupling constant, α_s, HQET relates the six form factors by a unique function,

$\xi_{QQ'}(\omega)$, [84]

$$F_i(\omega) = N_i(\omega)\ \xi_{QQ'}(\omega)\ , \tag{3.22}$$

$$G_i(\omega) = N_i^5(\omega)\ \xi_{QQ'}(\omega)\ . \tag{3.23}$$

$N_i(\omega)$ and $N_i^5(\omega)$ depend on the heavy quark mass through $\epsilon_Q = \overline{\Lambda}/2m_Q$. All the dependence in $\alpha_s(m_Q)$ is summarised in the short distance functions $\hat{C}_i$ and $\hat{C}_i^5$ - see [84, 90] for definitions. In terms of these functions, ϵ_Q and $\epsilon_{Q'}$, $N_i(\omega)$ and $N_i^5(\omega)$ are given by

$$N_1(\omega) = \hat{C}_1(\overline{\omega})\,(1 + \frac{2}{\omega+1}(\epsilon_Q + \epsilon_{Q'}))\ , \tag{3.24}$$

$$N_2(\omega) = \hat{C}_2(\overline{\omega})\,(1 + \frac{2\omega}{\omega+1}\epsilon_{Q'}) - [\hat{C}_1(\overline{\omega}) + \hat{C}_3(\overline{\omega})]\frac{2}{\omega+1}\epsilon_Q\ , \tag{3.25}$$

$$N_3(\omega) = \hat{C}_3(\overline{\omega})\,(1 + \frac{2\omega}{\omega+1}\epsilon_Q) - [\hat{C}_1(\overline{\omega}) + \hat{C}_2(\overline{\omega})]\frac{2}{\omega+1}\epsilon_{Q'}\ , \tag{3.26}$$

$$N_1^5(\omega) = \hat{C}_1^5(\overline{\omega})\ , \tag{3.27}$$

$$N_2^5(\omega) = \hat{C}_2^5(\overline{\omega})(1 + \frac{2}{\omega+1}\epsilon_Q + 2\epsilon_{Q'}) - [\hat{C}_1^5(\overline{\omega}) + \hat{C}_3^5(\overline{\omega})]\frac{2}{\omega+1}\epsilon_Q\ , \tag{3.28}$$

$$N_3^5(\omega) = \hat{C}_3^5(\overline{\omega})(1 + 2\epsilon_Q + \frac{2\omega}{\omega+1}\epsilon_{Q'}) + [\hat{C}_1^5(\overline{\omega}) - \hat{C}_2^5(\overline{\omega})]\frac{2}{\omega+1}\epsilon_{Q'}\ , \tag{3.29}$$

where

$$\overline{\omega} = \omega + \overline{\Lambda}(1/m_Q + 1/m_{Q'})\,(\omega - 1)\ , \tag{3.30}$$

and $\overline{\Lambda}$ is the mass of the light degrees of freedom.

The baryonic Isgur-Wise function, $\xi_{QQ'}(\omega)$, is not a universal function. However, $\xi_{QQ'}(\omega)$ can be expressed in terms of two universal, mass and renormalisation scheme independent functions of the velocity transfer, $\xi(\omega)$ and $\chi(\omega)$, as

$$\xi_{QQ'}(\omega) = \xi(\omega) + (\epsilon_Q + \epsilon_{Q'})[\,2\,\chi(\omega) + \frac{\omega-1}{\omega+1}\xi(\omega)\,]\ . \tag{3.31}$$

The function $\xi(\omega)$ is the form factor which describes the transition in the infinite mass limit[3], whereas $\chi(\omega)$ comes from insertions of $1/m_Q$ terms in the effective Lagrangian into matrix elements of the lowest order current, $\overline{h}\Gamma h$. At zero recoil,

[3]Usually called Isgur-Wise function.

i.e. $\omega = 1$, these functions satisfy the normalisation conditions

$$\xi(1) = 1 \quad \text{and} \quad \chi(1) = 0 \; . \tag{3.32}$$

Consequently, the baryonic Isgur-Wise function $\xi_{QQ'}(\omega)$ is also normalised at zero recoil,

$$\xi_{QQ'}(1) = 1 \; . \tag{3.33}$$

In the study of $1/m_Q$ corrections to the form factors, Luke's theorem provides results at zero recoil valid to all orders of perturbation theory in α_s [91, 92]. For the baryonic form factors, Luke's theorem means that

$$\sum_i F_i(1) = \eta_V + \mathcal{O}(1/m_Q^2) \; , \tag{3.34}$$

$$G_1(1) = \eta_A + \mathcal{O}(1/m_Q^2) \; , \tag{3.35}$$

where η_V, η_A are the values of the radiative corrections at zero recoil.

For transitions between heavy quarks with the same mass, the number of independent form factors is further reduced. The relations $F_2(\omega) = F_3(\omega)$ and $G_2(\omega) = -G_3(\omega)$ are valid for all values of ω and the vector current at zero recoil becomes conserved[4]. At zero recoil, the radiative corrections defined in (3.34) and (3.35) are

$$\eta_V = 1 \tag{3.36}$$

$$\eta_A = 1 - \frac{2\alpha_s(m_Q)}{3\pi} \; . \tag{3.37}$$

Luke's theorem protects the form factor $G_1(1)$ against $1/m_Q$ corrections. At zero recoil, the decay rate for $\Lambda_b \to \Lambda_c \, l \, \overline{\nu}$ only gets contributions from $G_1(1)$,

$$\frac{d\Gamma}{d\omega}(\Lambda_b \to \Lambda_c l \overline{\nu}) = \frac{G_F^2}{4\pi^3} |V_{cb}|^2 M_{\Lambda_c}^3 (M_{\Lambda_b} - M_{\Lambda_c})^2 \sqrt{\omega^2 - 1} \, |G_1(1)|^2 \; , \tag{3.38}$$

where G_F is the Fermi weak decay constant and V_{cb} is an element of the CKM

[4] In this case, the vector current is the conserved flavour current.

matrix. If the semi-leptonic $\Lambda_b \to \Lambda_c$ data can be continued reliably to zero recoil, this decay provides an accurate[5] and independent way of extracting V_{cb}. Besides, if the Isgur-Wise function is known, all the form factors describing the decay $\Lambda_b \to \Lambda_c \, l \, \overline{\nu}$ are determined and a complete theoretical description of these decay becomes available.

[5]The $1/m_Q^2$ corrections at zero recoil have been estimated, [93], and are of the order of a few percent.

Chapter 4

Heavy Baryon Spectroscopy

The spectroscopy of hadrons with heavy flavours (c or b) and their decays are currently under experimental investigation. For heavy baryons, the information available about the spectrum is still very limited. However, the expectations are that, during the next few years, a number of new heavy baryons will be discovered and a better description of the presently known ones will be achieved. For this reason, it is important that theory provides a clear and coherent picture of their physics.

The theoretical analysis of the quark dynamics requires solving QCD, a task not yet fully accomplished. Alternatively, one can try to model the quark interaction by, for example, introducing a potential interaction. This was done with considerable success for light quarks and for mesons with heavy quarks.

Previous studies of heavy baryon spectroscopy had to rely on modelling the quark interaction and/or quark wave function. Despite consistency of results between the different approaches[1], it is important to make QCD model-independent predictions. Lattice QCD is, currently, the only computational technique which allows for non-perturbative, first principles, model-independent predictions.

In this chapter, we describe a lattice study of heavy baryon spectroscopy using Quenched Lattice QCD [44].

4.1 Heavy Baryon States

Before embarking on explaining our calculation of the heavy baryon spectrum, we want to discuss the classification of the heavy baryon states and to describe the present experimental situation.

[1] See chapter 1 for references.

The spectroscopy of heavy-flavoured hadrons is not qualitatively different from the spectroscopy of light hadrons. Adopting the quark model language, baryons are bound states of three quarks in a colour singlet state. The quark wave function is assumed to factorize into a colour-dependent, a flavour-dependent, a spin-dependent and a space-dependent part. Baryons are fermionic particles, and their total wave function must be antisymmetric under the interchange of quarks. Since baryons are colour singlet states, their wave function is completely antisymmetric in the quark colour indices. Consequently, the baryonic wave function is totally symmetric under exchange of spin, flavour and space quark coordinates.

The determination of the spatial part of the wave function requires detailed information about the interaction. However, the spin and flavour parts of the wave function are fixed once exact flavour symmetry is assumed.

For particles composed only of light quarks, u, d, s, the $SU(3)$-flavour, $SU(3)_F$, scheme provides a systematic classification of meson and baryon states - see for example [94]. To allow for the possibility of having particles with one type of heavy quark, Q, and light quarks, the $SU(3)$-flavour scheme has to be replaced by $SU(4)_F$. Despite the fact that $SU(4)_F$ is badly broken, it offers a useful classification of the lowest-lying heavy hadrons.

In the $SU(4)_F$ scheme, the fundamental representation of the group, 4, is made up of the quark flavours u, d, s and Q. In terms of the fundamental representation, the baryon content is given by

$$4 \otimes 4 \otimes 4 \;=\; 20_S \oplus 20_M \oplus 20_M \oplus \overline{4}\,, \tag{4.1}$$

where the suffix S denotes a symmetric representation and M a representation with mixed symmetry. Of the two representations with mixed symmetry, one can be chosen symmetric under the interchange of the first two flavour indices, denoted by 20_{M_S}, whereas the other can be made antisymmetric with respect to the same flavour indices, the 20_{M_A} representation.

Each of the $SU(4)_F$ multiplets can be decomposed into $SU(3)_F$ multiplets. For

baryon representations, the $SU(3)_F$ content is

$$20_M \supset 8_0 \oplus 6_1 \oplus \overline{3}_1 \oplus 3_2 \ , \tag{4.2}$$

$$20_S \supset 10_0 \oplus 6_1 \oplus 3_2 \oplus 1_3 \ , \tag{4.3}$$

$$\overline{4} \supset 1_0 \oplus 3_1 \ , \tag{4.4}$$

where the subscript refers to the heavy quark content of each multiplet. The 20_M representation includes an $SU(3)_F$ octet with no heavy quark content, whereas 20_S representation contains an $SU(3)_F$ decuplet with zero heavy quark content. These $SU(3)_F$ multiplets are identified with the usual $SU(3)_F$ states. Then, according to the quark model description, the $J^P = \frac{1}{2}^+$ ground-state baryons with one heavy quark belong to the 20_{M_A} representation[2]. The 20_{M_S} representation describes another family of $J^P = \frac{1}{2}^+$ heavy baryons, whereas the 20_S representation include the $J^P = \frac{3}{2}^+$ heavy baryons.

In the tables 4.1 and 4.2, we list the quantum numbers of charm baryons; only states with one charm quark are considered. We follow the notation of the Particle Data Group (PDG) [26], and I and I_3 denote the isospin, S, C, B refer to strangeness, charm and bottom quantum numbers. The values quoted for the particle masses are from [26], except where otherwise stated. Table 4.3 reports on b-baryons.

The actual experimental situation is that, for charm-baryons, almost all the lowest-lying $J^P = \frac{1}{2}^+$ states have been observed, their masses determined and some of their decays studied - see [26]. First claims of $J^P = \frac{3}{2}^+$ baryon states have also been reported. For b-baryons, only the Λ_b is established unambiguously.

4.2 Particles and Operators

The work described in this chapter is about QCD and heavy baryon spectroscopy. Ignoring electromagnetic splittings, there are only eight lowest-lying baryons containing one heavy quark and two light quarks. In table 4.4 we list their quantum numbers.

[2]In the quark model, states which are symmetric under the interchange of space coordinates are lower in energy for attractive potentials.

Notation	Quark Content	I	I_3	S	C	Mass (MeV)
Λ_c^+	$[ud]c$	0	0	0	1	2284.9 ± 0.6
Ξ_c^+	$[us]c$	$\frac{1}{2}$	$\frac{1}{2}$	-1	1	2465.6 ± 1.4
Ξ_c^0	$[ds]c$	$\frac{1}{2}$	$-\frac{1}{2}$	-1	1	2470.3 ± 1.8
Σ_c^{++}	uuc	1	1	0	1	2452.9 ± 0.6
Σ_c^+	$\{ud\}c$	1	0	0	1	2453.5 ± 0.9
Σ_c^0	ddc	1	-1	0	1	2452.1 ± 0.7
$\Xi_c'^+$	$\{us\}c$	$\frac{1}{2}$	$\frac{1}{2}$	-1	1	–
$\Xi_c'^0$	$\{ds\}c$	$\frac{1}{2}$	$-\frac{1}{2}$	-1	1	–
Ω_c^0	ssc	0	0	-2	1	2704.9 ± 4

Table 4.1: $J^P = \frac{1}{2}^+$ charm-baryons. In the quark content column, $[qq']$ means that the flavour wave function is antisymmetric under intercharge of the flavour indices of these quarks, and $\{qq'\}$ refers to symmetric flavour wave functions.

Notation	Quark Content	I	I_3	S	C	Mass (MeV)
$\Sigma_c^{*\,++}$	uuc	1	1	0	1	seen
$\Sigma_c^{*\,+}$	udc	1	0	0	1	seen
$\Sigma_c^{*\,0}$	ddc	1	-1	0	1	seen
$\Xi_c^{*\,+}$	usc	$\frac{1}{2}$	$\frac{1}{2}$	-1	1	2644.6 ± 2.3
$\Xi_c^{*\,0}$	dsc	$\frac{1}{2}$	$-\frac{1}{2}$	-1	1	2643.3 ± 2.2
$\Omega_c^{*\,0}$	ssc	0	0	-2	1	-

Table 4.2: $J^P = \frac{3}{2}^+$ charm-baryons. All data concerning the $\frac{3}{2}^+$ baryons are reported by just one experiment. The Σ^* was seen by the SKAT collaboration [27] and a mass of $2530 \pm 5 \pm 5\,MeV$ was claimed. The mass values for Ξ^* are from the CLEO collaboration [28, 29].

The baryons which are the object of our study are particles with one heavy quark and two light quarks. For this type of particles, QCD can be approximated by Heavy Quark Effective Theory.

In the context of HQET, hadron states with one type of heavy quark are distinguished by the quantum numbers of their light degrees of freedom (gluons and quarks), i.e. by their spin, parity and flavour (isospin and strangeness) quantum numbers. The quantum numbers of a hadron are the result of combining the quantum numbers both of the light degrees of freedom and of the heavy quark. Our choice of interpolating operators for studying heavy baryon spectroscopy embraces the HQET description of hadrons.

To compute the spectrum of the heavy baryons on the lattice, we define the following three interpolating operators

$$\mathcal{O}_5 = \varepsilon_{ABC}\,(q^{A\,T} C\gamma_5 q'^{\,B})\,Q^C\,, \tag{4.5}$$

$$\mathcal{O}_\mu = \varepsilon_{ABC}\,(q^{A\,T} C\gamma_\mu q^B)\,Q^C\,, \tag{4.6}$$

Notation	Quark Content	J^P	I	I_3	S	B	Mass (MeV)
Λ_b^0	$[ud]c$	$\frac{1}{2}^+$	0	0	0	-1	5641 ± 50
Ξ_b^0	$[us]c$	$\frac{1}{2}^+$	$\frac{1}{2}$	$\frac{1}{2}$	-1	-1	–
Ξ_b^-	$[ds]c$	$\frac{1}{2}^+$	$\frac{1}{2}$	$-\frac{1}{2}$	-1	-1	–
Σ_b^+	uuc	$\frac{1}{2}^+$	1	1	0	-1	–
Σ_b^0	udc	$\frac{1}{2}^+$	1	0	0	-1	–
Σ_b^-	ddc	$\frac{1}{2}^+$	1	-1	0	-1	–
$\Xi_b^{\prime 0}$	usc	$\frac{1}{2}^+$	$\frac{1}{2}$	$\frac{1}{2}$	-1	-1	–
$\Xi_b^{\prime -}$	dsc	$\frac{1}{2}^+$	$\frac{1}{2}$	$-\frac{1}{2}$	-1	-1	–
Ω_b^-	ssc	$\frac{1}{2}^+$	0	0	-2	-1	–
Σ_b^{*+}	uuc	$\frac{3}{2}^+$	1	1	0	-1	–
Σ_b^{*0}	udc	$\frac{3}{2}^+$	1	0	0	-1	–
Σ_b^{*-}	ddc	$\frac{3}{2}^+$	1	-1	0	-1	–
Ξ_b^{*0}	usc	$\frac{3}{2}^+$	$\frac{1}{2}$	$\frac{1}{2}$	-1	-1	–
Ξ_b^{*-}	dsc	$\frac{3}{2}^+$	$\frac{1}{2}$	$-\frac{1}{2}$	-1	-1	–
Ω_b^{*-}	ssc	$\frac{3}{2}^+$	0	0	-2	-1	–

Table 4.3: $J^P = \frac{1}{2}^+, \frac{3}{2}^+$ b-baryons. For notation see table 4.1.

Baryon	J^P	S	I	Quark Content	$s_l^{\pi_l}$	Operator
$\Lambda_{c,b}$	$\frac{1}{2}^+$	0	0	$(ud)c,b$	0^+	$\mathcal{O}_5$
$\Xi_{c,b}$	$\frac{1}{2}^+$	-1	$\frac{1}{2}$	$(us)c,b$	0^+	$\mathcal{O}_5$
$\Sigma_{c,b}$	$\frac{1}{2}^+$	0	1	$(uu)c,b$	1^+	$\mathcal{O}_\mu$
$\Xi'_{c,b}$	$\frac{1}{2}^+$	-1	$\frac{1}{2}$	$(us)c,b$	1^+	$\mathcal{O}'_\mu$
$\Omega_{c,b}$	$\frac{1}{2}^+$	-2	$\frac{1}{2}$	$(ss)c,b$	1^+	$\mathcal{O}_\mu$
$\Sigma^*_{c,b}$	$\frac{3}{2}^+$	0	1	$(uu)c,b$	1^+	$\mathcal{O}_\mu$
$\Xi^*_{c,b}$	$\frac{3}{2}^+$	-1	$\frac{1}{2}$	$(us)c,b$	1^+	$\mathcal{O}'_\mu$
$\Omega^*_{c,b}$	$\frac{3}{2}^+$	-2	$\frac{1}{2}$	$(ss)c,b$	1^+	$\mathcal{O}_\mu$

Table 4.4: Summary of the quantum numbers of the eight baryons containing a single heavy quark. $s_l^{\pi_l}$ is the spin-parity of the light degrees of freedom.

$$\mathcal{O}'_\mu \;=\; \varepsilon_{ABC}\,(q^{A\,T}\mathcal{C}\gamma_\mu q'^{B})\,Q^C\;, \tag{4.7}$$

where A, B, C are colour indices, ε_{ABC} is the totally antisymmetric Levi-Civita tensor, $\mathcal{C}$ is the charge conjugation matrix, q, q' are light quark fields, and Q is the heavy quark field. The spinorial index of the three operators is the uncontracted Dirac index carried by the heavy quark field.

On the lattice, the Euclidean symmetry associated with the orthogonal group $O(4)$ is reduced to symmetry under the hypercubic group. An irreducible representation of $O(4)$ or of its covering group, $SU(2)\otimes SU(2)$, is not necessarily irreducible in the discretised version of the theory [95, 96]. Typically, in an irreducible representation of the hypercubic group different continuum spins are mixed. Then, one should first check that our choice of operators is suitable for the study we want to realize.

The operator $\mathcal{O}_5$ behaves under Lorentz transformations as a Dirac spinor, and $\mathcal{O}_\mu$ and $\mathcal{O}'_\mu$ are the tensor product of a four vector and a Dirac spinor. In the $SU(2)\otimes SU(2)$ notation for the parity extended Lorentz group, $\mathcal{O}_5$ belong to $(\frac{1}{2},0)\oplus(0,\frac{1}{2})$ representation and $\mathcal{O}_\mu$, $\mathcal{O}'_\mu$ transform us $(1,\frac{1}{2})\oplus(\frac{1}{2},1)\oplus(\frac{1}{2},0)\oplus(0,\frac{1}{2})$. Mandula and Shpiz [96] have shown that of the $SU(2)\otimes SU(2)$ double-valued representations, the following ones

$$(\frac{1}{2},0)\;,\;\;(0,\frac{1}{2})\;,\;\;(1,\frac{1}{2})\;,\;\;(\frac{1}{2},1)\;,\;\;(\frac{3}{2},0)\;,\;\;(0,\frac{3}{2})\;, \tag{4.8}$$

are also irreducible under the hypercubic cover group. Furthermore, they computed the full list of continuum spins contributing to each of the above representations of the hypercubic cover group. For the representations of interest in our case, their result is

$$(\tfrac{1}{2},0)_{\text{hypercubic}}\;\;(0,\tfrac{1}{2})_{\text{hypercubic}}\;:\frac{1}{2}\,,\frac{7}{2},\cdots \tag{4.9}$$

$$(1,\tfrac{1}{2})_{\text{hypercubic}}\;\;(\tfrac{1}{2},1)_{\text{hypercubic}}\;:\frac{1}{2}\,,\cdots \tag{4.10}$$

where the dots denotes all half-integral spins higher than the last indicated.

Assuming that higher spin states are heavier, then the large time behaviour of the

lattice two-point correlation function

$$G_5(\vec{p},t) = \sum_{\vec{x}} e^{-i\vec{p}\cdot\vec{x}} \langle \mathcal{O}_5(\vec{x},t)\, \overline{\mathcal{O}}_5(\vec{0},0)\rangle \tag{4.11}$$

is dominated by a spin-1/2 state with three momentum $\vec{p}$.

For the two-point function associated with the operator $\mathcal{O}_\mu$,

$$G_{\mu\nu}(\vec{p},t) = \sum_{\vec{x}} e^{-i\vec{p}\cdot\vec{x}} \langle \mathcal{O}_\mu(\vec{x},t)\, \overline{\mathcal{O}}_\nu(\vec{0},0)\rangle \ , \tag{4.12}$$

the identification of the different spins is more involved. In the continuum, this correlation function has contributions from spin-1/2 and spin-3/2 particles. The separation of the different spins can be made with the help of the spin-projection operators[3] of ref. [97],

$$(P^{3/2})_{\mu\nu}(p) = g_{\mu\nu} - \frac{1}{3}\gamma_\mu\gamma_\nu - \frac{1}{3p^2}(\not{p}\gamma_\mu p_\nu + p_\mu\gamma_\nu \not{p}) \ , \tag{4.13}$$

$$(P_{11}^{1/2})_{\mu\nu}(p) = \frac{1}{3}\gamma_\mu\gamma_\nu - \frac{1}{p^2}p_\mu p_\nu + \frac{1}{3p^2}(\not{p}\gamma_\mu p_\nu + p_\mu\gamma_\nu \not{p}) \ , \tag{4.14}$$

$$(P_{22}^{1/2})_{\mu\nu}(p) = \frac{1}{p^2}p_\mu p_\nu \ , \tag{4.15}$$

$$(P_{12}^{1/2})_{\mu\nu}(p) = \frac{1}{\sqrt{3}p^2}(\, p_\mu p_\nu - \not{p}\gamma_\mu p_\nu \,) \ , \tag{4.16}$$

$$(P_{21}^{1/2})_{\mu\nu}(p) = \frac{1}{\sqrt{3}p^2}(\not{p} p_\mu\gamma_\nu - p_\mu p_\nu \,) \ . \tag{4.17}$$

These projectors are orthonormal and idempotent

$$(P^I_{ij})_{\mu\rho}(p)\,(P^J_{kl})^{\rho\nu}(p) = \delta^{IJ}\,\delta_{jk}\,(P^J_{il})_\mu{}^\nu \ , \tag{4.18}$$

where I, J take the values $1/2$ and $3/2$, and complete

$$g_{\mu\nu} = (P^{3/2})_{\mu\nu}(p) + (P_{11}^{1/2})_{\mu\nu}(p) + (P_{22}^{1/2})_{\mu\nu}(p) \ . \tag{4.19}$$

They satisfy the relations

$$\gamma_\mu(P^{3/2})^\mu_\nu(p) = 0 \ , \tag{4.20}$$

[3]Note that now we are using again the Minkowski space notation.

$$p_\mu (P^{3/2})^{\mu\nu}(p) = (P^{3/2})^{\mu\nu}(p) p_\nu = 0 \ , \tag{4.21}$$

$$p_\mu (P_{1j}^{1/2})^{\mu\nu}(p) = (P_{i1}^{1/2})^{\mu\nu}(p) p_\nu = 0 \quad , i,j = 1,2 \ , \tag{4.22}$$

and the following properties

$$\not{p} (P^{3/2})^{\mu\nu}(p) = (P^{3/2})^{\mu\nu}(p) \not{p} \ , \tag{4.23}$$

$$\not{p} (P_{ij}^{1/2})^{\mu\nu}(p) = \pm (P_{ij}^{1/2})^{\mu\nu}(p) \not{p} \quad , + \text{ for } i = j, - \text{ for } i \neq j \ . \tag{4.24}$$

Using (4.20) - (4.24), it is straightforward to prove that if the spinor $u_\mu(p)$ satisfies the Dirac equation for all values of the Lorentz index μ, then $(P^{3/2})^{\mu\nu}(p)\, u_\nu(p)$ satisfy the Rarita-Schwinger equations [98].

To extract the masses of the spin-1/2 and spin-3/2 particles, one needs to consider only the correlators at zero momentum[4]. In this case, the projectors simplify to

$$(P^{3/2})_{ij}(p) = g_{ij} - \frac{1}{3}\gamma_i \gamma_j \ , \tag{4.25}$$

$$(P_{11}^{1/2})_{ij}(p) = \frac{1}{3}\gamma_i \gamma_j \ , \tag{4.26}$$

with the remaining components vanishing. We define the two-point correlation function for the spin-1/2 particle as

$$G_{\mu\nu}^{(1/2)}(\vec{0},t) = (P_{11}^{1/2})_{\mu\rho}(\vec{0})\, G^\rho{}_\nu(\vec{0},t) \ , \tag{4.27}$$

and the spin-3/2 correlation function by

$$G_{\mu\nu}^{(3/2)}(\vec{0},t) = (P^{3/2})_{\mu\rho}(\vec{0})\, G^\rho_\nu(\vec{0},t) \ . \tag{4.28}$$

The question which we have to answer now is if this spin decomposition survives on the lattice. Again, Mandula and Shpiz [96] were able to prove that the spin-1/2 and spin-3/2 $SU(2)$ representations are also irreducible under the action of the cubic lattice rotation group. Moreover, they computed the continuum spin

[4]The use of the spin-projectors for nonzero momentum is to be done with care. Since each particle has a different mass, their four-momenta are different and the orthogonality of the projectors for the different particles is spoiled. As we will see, at zero momentum the projectors do not depend on the particle mass.

content of the double-valued cubic lattice rotation representations and found

$$(\frac{1}{2})_{\text{cubic}} : \frac{1}{2}, \frac{7}{2}, \cdots \quad (\frac{3}{2})_{\text{cubic}} : \frac{3}{2}, \cdots , \tag{4.29}$$

with the dots denoting all half-integral spins higher than the last indicated.

Once more, as long as the higher spin states are heavier, the lattice Euclidean correlation functions $G_{\mu\nu}^{(1/2)}(\vec{0}, t)$ and $G_{\mu\nu}^{(3/2)}(\vec{0}, t)$ are dominated for large times by spin-parity $\frac{1}{2}^+$ and $\frac{3}{2}^+$ particles at rest, respectively.

The analysis of the correlation functions for the operator $\mathcal{O}'_\mu$ is, in all aspects, similar to the analysis just performed for the operator $\mathcal{O}_\mu$. The results for the correlation functions of the latter operator apply equally to correlation functions of $\mathcal{O}'_\mu$.

In this section, we have defined two-point correlation functions which are directly related to the different physical baryon states. In the following sections, we shall use these correlators to compute the heavy-light baryon spectrum.

4.3 Simulation Details

In our simulation we use 60 $SU(3)$ configurations generated on a $24^3 \times 48$ lattice at $\beta = 6.2$. The configurations were generated by the hybrid over-relaxed algorithm described in [99].

For the quark action we use the $\mathcal{O}(a)$-improved Sheikholeslami-Wohlert (2.54) action with $r = 1$. By adopting this fermionic action, the discretisation errors are reduced from $\mathcal{O}(ma)$ to $\mathcal{O}(\alpha_s ma)$. This feature of the Sheikholeslami-Wohlert action is of particular importance in our study, since the heavy baryon masses we consider are typically between 0.8 and one inverse lattice spacing.

The gauge field configurations and light quark propagators were generated on the 64-node $i860$ Meiko Computing Surface at the University of Edinburgh. The heavy quark propagators were computed on the Cray T3D, presently with 512 nodes, also at Edinburgh.

In order to convert our results into physical units we take the inverse lattice spacing from R_0 [100]. The rationale for using R_0 to compute the inverse lattice

spacing is that all fundamental parameters of the simulation should come from heavy quark data. Our value for the inverse lattice spacing [101],

$$a^{-1} = 2.9 \pm 0.2\,GeV\ , \tag{4.30}$$

is slightly bigger than the number quoted on previous UKQCD publications [99, 102, 71], $a^{-1} = 2.73(5)\,GeV$, but both results are compatible within errors. The agreement between the inverse lattice spacing computed from light quark and from heavy quark data can be seen as a consistency test on the Lattice QCD procedure.

For light quarks we consider two mass values around the strange quark mass. The corresponding hopping parameters are $\kappa = 0.14144$ and 0.14226. Because each baryon contains two light quarks, for each heavy quark mass we can form three baryon correlators, of which two have degenerate light-quark masses and one has non-degenerate light-quark masses. In this way we have a minimum number of combinations for studying the chiral limit.

For the simulation of the heavy quark we take four values of the heavy quark mass around the charm quark mass. The corresponding hopping parameters are $\kappa_Q = 0.133, 0.129,\ 0.125$ and 0.121.

The masses of the light pseudoscalar meson needed for this study were obtained in ref. [71]. Results extrapolated to the chiral limit (corresponding to a hopping parameter $\kappa_{\rm crit} = 0.14315^{+2}_{-2}$) and to the mass of the strange quark($\kappa_s = 0.1419^{+1}_{-1}$) are also tabulated there. The masses of the heavy-light pseudoscalar mesons can be found in ref. [103].

In order to improve the signal for the baryon correlation functions, we use the Jacobi smearing method [104, 105]. The light- and heavy-quark fields were either smeared at the source only (SL) or smeared both at the source and the sink (SS). Smearing is not a Lorentz-invariant operation, and it might alter some of the transformation properties of non-scalar observables. According to the analysis of appendix B for the baryonic propagator, smearing effects are expected to be seen only for nonzero momentum. Since the spectroscopy study is concerned only with zero-momentum propagators, we postpone the discussion of smearing effects to

the next chapter.

4.4 Analysis Details

In section 4.2, we defined the correlation functions used in our study. Here we want to have a closer look at them, with the aim of identifying combinations of components which provide the clearest signal.

For large positive time, the correlation function (4.11) at zero momentum is given by

$$\begin{aligned} G_5(\vec{0},t) &= \frac{Z_\Lambda^2}{2}\left[(1+\gamma_4)e^{-M_\Lambda t} - (1-\gamma_4)e^{-M_\Lambda(T-t)}\right] + \\ &\quad \frac{Z_{\Lambda_{PP}}^2}{2}\left[(1-\gamma_4)e^{-M_{\Lambda_{PP}} t} - (1+\gamma_4)e^{-M_{\Lambda_{PP}}(T-t)}\right], \end{aligned} \tag{4.31}$$

where M_Λ, $M_{\Lambda_{PP}}$ are the masses of the Λ-type particle and its parity partner, Z_Λ ($Z_{\Lambda_{PP}}$) the wave function overlap factor of the Λ-type particle (parity partner) and T is the lattice extension on the time direction. The only nonzero components of (4.31) are the diagonal ones and they satisfy the relations

$$\begin{aligned} [G_5(\vec{0},t)]_{11} &= [G_5(\vec{0},t)]_{22} = -[G_5(\vec{0},T-t)]_{33} = -[G_5(\vec{0},T-t)]_{44} \\ &= Z_\Lambda^2\, e^{-M_\Lambda t} - Z_{\Lambda_{PP}}^2\, e^{-M_{\Lambda_{PP}}(T-t)}\,. \end{aligned} \tag{4.32}$$

A measure of the Λ particle mass and Z_Λ should involve only these components. Then, we define the Λ correlator

$$\begin{aligned} G_\Lambda(t) &= \frac{1}{4}\{[G_5(\vec{0},t)]_{11} + [G_5(\vec{0},t)]_{22} - \\ &\qquad [G_5(\vec{0},T-t)]_{33} - [G_5(\vec{0},T-t)]_{44}\} \\ &= Z_\Lambda^2\, e^{-M_\Lambda t} - Z_{\Lambda_{PP}}^2\, e^{-M_{\Lambda_{PP}}(T-t)}\,, \end{aligned} \tag{4.33}$$

and in the analysis program only (4.33) is considered.

For $t < T/2$, $G_\Lambda(t)$ is dominated by the contribution of the Λ-type particle. Its parity partner, which propagates backwards in time, is responsible for the dominant contribution to (4.33) for $t > T/2$.

In the analysis, we use only the forward part of the lattice, $t < T/2$, where the

contribution of the parity partner can be neglected [5]. Therefore, we assume

$$G_\Lambda(t) \;=\; Z_\Lambda^2\, e^{-M_\Lambda t}\;. \tag{4.34}$$

For each of the correlation functions $G^{(1/2)}_{\mu\nu}(\vec{0},t)$ and $G^{(3/2)}_{\mu\nu}(\vec{0},t)$ it is possible to choose a combination of components that define particle correlators equivalent to (4.34). The procedure is similar to the one used for $G_\Lambda(t)$ and will not be shown here. For completeness, we write the definitions of the Σ correlator,

$$\begin{aligned}
G_\Sigma(t) \;=\; & \frac{1}{12}\sum_{i=1}^{3}\Re\{\,[G^{(1/2)}_{ii}(\vec{0},t)]_{11} + [G^{(1/2)}_{ii}(\vec{0},t)]_{22} - \\
& \qquad [G^{(1/2)}_{ii}(\vec{0},T-t)]_{33} - [G^{(1/2)}_{ii}(\vec{0},T-t)]_{33}\,\} + \\
& \frac{1}{12}\Re\{\,-[G^{(1/2)}_{13}(\vec{0},t)]_{12} + [G^{(1/2)}_{13}(\vec{0},t)]_{21} + \\
& \qquad [G^{(1/2)}_{31}(\vec{0},t)]_{12} - [G^{(1/2)}_{31}(\vec{0},t)]_{21} + \\
& \qquad [G^{(1/2)}_{13}(\vec{0},T-t)]_{34} - [G^{(1/2)}_{13}(\vec{0},T-t)]_{43} - \\
& \qquad [G^{(1/2)}_{31}(\vec{0},T-t)]_{34} + [G^{(1/2)}_{31}(\vec{0},T-t)]_{43}\,\} + \\
& \frac{1}{12}\Im\{\,[G^{(1/2)}_{12}(\vec{0},t)]_{11} - [G^{(1/2)}_{12}(\vec{0},t)]_{22} - \\
& \qquad [G^{(1/2)}_{21}(\vec{0},t)]_{11} + [G^{(1/2)}_{21}(\vec{0},t)]_{22} + \\
& \qquad [G^{(1/2)}_{23}(\vec{0},t)]_{12} + [G^{(1/2)}_{23}(\vec{0},t)]_{21} - \\
& \qquad [G^{(1/2)}_{32}(\vec{0},t)]_{12} - [G^{(1/2)}_{32}(\vec{0},t)]_{21} - \\
& \qquad [G^{(1/2)}_{12}(\vec{0},T-t)]_{33} + [G^{(1/2)}_{12}(\vec{0},T-t)]_{44} + \\
& \qquad [G^{(1/2)}_{21}(\vec{0},T-t)]_{33} - [G^{(1/2)}_{21}(\vec{0},T-t)]_{44} - \\
& \qquad [G^{(1/2)}_{23}(\vec{0},T-t)]_{34} - [G^{(1/2)}_{23}(\vec{0},T-t)]_{43} + \\
& \qquad [G^{(1/2)}_{32}(\vec{0},T-t)]_{34} + [G^{(1/2)}_{32}(\vec{0},T-t)]_{43}\,\} \\
=\; & Z_\Sigma^2\, e^{-M_\Sigma t}\;,
\end{aligned} \tag{4.35}$$

and the Σ^* correlator

$$G_{\Sigma^*}(t) \;=$$

[5] The analysis of the backward part of the lattice, i.e. for $t > T/2$, shows that the amplitude $Z^2_{\Lambda_{PP}}$ is much smaller than Z^2_Λ.

$$
\begin{aligned}
&\frac{1}{24}\sum_{i=1}^{3}\Re\{\,[G_{ii}^{(3/2)}(\vec{0},t)]_{11}+[G_{ii}^{(3/2)}(\vec{0},t)]_{22}- \\
&\qquad [G_{ii}^{(3/2)}(\vec{0},T-t)]_{33}-[G_{ii}^{(3/2)}(\vec{0},T-t)]_{33}\,\}- \\
&\frac{1}{12}\Re\{\,-[G_{13}^{(3/2)}(\vec{0},t)]_{12}+[G_{13}^{(3/2)}(\vec{0},t)]_{21}+ \\
&\qquad [G_{31}^{(3/2)}(\vec{0},t)]_{12}-[G_{31}^{(3/2)}(\vec{0},t)]_{21}+ \\
&\qquad [G_{13}^{(3/2)}(\vec{0},T-t)]_{34}-[G_{13}^{(3/2)}(\vec{0},T-t)]_{43}- \\
&\qquad [G_{31}^{(3/2)}(\vec{0},T-t)]_{34}+[G_{31}^{(3/2)}(\vec{0},T-t)]_{43}\,\}- \\
&\frac{1}{12}\Im\{\,[G_{12}^{(3/2)}(\vec{0},t)]_{11}-[G_{12}^{(3/2)}(\vec{0},t)]_{22}- \\
&\qquad [G_{21}^{(3/2)}(\vec{0},t)]_{11}+[G_{21}^{(3/2)}(\vec{0},t)]_{22}+ \\
&\qquad [G_{23}^{(3/2)}(\vec{0},t)]_{12}+[G_{23}^{(3/2)}(\vec{0},t)]_{21}- \\
&\qquad [G_{32}^{(3/2)}(\vec{0},t)]_{12}-[G_{32}^{(3/2)}(\vec{0},t)]_{21}- \\
&\qquad [G_{12}^{(3/2)}(\vec{0},T-t)]_{33}+[G_{12}^{(3/2)}(\vec{0},T-t)]_{44}+ \\
&\qquad [G_{21}^{(3/2)}(\vec{0},T-t)]_{33}-[G_{21}^{(3/2)}(\vec{0},T-t)]_{44}- \\
&\qquad [G_{23}^{(3/2)}(\vec{0},T-t)]_{34}-[G_{23}^{(3/2)}(\vec{0},T-t)]_{43}+ \\
&\qquad [G_{32}^{(3/2)}(\vec{0},T-t)]_{34}+[G_{32}^{(3/2)}(\vec{0},T-t)]_{43}\,\} \\
=\;& Z_{\Sigma^*}^2\, e^{-M_{\Sigma^*}t}\,. \qquad (4.36)
\end{aligned}
$$

4.4.1 The Effective Mass

The correlators (4.34), (4.35) and (4.36) are all of the type

$$c(t) = Z^2\, e^{-Mt}\,, \qquad (4.37)$$

wher Z is the wave function overlap factor and M the particle mass. This expression is valid only for large values of t. For small t, the contributions from excited states are sizeable and the correct functional form for $c(t)$ is a sum of exponentials. To check if the correlator is saturated by the ground state, we look for a plateau in the effective mass,

$$M_{eff}(t) = \ln\frac{c(t)}{c(t+1)}\,. \qquad (4.38)$$

The analysis of $M_{eff}(t)$ also gives an idea of the time interval that should be used to fit the lattice data.

4.4.2 Fitting Procedure

Given a set of data points, we need a measure which indicates how a particular theoretical model describes the data.

In a least-χ^2 fitting, the χ^2 function is minimised with respect to the parameters of the theoretical model, and the value of the χ^2 function, at the minimum, is used to evaluate how the model fits the data points.

For each correlator, the mass and Z factor were computed from a least-χ^2 fitting of the lattice data to the functional form (4.37). The χ^2 was minimised using the Levenberg-Marquardt method - see [106] for an explanation of the method.

In the definition of the χ^2 function,

$$\chi^2(Z,m) = \sum_{t_i=t_{min}}^{t_{max}} \sum_{t_f=t_{min}}^{t_{max}} \delta C(t_i;Z,m)\, Corr^{-1}(t_i,t_f)\, \delta C(t_f;Z,m) \ , \qquad (4.39)$$

we take into account possible statistical correlations of the lattice data between the different time-slices. In (4.39)

$$\delta C(t;Z,m) = \frac{1}{\sigma(t)}[\overline{c}(t) - C_{fit}(t;Z,m)] \ , \qquad (4.40)$$

$$\overline{c}(t) = \frac{1}{N}\sum_{n=1}^{N} c^{(n)}(t) \ , \qquad (4.41)$$

$c^{(n)}(t), n = 1 \cdots N$ are the correlators evaluated for each of the N configurations, $C_{fit}(t;Z,m)$ is the theoretical functional form (4.37) and $\sigma(t)$ is the Jackknife estimate of the error on $\overline{c}(t)$. The time-slices t_{min} and t_{max} define the fitting range used to match the data to a single exponential function.

The statistical correlations between the different time-slices are measured by the correlation matrix $Corr(t_i,t_f)$. This matrix is defined in terms of the covariance matrix,

$$Cov(t_i,t_j) = \frac{1}{N(N-1)}\sum_{n=1}^{N}[c^{(n)}(t_i) - \overline{c}(t_i)][c^{(n)}(t_f) - \overline{c}(t_f)] \ , \qquad (4.42)$$

a generalisation of the variance for a correlated data set, as

$$Corr(t_i, t_f) = \frac{Cov(t_i, t_j)}{\sigma(t_i)\sigma(t_f)} . \tag{4.43}$$

By definition, $Corr$ has 1 on its diagonal and numbers between 0 and 1 elsewhere. A strongly correlated data set has nondiagonal elements close to 1, whereas for a set of uncorrelated data the nondiagonal elements of $Corr$ are zero.

In an ideal situation, where the data points follow the theoretical description, the value of χ^2 at the minimum should be equal to the number of degrees of freedom ($d.o.f$). The number of $d.o.f$ is the number of fitted data points, i.e. the number of time-slices used in the fit, minus the number of fitted parameters. A value of $\chi^2/d.o.f$ much bigger than 1 indicates that either the model does not provide a good description of the data points or the errors on the data were underestimated. On the other hand, a value of $\chi^2/d.o.f$ much smaller than 1 is a sign that the errors on the data were overestimated or that the correlations between the time-slices were underestimated.

4.4.3 Determination of the Fitting Range

In order to choose a fitting range, we fit the correlators to a single exponential in the range $[t_{min}, t_{max}]$. The upper limit of the interval is taken from the analysis of the effective mass plot, and t_{min} is computed from a sliding window analysis, where t_{max} is keep fixed. We choose t_{min} as the lowest value for which the $\chi^2/d.o.f$ is reasonably close to 1, and the fitted parameters are stable against variations of t_{min}.

4.4.4 Statistical Errors

The statistical errors were computed by the bootstrap method - see [107] for the description of the method. All quoted statistical errors correspond to 68% confidence limits of the distribution obtained from 1000 bootstrap samples.

4.5 Heavy Baryon Masses

The calculation of the heavy baryon spectrum is performed by fitting the correlators (4.34), (4.35) and (4.36) to the functional form (4.37). For each of the

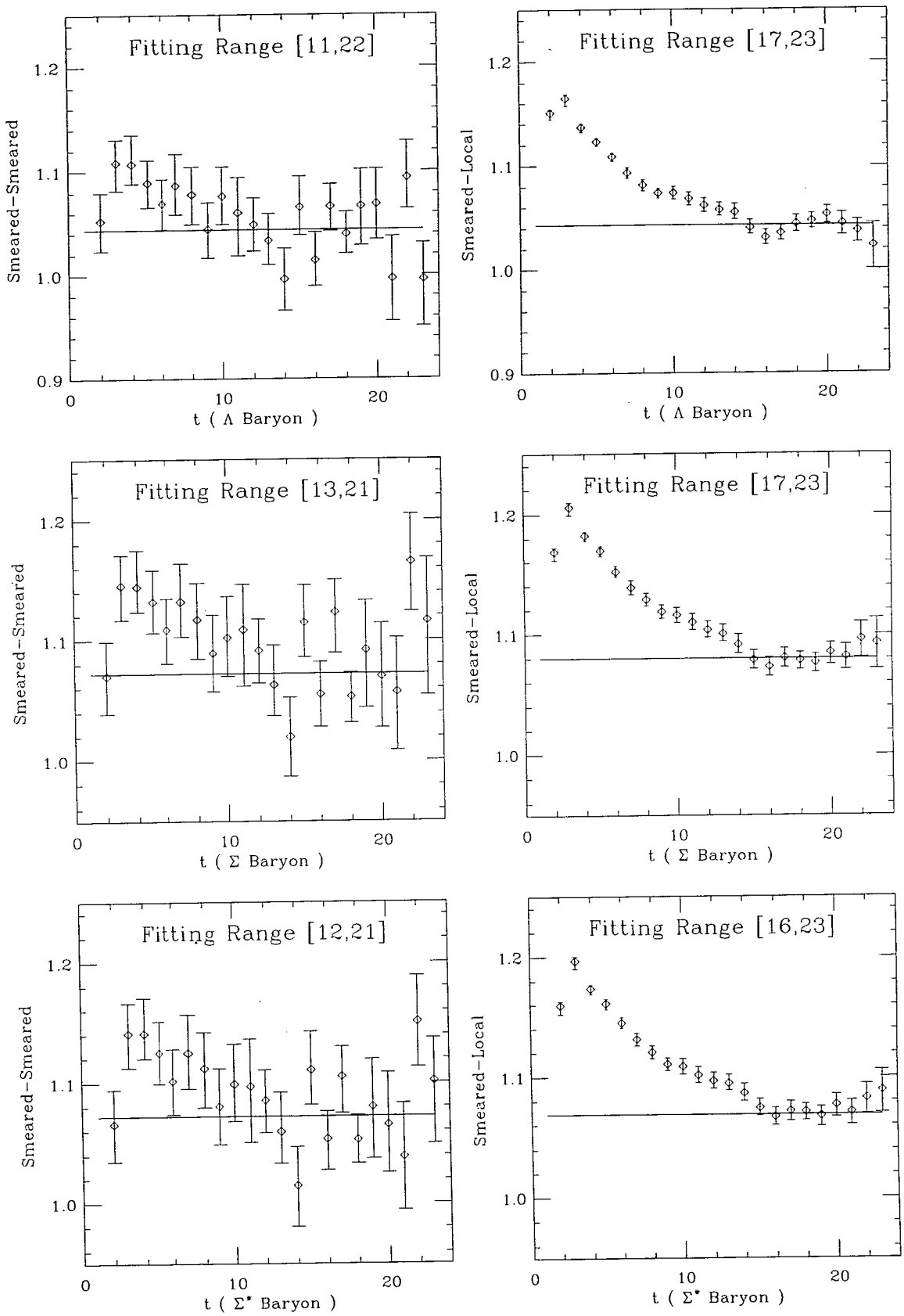

Figure 4.1: Effective masses for the Λ, Σ and Σ^* baryons for $\kappa_h = 0.125$ and $\kappa_{l_1} = \kappa_{l_2} = 0.14144$. The straight lines are the results of our best fits.

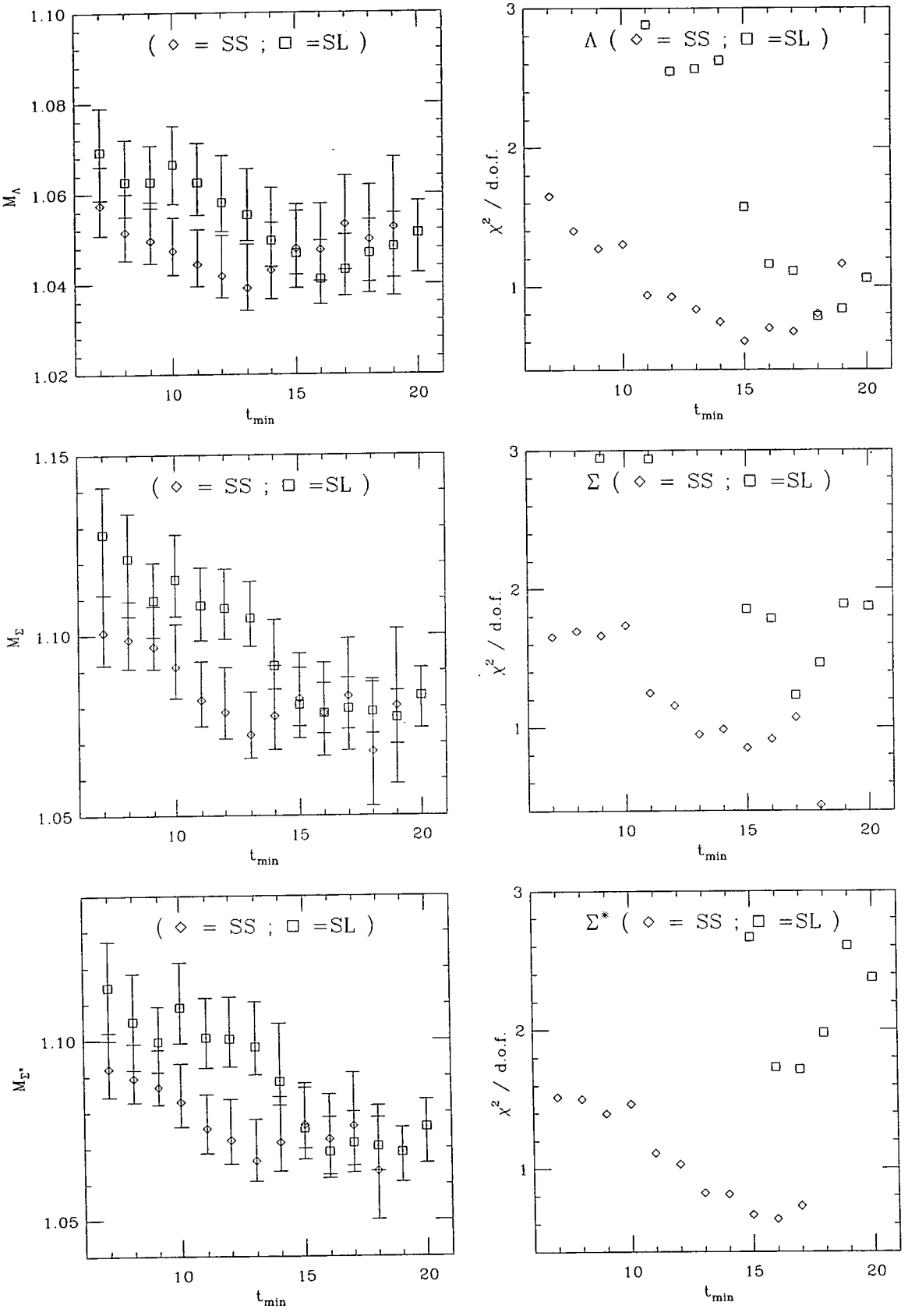

Figure 4.2: Masses and $\chi^2/d.o.f$ obtained from a sliding window analysis for the Λ, Σ and Σ^* baryons. t_{max} is defined from the effective mass plots.

$(\kappa_{l_1}, \kappa_{l_2})$	$\kappa_h = 0.121$	$\kappa_h = 0.125$	$\kappa_h = 0.129$	$\kappa_h = 0.133$
Λ Correlator				
(0.14144, 0.14144)				
SS correlators	[11, 22]	[11, 22]	[11, 22]	[11, 22]
SL correlators	[17, 23]	[17, 23]	[16, 23]	[16, 23]
(0.14144, 0.14226)				
SS correlators	[11, 22]	[9, 22]	[9, 22]	[10, 22]
SL correlators	[17, 23]	[17, 23]	[16, 23]	[16, 23]
(0.14226, 0.14226)				
SS correlators	[10, 22]	[10, 22]	[9, 22]	[9, 22]
SL correlators	[17, 23]	[17, 23]	[17, 23]	[17, 23]
Σ Correlator				
(0.14144, 0.14144)				
SS correlators	[13, 21]	[13, 21]	[13, 21]	[13, 21]
SL correlators	[17, 23]	[17, 23]	[17, 23]	[17, 23]
(0.14144, 0.14226)				
SS correlators	[12, 21]	[12, 21]	[12, 21]	[12, 21]
SL correlators	[17, 23]	[17, 23]	[17, 23]	[17, 23]
(0.14226, 0.14226)				
SS correlators	[13, 21]	[13, 21]	[13, 21]	[12, 21]
SL correlators	[17, 23]	[17, 23]	[17, 23]	[16, 23]
Σ^* Correlator				
(0.14144, 0.14144)				
SS correlators	[12, 21]	[12, 21]	[12, 21]	[12, 21]
SL correlators	[17, 23]	[16, 23]	[16, 23]	[16, 23]
(0.14144, 0.14226)				
SS correlators	[11, 21]	[11, 21]	[11, 21]	[11, 21]
SL correlators	[17, 23]	[17, 23]	[17, 23]	[16, 23]
(0.14226, 0.14226)				
SS correlators	[11, 21]	[11, 21]	[11, 21]	[11, 21]
SL correlators	[17, 23]	[16, 23]	[16, 23]	[15, 23]

Table 4.5: Fitting range for the different particle correlators.

$(\kappa_{light}, \kappa_{light}, \kappa_{heavy})$ combinations, both for SL and SS correlators, and for each type of particle correlator, the choice of the fitting range was made according to the procedure described in 4.4.3.

As an example, in figure 4.1 we show effective mass plots for the Λ, Σ and Σ^* baryons, using either SL or SS correlators, for degenerate light quarks, $\kappa_{light} = 0.14144$, and $\kappa_{heavy} = 0.125$. The analysis of these plots together with fig. 4.2 shows

i) that for all graphs a plateau can be identified. The extent of the plateau is smaller for SL data, when compared with SS data. This behaviour supports the hypothesis that by smearing both at the sink and at the source, the overlap with the ground-state is increased.

ii) The signal for the effective mass becomes noisy when t is close to half of the lattice time extension. Our criterion for choosing the upper limit of the fitting range, t_{max}, is based on an empirical recognition of a large noise/signal ratio when t is close to $T/2$. We take $t_{max} = 22, 21, 21$ for the Λ, Σ, Σ^* particles (SS data) and $t_{max} = 23$ for all particles in the case of SL data.

The behaviour of the effective mass for the remaining κ combinations show a similar pattern to the one just described.

In Figure 4.2 we present the results of the sliding window analysis for the same κ combination and both types of correlators. Considering the $\chi^2/d.o.f.$ of the fits, as well the stability of the results under variation of t_{min}, we make the following observations

i) the masses obtained from the fits to the SS correlators are stable and the $\chi^2/d.o.f.$ is acceptable for $t_{min} \geq 11$ ($t_{min} \geq 15$ for SL data).

ii) The masses obtained from fitting SL correlators and SS correlators agree for $t_{min} \geq 15$.

We define t_{min} from the interval in which the fitted mass is stable, taking the smallest value for which the $\chi^2/d.o.f.$ is acceptable. Our choice is $t_{min} = 11$, 13,

12 for the Λ, Σ, Σ^* particles when using SS correlators and t_{min} = 17, 17, 16 for the Λ, Σ, Σ^* particles and SL data. The observations drawn for this particular κ combination are naturally extended to the data not shown here.

In table 4.5 we report the fitting ranges used for all baryons, all κ combinations and for both types of data.

In appendix C, we give the values of the fitted masses and $\chi^2/d.o.f$ for all particles. The overall picture which emerges from the fits is :

- The plateau from the SS data is longer than the plateau from the corresponding SL data. Typically, the fitting range for SS correlators contains 10 time-slices, being smaller for SL data ($\sim$ 7 time-slices).
- The results from fitting the SL and SS data agree within errors.
- The statistical errors show no dependence on the heavy-quark mass, but increase slightly for lighter-quark masses.
- For the Λ particle, the SS data gives smaller statistical errors for the mass values. This is not a general trend of the data, as for Σ and Σ^* the smaller errors are obtained from SL data. The analysis of the wave function overlap factors confirms this observation.

  A possible explanation for this behaviour could come from the type of smearing functions used. In the Σ and Σ^* particles, the light degrees of freedom have spin-parity 1^+, whereas for the Λ they are in a state with $J^P = 0^+$. The smearing functions are S waves and this may make the overlap of the interpolating operators with the light sector of the baryon for Σ and Σ^* particles non-optimal. From the effective mass plots, we conclude that for the Σ and Σ^*, smearing the quark fields both at the source and at the sink increases the overlap with the ground state. However, it seems that by smearing states with spin 1, both at the sink and the source, with S waves the noise increases when compared with smearing only at the source. For the Λ particle, naively, one expects an increase of the overlap and a reduction of the noise.

  This different statistical behaviour disappears after extrapolations in the

light and heavy quark mass. Then, the SS data shows the smallest statistical errors.

Despite the good agreement between SL and SS data, to build confidence in the results, in all our studies we always consider both types of data. However, the numbers which will be quoted are those with smaller statistical errors.

4.6 Mass Extrapolations

The correlators used in our simulation were computed with quark masses that do not correspond to their physical values. To obtain the masses of the eight charm and b-baryons, the results discussed in the previous section have to be extrapolated to physical quark masses. We first do the extrapolation in the light quark mass and then in the heavy quark mass.

4.6.1 Extrapolation in the Light Quark Mass

For each heavy quark mass, three correlators with different light contents were computed, two degenerate combinations ($\kappa_{l_1} = \kappa_{l_2} = 0.14144$ or 0.14226) and one non-degenerate ($\kappa_{l_1} = 0.14144$, $\kappa_{l_2} = 0.14226$). For the extrapolation in the light quark mass we assume a linear dependence of M_{baryon} with the quark mass. Furthermore, because we are limited to two light-quark masses, we have to assume exact $SU(3)$-flavour, i.e.

$$\begin{aligned} M_{baryon}(\kappa_{l_1}, \kappa_{l_2}, \kappa_h) &= M_{baryon}(\kappa_h) + A\left(\frac{1}{2\kappa_{l_1}} + \frac{1}{2\kappa_{l_2}} - \frac{1}{\kappa_{crit}}\right) \\ &= M_{baryon}(\kappa_h) + A\left(\frac{1}{\kappa_{eff}} - \frac{1}{\kappa_{crit}}\right), \end{aligned} \tag{4.44}$$

where $\kappa_{eff}^{-1} = (\kappa_{l_1}^{-1} + \kappa_{l_2}^{-1})/2$, κ_l is the light quark hopping parameter, κ_h is the hopping parameter for the heavy quark and $M_{baryon}(\kappa_h)$ is the chirally extrapolated baryon mass.

For each particle, the value of κ_{eff}^{-1} is fixed by its light quark content - see table 4.4. The mass of Λ_h is given by extrapolating the Λ correlator data to $\kappa_{l_1} = \kappa_{l_2} = \kappa_{crit}$. By extrapolating κ_{l_1} to κ_{crit} and interpolating κ_{l_2} to κ_s we compute the mass of Ξ_h. Similarly, from the Σ (Σ^*) correlator we extract the mass of Σ_h (Σ_h^*), Ξ_h' (Ξ_h^*). The masses of Ω_h and Ω_h^* are computed by interpolating the Σ and Σ^* correlator

data to $\kappa_{l_1} = \kappa_{l_2} = \kappa_s$.

κ_h		$\chi^2/d.o.f.$	$chiral/chiral$	$Strange/Strange$	$chiral/strange$
0.121	SS	0.26	$1.022 \pm^{14}_{9}$	$1.111 \pm^{8}_{5}$	$1.066 \pm^{11}_{7}$
	SL	0.05	$1.004 \pm^{19}_{12}$	$1.104 \pm^{9}_{7}$	$1.054 \pm^{14}_{10}$
0.125	SS	0.76	$0.922 \pm^{16}_{9}$	$1.011 \pm^{9}_{5}$	$0.967 \pm^{12}_{6}$
	SS	0.20	$0.905 \pm^{18}_{12}$	$1.005 \pm^{10}_{7}$	$0.955 \pm^{14}_{10}$
0.129	SS	1.11	$0.813 \pm^{17}_{9}$	$0.907 \pm^{9}_{4}$	$0.860 \pm^{12}_{6}$
	SL	0.01	$0.803 \pm^{19}_{12}$	$0.901 \pm^{10}_{7}$	$0.852 \pm^{14}_{10}$
0.133	SS	0.04	$0.710 \pm^{21}_{8}$	$0.799 \pm^{9}_{4}$	$0.754 \pm^{14}_{5}$
	SL	0.06	$0.694 \pm^{19}_{13}$	$0.792 \pm^{10}_{7}$	$0.743 \pm^{14}_{10}$

Table 4.6: Extrapolations in light quark mass - Λ correlator.

κ_h		$\chi^2/d.o.f.$	$chiral/chiral$	$Strange/Strange$	$chiral/strange$
0.121	SS	0.48	$1.073 \pm^{23}_{14}$	$1.145 \pm^{15}_{7}$	$1.109 \pm^{18}_{10}$
	SL	0.17	$1.065 \pm^{19}_{15}$	$1.146 \pm^{11}_{8}$	$1.105 \pm^{15}_{11}$
0.125	SS	0.51	$0.973 \pm^{22}_{13}$	$1.046 \pm^{14}_{7}$	$1.010 \pm^{18}_{10}$
	SL	0.10	$0.967 \pm^{19}_{14}$	$1.049 \pm^{11}_{7}$	$1.008 \pm^{15}_{10}$
0.129	SS	0.55	$0.868 \pm^{21}_{13}$	$0.944 \pm^{14}_{7}$	$0.906 \pm^{18}_{9}$
	SL	0.04	$0.864 \pm^{21}_{14}$	$0.947 \pm^{11}_{7}$	$0.906 \pm^{15}_{10}$
0.133	SS	0.38	$0.762 \pm^{24}_{15}$	$0.836 \pm^{14}_{7}$	$0.799 \pm^{18}_{11}$
	SL	1.01	$0.748 \pm^{22}_{11}$	$0.836 \pm^{11}_{6}$	$0.792 \pm^{16}_{9}$

Table 4.7: Extrapolations in light quark mass - Σ correlator.

In figure 4.3 and in tables 4.6, 4.7 and 4.8 we summarise the results of the chiral extrapolations.

The results from the fits seem to support a linear dependence of the baryon mass on the light quark mass. Concerning the statistical errors, the general trend described in section 4.5 is reproduced here, with the SS data giving smaller errors for the Λ type particles, and the SL data producing smaller errors for the other particle types. The analysis of the $\chi^2/d.o.f.$ suggests that the SS data is better described by (4.44) than the SL data. Finally, we note the good agreement between the results coming from the two types of data.

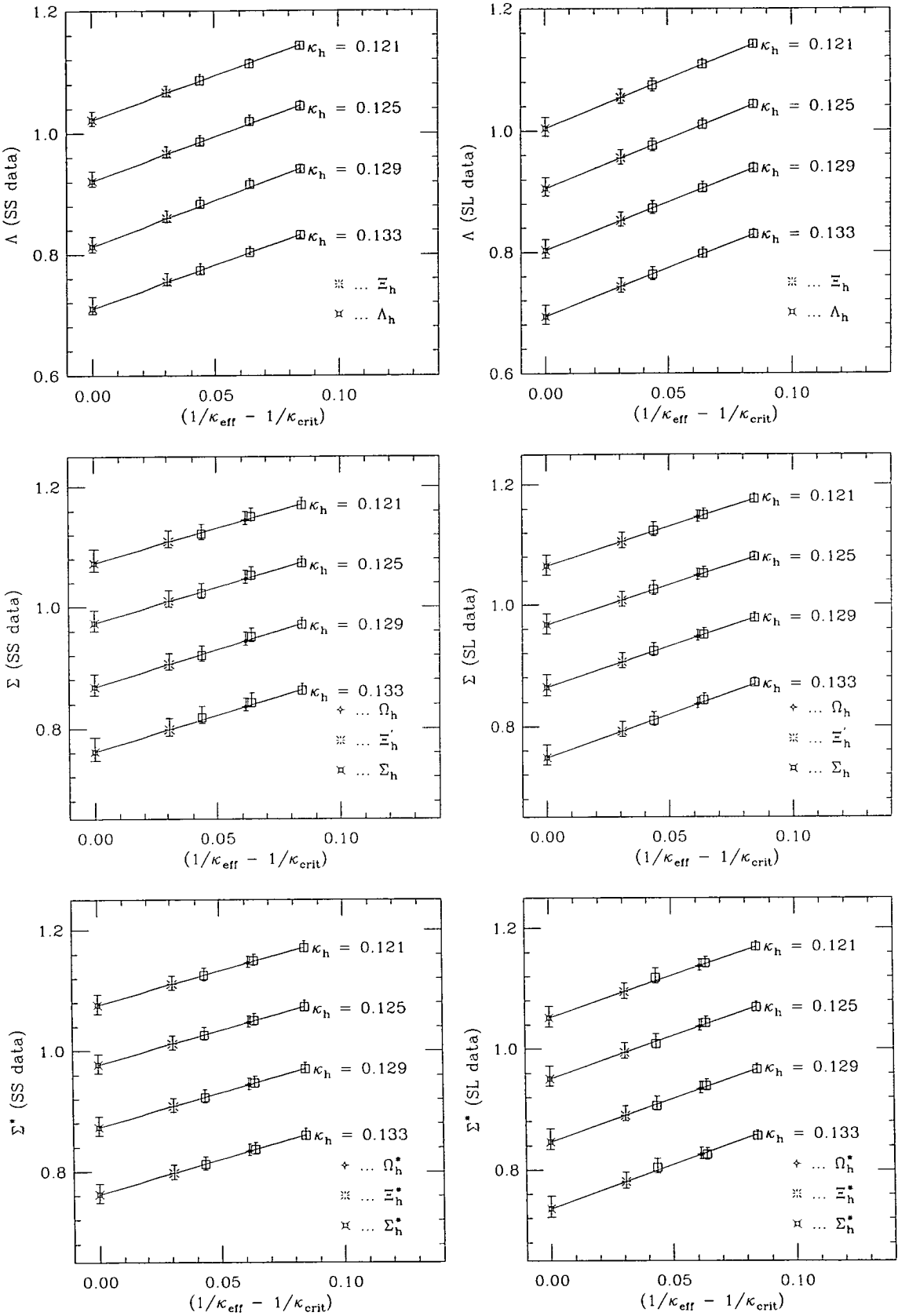

Figure 4.3: Chiral behaviour of the Λ, Σ and Σ^* masses.

κ_h		$\chi^2/d.o.f.$	*chiral/chiral*	*Strange/Strange*	*chiral/strange*
0.121	SS	0.21	$1.076 \pm^{17}_{14}$	$1.145 \pm^{11}_{8}$	$1.110 \pm^{14}_{10}$
	SL	1.00	$1.052 \pm^{19}_{15}$	$1.137 \pm^{11}_{8}$	$1.095 \pm^{15}_{11}$
0.125	SS	0.18	$0.977 \pm^{17}_{14}$	$1.047 \pm^{11}_{8}$	$1.012 \pm^{14}_{10}$
	SL	1.03	$0.950 \pm^{22}_{12}$	$1.038 \pm^{12}_{7}$	$0.994 \pm^{16}_{9}$
0.129	SS	0.16	$0.873 \pm^{18}_{14}$	$0.944 \pm^{11}_{8}$	$0.908 \pm^{13}_{10}$
	SL	0.59	$0.846 \pm^{22}_{12}$	$0.934 \pm^{12}_{7}$	$0.890 \pm^{16}_{9}$
0.133	SS	0.16	$0.762 \pm^{18}_{14}$	$0.834 \pm^{11}_{8}$	$0.798 \pm^{13}_{10}$
	SL	1.90	$0.736 \pm^{21}_{14}$	$0.825 \pm^{12}_{7}$	$0.781 \pm^{16}_{10}$

Table 4.8: Extrapolations in light quark mass - Σ^* correlator.

4.6.2 Heavy Quark Extrapolation

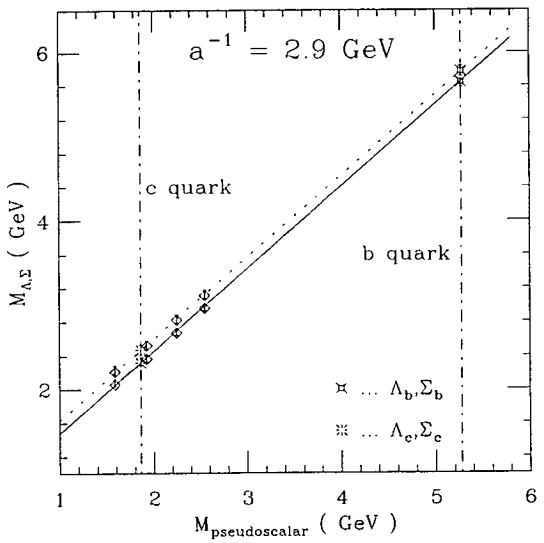

Figure 4.4: Heavy quark extrapolations for Λ (solid line) and Σ (dash line) particles. The figure also shows the results of the best fit including $1/M_Q$ corrections.

The physical masses of the charmed and b-baryons are obtained by extrapolating the four data sets $\kappa_h = 0.121$, 0.125, 0.129 and 0.133. For the extrapolation to the physical heavy quark mass we use HQET as a guide.

In the context of Heavy Quark Effective Theory, any physical quantity can be expanded in inverse powers of the heavy quark mass, M_Q. For example, the

baryon mass can written as

$$M_{Baryon}(M_Q) = M_Q + \overline{\Lambda} + \frac{A_1}{M_Q} + \frac{A_2}{M_Q^2} + \cdots \tag{4.45}$$

Similarly, the mass of a heavy-light meson is given by

$$M_{Meson}(M_Q) = M_Q + \overline{\Lambda}' + \frac{A_1'}{M_Q} + \frac{A_2'}{M_Q^2} + \cdots \tag{4.46}$$

The latter expression can be inverted and the result used in (4.45) to eliminate M_Q. In this way, we achieve to express M_{Baryon} only in terms of the heavy-light meson mass. After rearranging the series,

$$\begin{aligned} M_{Baryon}(M_{Meson}) &= M_{Baryon}(M_0) + (M_{Meson} - M_0) \\ &+ d_1 \left(\frac{1}{M_{Meson}} - \frac{1}{M_0}\right) \\ &+ d_2 \left(\frac{1}{M_{Meson}^2} - \frac{1}{M_0^2}\right) \\ &+ \cdots , \end{aligned} \tag{4.47}$$

where $M_{Baryon}(M)$ is the mass of the heavy baryon at the meson mass M. In the extrapolation in heavy quark mass, we use the chirally extrapolated heavy-light pseudoscalar meson mass[6] to define M_0. The masses of the charm and b-baryons are obtained for $M_0 = M_D$ and $M_0 = M_B$, respectively, and assuming[7] $a^{-1} = 2.9\, GeV$.

In order to study the dependence on the heavy quark mass, we consider several functional forms,

$$M_{Baryon}(M_{Meson}) = M_{Baryon} + d_0 (M_{Meson} - M_0) , \tag{4.48}$$

$$\begin{aligned} M_{Baryon}(M_{Meson}) &= M_{Baryon} + d_0 (M_{Meson} - M_0) + \\ &\quad d_1 \left(\frac{1}{M_{Meson}} - \frac{1}{M_0}\right) , \end{aligned} \tag{4.49}$$

$$M_{Baryon}(M_{Meson}) = M_{Baryon} + (M_{Meson} - M_0) +$$

[6]The meson mass was computed by fitting the meson correlators in the range $t \in [12, 21]$, as in [103]. Then, chiral extrapolation, assuming a linear dependence of the meson mass on the light quark mass was performed.

[7]In this section, we only report statistical errors. In the last section of this chapter, we include an estimate of the error from the lattice spacing.

$$d_1\left(\frac{1}{M_{Meson}} - \frac{1}{M_0}\right), \tag{4.50}$$

$$\begin{aligned} M_{Baryon}(M_{Meson}) &= M_{Baryon} + (M_{Meson} - M_0) + \\ & d_1\left(\frac{1}{M_{Meson}} - \frac{1}{M_0}\right) + \\ & d_2\left(\frac{1}{M_M^2} - \frac{1}{M_0^2}\right), \end{aligned} \tag{4.51}$$

all motivated by HQET. From the analysis of the results from the fits to (4.48)-(4.51), one can test the validity of HQET as a theoretical tool to investigate heavy baryons.

In the heavy quark extrapolation, the fits to any of the theoretical formulae (4.48)-(4.51) have to use both meson and baryon masses. The correlators for the pseudoscalar mesons were computed by smearing only the heavy quark. They have a different smearing than the baryon correlators and, consequently, different statistical correlations between time slices. In principle, the fits do a correct evaluation of these correlations. However, because the baryon and meson masses came from correlators with different smearing, we choose to set the correlation matrix to one. This correlation matrix was used in all heavy extrapolations[8]

By considering the analysis of the results of the fits we make the following observations :

- The fits always show low values for the $\chi^2/d.o.f.$, typically around 0.3 or smaller. Moreover, the results from using the different functional forms agree within one standard deviation.
- The results for d_0 from fitting to (4.48) are compatible with 1 within less than 1.5 standard deviations. However, when the $1/M_Q$ corrections are included, (4.49), d_0 becomes 1 or compatible with this value to less than one standard deviation. d_1 is nonzero within 3 standard deviations. This seems to confirm that heavy quark symmetry is very well satisfied here, and that the $1/M_Q$ terms play an important role for heavy baryons.
- Due to the limited statistics we have, our results are not sensitive to $1/M_Q^2$

[8]In an uncorrelated fit the $\chi^2/d.o.f.$ is underestimated. However, it still provides an idea of the goodness of the fit.

corrections. The fits to (4.51) always give d_2 compatible with zero. The analysis of the central values seems to suggest that the contribution of higher-order terms in the $1/M_Q$ expansion decreases with order.

- As far as the particle masses are concerned, the difference arising from using one of the above expressions only shows up in the statistical error. The charm baryons are obtained by interpolating our data, and the statistical errors are independent of the type of fitting function. On the other hand, for b-baryons the statistical errors are very sensitive to the fitting function. The smallest errors were found from fitting (4.50); the fit to (4.51) produced the largest statistical errors.

Furthermore, the final numbers obtained from using SS and SL correlators agree within statistical errors.

Our conclusion is that HQET seems to hold for heavy baryons. Concerning the $1/M_Q$ effects, the data suggests that they play an important role here. However their contribution to M_{baryon} is small. This conclusion is also supported by the analysis of the mass splittings. The stability of the fitting results against the different modelling functions gives us further confidence on the procedure devised to compute the baryon spectrum.

In table 4.9 we report the results for hadron masses in physical units, from fitting to (4.50). Only statistical errors are quoted there. As an example, in figure 4.4 we show the heavy quark extrapolations for the Λ and Σ particles.

4.7 Calculation of Mass Splittings

The mass splittings are interesting quantities to compute because they are probes of the details of the quark dynamics. Thus, they provide important tests of the theoretical description of strong interactions.

The mass splittings are small quantities when compared with the baryon masses themselves. On the lattice, they are difficult to measure because they are affected by relatively large statistical errors.

To achieve a better control in the determination of the mass splittings we study both ratios of correlators and the difference of the masses from fits to a single

Baryon	Quark Content	charm baryons Exp. (GeV)	charm baryons Latt. (GeV)	b-baryons Exp. (GeV)	b-baryons Latt. (GeV)
Λ_Q	$(ud)Q$	2.285(1)	$2.31 \pm \frac{5}{3}$	5.641(50)	$5.64 \pm \frac{4}{7}$
Ξ_Q	$(us)Q$	2.468(4)	$2.44 \pm \frac{3}{3}$		$5.77 \pm \frac{3}{6}$
Σ_Q	$(uu)Q$	2.453(1)	$2.46 \pm \frac{6}{5}$	5.814(60)	$5.79 \pm \frac{7}{7}$
Σ_Q^*	$(uu)Q$	2.530(7)	$2.47 \pm \frac{4}{4}$	5.870(60)	$5.80 \pm \frac{5}{7}$
Ξ_Q'	$(us)Q$		$2.57 \pm \frac{5}{4}$		$5.89 \pm \frac{5}{6}$
Ξ_Q^*	$(us)Q$	2.643(2)	$2.57 \pm \frac{3}{4}$		$5.90 \pm \frac{3}{4}$
Ω_Q	$(ss)Q$	2.704(20)	$2.68 \pm \frac{4}{3}$		$5.99 \pm \frac{4}{5}$
Ω_Q^*	$(ss)Q$		$2.67 \pm \frac{3}{3}$		$6.00 \pm \frac{3}{5}$

Table 4.9: Heavy baryon masses. Our results are quoted with statistical errors only. Where available, we report the experimental data.

exponential[9], and look for consistency between the two different ways of extracting the mass splittings within the SS and SL data.

4.7.1 The Λ-Pseudoscalar Meson Mass Splitting

In the calculation of the heavy baryon spectrum, we use the pseudoscalar meson to fix the value of the heavy quark hopping parameter. The determination of the Λ-Pseudoscalar meson mass splitting is a test of our procedure. Furthermore, since the splitting has been very precisely measured experimentally, especially in the charm sector, it is an interesting quantity per se.

There are already several lattice studies which computed the Λ-Pseudoscalar meson mass splitting. In [108, 109, 110] the static approximation was used to describe the heavy quark, whereas in [42] the splitting was computed with Wilson fermions. Also, the Λ-Pseudoscalar meson mass splitting have been investigated using NRQCD simulations on the lattice [111]. However, none of these investigations used a fully relativistic improved fermionic action to describe the heavy quark.

The determination of this splitting needs the correlation functions for the heavy-light pseudoscalar meson. These functions, with an additional light quark mass $\kappa_l = 0.14262$, were computed in a previous study [103]. They were evaluated using local light quark propagators and smeared heavy propagators. Therefore, the meson and baryon correlation functions have different statistical correlations between the time-slices, and taking ratios of baryon and meson correlators does not suppress the statistical correlations. Besides, if we use the ratio method in the chiral extrapolation, we are limited to using only the two degenerate light-quark combinations which give poor control of the extrapolation.

In order to avoid the problems just mentioned, we compute the Λ-Pseudoscalar meson mass splitting by taking the differences between the chirally extrapolated baryon and mesons masses. In table 4.10 we report the chirally extrapolated mass differences in lattice units. We stress the good agreement between the two sets of data and note that the mass differences computed from SL data have bigger

[9]The determination of the Λ-Pseudoscalar meson splitting is the only exception. For reasons seen below, we consider only mass differences.

	$\kappa_Q = 0.121$	$\kappa_Q = 0.125$	$\kappa_Q = 0.129$	$\kappa_Q = 0.133$
SS	$0.14 \pm^{1}_{1}$	$0.15 \pm^{1}_{1}$	$0.15 \pm^{2}_{1}$	$0.16 \pm^{2}_{1}$
SL	$0.12 \pm^{2}_{2}$	$0.13 \pm^{2}_{2}$	$0.14 \pm^{2}_{2}$	$0.15 \pm^{2}_{2}$

Table 4.10: $M_\Lambda - M_{pseudo}$ obtained from the difference of chirally extrapolated fitted masses.

statistical errors. From now on we will report only results from SS correlators.

The dependence of the mass difference on the heavy quark mass was studied in a similar way to the dependence of the baryon mass. We fit the mass differences to the following functional forms suggested by HQET

$$\Delta M_{Baryon}(M_{Meson}) = \Delta M_{Baryon} + d_0(M_{Meson} - M_0) , \quad (4.52)$$

$$\Delta M_{Baryon}(M_{Meson}) = \Delta M_{Baryon} + d_1(\frac{1}{M_{Meson}} - \frac{1}{M_0}) , \quad (4.53)$$

$$\Delta M_{Baryon}(M_{Meson}) = \Delta M_{Baryon} + d_1(\frac{1}{M_{Meson}} - \frac{1}{M_0}) + d_2(\frac{1}{M^2_{Meson}} - \frac{1}{M^2_0}) , \quad (4.54)$$

where ΔM is the mass difference at the scale M_0. From the results of the fits, we make the following observations

- The $\chi^2/d.o.f$ of the fits is always below 0.24. This seems to indicate that the expansion suggested by HQET reproduces well the data in our simulation.
- For expression (4.52), d_0 is not zero but is compatible with zero within two to three standard deviations. If (4.54) is used to fit the data, the central value for d_2 is one order of magnitude smaller than d_1. However, the statistical errors on both coefficients are of the same order as their central values.
- The results from the fits to (4.53) and (4.54) are compatible within errors. If (4.52) is used to describe the data, the results are compatible with the

other functional forms within 1.5 standard deviations.

- As in the study of the heavy baryon mass, the results of using SL or SS data agree within errors, with the SS data giving the smaller statistical errors. The final numbers at the charm quark mass are stable against changing the fitting function. For the b quark mass, the statistical errors show dependence on the functional form, with (4.53) giving the smallest statistical errors and (4.54) the biggest errors.

Again, the conclusion is that HQET seems to be very well satisfied here. Moreover, the insensitivity of the results to the different modelling functions strengthens our confidence in the results.

In table 4.11 we report the mass splittings obtained from SS data. Figure 4.5 illustrates the data for the heavy extrapolation. Once more, we stress the good agreement with the experimental result.

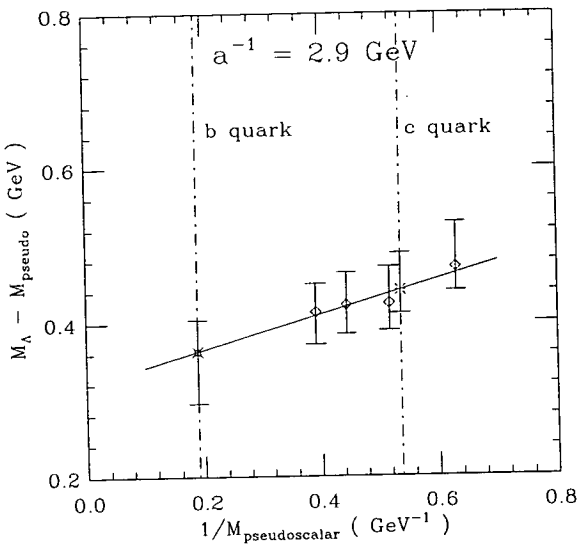

Figure 4.5: Heavy quark extrapolation for $M_\Lambda - M_{pseudoscalar}$. The solid line shows the best fit to (4.53).

4.7.2 The Σ - Λ Splitting

The Σ - Λ mass splitting was obtained for the various κ, both by taking the difference of the fitted masses and by fitting the time evolution of the ratio of

	Exp. $[MeV]$	Function (4.52) $[MeV]$	Function (4.53) $[MeV]$	Function (4.54) $[MeV]$
charm	415(1)	$443 \pm^{50}_{30}$	$441 \pm^{48}_{30}$	$433 \pm^{48}_{32}$
bottom	362(50)	$264 \pm^{62}_{155}$	$363 \pm^{41}_{68}$	$468 \pm^{123}_{131}$

Table 4.11: Results for the $M_\Lambda - M_{pseudo}$ splitting, at the physical masses, corresponding to $a^{-1} = 2.9 GeV$.

Σ and Λ correlators. The numbers from the two methods agree within errors, with the former showing bigger statistical errors. The results at each value of the computed masses and after extrapolation in the light quark mass are given in table 4.12.

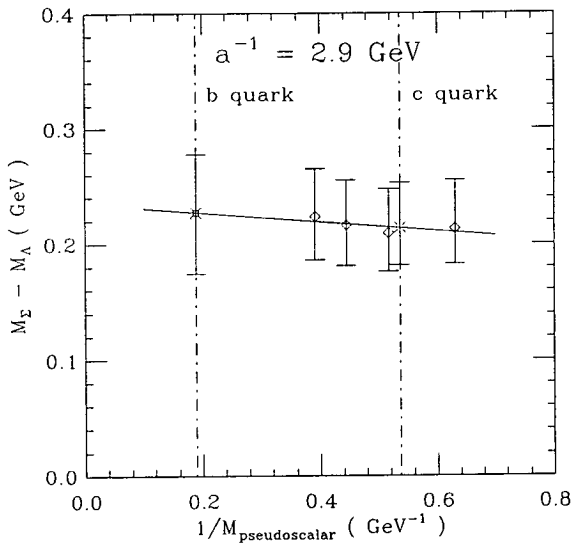

Figure 4.6: Heavy quark extrapolation for $M_\Sigma - M_\Lambda$ from ratio method. The solid line shows the best fit to (4.53).

The mass splitting shows a very mild dependence on the heavy-quark mass, suggesting that the $1/M_Q$ corrections to the masses of the two baryons must be very similar and nearly cancel in the difference. In the extrapolation to physical quark masses, this feature make the results from (4.53) and (4.54) indistinguishable. We note that our results, presented in table 4.13 (see also figure 4.6), compare very well with the experimental numbers.

$(\kappa_{l1}, \kappa_{l2})$	$\kappa_Q = 0.121$		$\kappa_Q = 0.125$	
$(0.14144, 0.14144)$	$0.034 \pm^{5}_{6}$	$[13,21]$ 1.15	$0.035 \pm^{5}_{6}$	$[13,21]$ 1.18
$(0.14144, 0.14226)$	$0.045 \pm^{7}_{7}$	$[12,22]$ 1.12	$0.045 \pm^{6}_{7}$	$[12,22]$ 1.20
$(0.14226, 0.14226)$	$0.054 \pm^{10}_{10}$	$[13,22]$ 1.02	$0.053 \pm^{9}_{9}$	$[13,22]$ 0.95
chiral/chiral	$0.077 \pm^{14}_{13}$	0.11	$0.074 \pm^{14}_{12}$	0.15
chiral/strange	$0.061 \pm^{11}_{10}$	0.11	$0.060 \pm^{10}_{9}$	0.15
$(\kappa_{l1}, \kappa_{l2})$	$\kappa_Q = 0.129$		$\kappa_h = 0.133$	
$(0.14144, 0.14144)$	$0.035 \pm^{5}_{6}$	$[13,21]$ 1.19	$0.036 \pm^{5}_{6}$	$[13,21]$ 1.18
$(0.14144, 0.14226)$	$0.45 \pm^{6}_{7}$	$[12,21]$ 1.16	$0.45 \pm^{6}_{6}$	$[12,21]$ 1.10
$(0.14226, 0.14226)$	$0.052 \pm^{9}_{9}$	$[13,21]$ 1.01	$0.054 \pm^{9}_{7}$	$[12,21]$ 1.01
chiral/chiral	$0.072 \pm^{13}_{11}$	0.22	$0.073 \pm^{15}_{10}$	0.002
chiral/strange	$0.059 \pm^{10}_{9}$	0.22	$0.060 \pm^{10}_{9}$	0.002

Table 4.12: Estimates of M_Σ - M_Λ in lattice units, for various κ combinations with the ratio method and for SS data. Also indicated is the fitting range and $\chi^2/d.o.f$. The extrapolations assume linear behaviour in the light quark mass.

4.7.3 The Spin Splitting

	Exp. $[MeV]$	Ratio Method $[MeV]$	$\chi^2/d.o.f.$	Mass Difference $[MeV]$	$\chi^2/d.o.f.$
Charm Results					
$M_\Sigma - M_\Lambda$	169(2)	$213 \pm^{39}_{32}$	0.04	$149 \pm^{61}_{64}$	0.18
$M_{\Xi'} - M_\Xi$	92	$173 \pm^{29}_{25}$	0.02	$127 \pm^{47}_{45}$	0.16
$M_{\Sigma^*} - M_\Sigma$	77(6)	$-30 \pm^{13}_{13}$	0.003	$-1 \pm^{27}_{42}$	0.06
$M_{\Xi^*} - M_{\Xi'}$	83	$-26 \pm^{9}_{9}$	0.003	$-4 \pm^{18}_{29}$	0.05
$M_{\Omega^*} - M_\Omega$	-	$-21 \pm^{6}_{5}$	0.002	$-8 \pm^{7}_{18}$	0.01
b Results					
$M_\Sigma - M_\Lambda$	173(11)	$227 \pm^{51}_{53}$	0.04	$126 \pm^{83}_{69}$	0.18
$M_{\Xi'} - M_\Xi$	-	$179 \pm^{36}_{38}$	0.02	$107 \pm^{56}_{47}$	0.16
$M_{\Sigma^*} - M_\Sigma$	56(16)	$-9 \pm^{13}_{8}$	0.003	$36 \pm^{46}_{73}$	0.06
$M_{\Xi^*} - M_{\Xi'}$	-	$-7 \pm^{10}_{6}$	0.002	$22 \pm^{27}_{45}$	0.05
$M_{\Omega^*} - M_\Omega$	-	$-4 \pm^{6}_{4}$	0.002	$8 \pm^{11}_{20}$	0.01

Table 4.13: Baryon mass splittings.

In the context of HQET, the mass difference within the spin doublets (Σ,Σ^*), (Ξ',Ξ^*) and (Ω,Ω^*) is due to the coupling of the heavy quark spin to the spin of the light degrees of freedom. Therefore, the spin splitting is suppressed by an inverse power of the heavy quark mass and vanishes in the infinite mass (spin-flavour symmetry) limit. The spin splitting is expected to be smaller than the Σ-Λ splitting, which makes its measurement even more difficult to realize.

In order to have better control over the extrapolations, we fit the chirally extrapolated SS and SL local data to the following function

$$[M_{\Sigma^*} - M_{\Sigma}](M_{Meson}) = \frac{A}{M_{Meson}} + \frac{B}{M^2_{Meson}} \tag{4.55}$$

either setting B to zero or leaving it as a free parameter. We also allow for a possible nonzero intercept at $1/M_{Meson} = 0$.

The results of all the fits we performed are perfectly consistent. Their $\chi^2/d.o.f.$ is always small (less than 0.7). The point we would like to stress is that the fitting results are compatible with zero within one to three standard deviations. This suggests that our statistics are not enough to allow a study of spin splitting. In HQET, the spin splittings are $1/M_Q$ effects. Experience from the baryon masses tell us that the $1/M_Q$ corrections are important but their contribution to physical quantities is small. Due to our limited statistics, firm conclusion about the consistency or our results with heavy quark scaling laws cannot be drawn. It would be interesting to see how the measurements change with better statistics.

In table 4.13 we report the spin splittings from SS data, computed from ratio of correlators and difference of fitted mass, assuming $B = 0$. We note that our numbers for the spin splitting disagree with the the experimental results. A similar result was found for the spin splitting of heavy-light mesons.

For heavy-light mesons, the spin splitting from quenched lattice QCD is about a factor of two lower than the experimental numbers [102]. The conclusion of [102] is that the spin splitting is very sensitive to the coefficient of the clover term c_{SW}, with bigger values of c_{SW} leading to results close to the experimental numbers.

The resolution of the spin splitting puzzle is believed to lie in a combination of discretisation errors[10] and quenching effects.

[10] According to Lüscher *et al.* [74], full $\mathcal{O}(a)$ improvement requires large values of the clover term (~ 1.6). The study of heavy-light meson spin splittings [103] suggests that they depend strongly on c_{SW}, with larger values of c_{SW} improving the lattice prediction.

4.8 Physical Results and Conclusions

In this section, we present a summary of the results. In the tables 4.14, 4.15 and 4.16 both the statistical (first) and a systematic (second) error are quoted. The systematic error is that arising from the uncertainty in the scale, and was computed allowing a^{-1} to vary within one standard deviations.

Baryon	Quark Content	charm baryons Exp. (GeV)	charm baryons Latt. (GeV)	b-baryons Exp. (GeV)	b-baryons Latt. (GeV)
Λ_Q	$(ud)Q$	2.285(1)	$2.31\ ^{+5}_{-3}\ ^{+4}_{-4}$	5.641(50)	$5.64\ ^{+4}_{-7}\ ^{+3}_{-2}$
Ξ_Q	$(us)Q$	2.468(4)	$2.44\ ^{+3}_{-3}\ ^{+5}_{-5}$		$5.77\ ^{+3}_{-6}\ ^{+4}_{-4}$
Σ_Q	$(uu)Q$	2.453(1)	$2.46\ ^{+6}_{-5}\ ^{+5}_{-5}$	5.814(60)	$5.79\ ^{+7}_{-7}\ ^{+3}_{-4}$
Σ^*_Q	$(uu)Q$	2.530(7)	$2.47\ ^{+4}_{-4}\ ^{+5}_{-5}$	5.870(60)	$5.80\ ^{+5}_{-7}\ ^{+4}_{-3}$
Ξ'_Q	$(us)Q$		$2.57\ ^{+5}_{-4}\ ^{+6}_{-6}$		$5.89\ ^{+5}_{-6}\ ^{+4}_{-5}$
Ξ^*_Q	$(us)Q$	2.643(2)	$2.57\ ^{+3}_{-4}\ ^{+6}_{-5}$		$5.90\ ^{+3}_{-4}\ ^{+5}_{-4}$
Ω_Q	$(ss)Q$	2.704(20)	$2.68\ ^{+4}_{-3}\ ^{+6}_{-7}$		$5.99\ ^{+4}_{-5}\ ^{+6}_{-5}$
Ω^*_Q	$(ss)Q$		$2.67\ ^{+3}_{-3}\ ^{+7}_{-6}$		$6.00\ ^{+3}_{-5}\ ^{+5}_{-5}$

Table 4.14: Heavy baryon masses. The quoted errors are statistical (first) and systematic (second) from the uncertainty in the calibration of the lattice spacing.

The beautiful agreement between the mass values we quote for the charm and b baryons already discovered and the experimental numbers, gives confidence in our predictions for the yet unseen particles.

For b baryons, the use of four values of the heavy quark mass proved important in the quality of the results. Unfortunately, the small number of light quark combinations did not made possible a very detailed study of the extrapolation to the chiral limit. Nevertheless, the behaviour observed is consistent with current

theoretical beliefs.

	Exp. $[MeV]$	Function (4.53) $[MeV]$
charm	415(1)	$441\ ^{+48}_{-30}\ ^{+40}_{-38}$
bottom	362(50)	$363\ ^{+41}_{-68}\ ^{+28}_{-28}$

Table 4.15: The $M_\Lambda - M_{pseudo}$ splitting.

For mass splittings we choose to quote the numbers obtained from the mass differences. The reason for this choice comes from the behaviour in the heavy mass extrapolations. In both methods, the $\chi^2/d.o.f.$ of the fits is very small (see table 4.13). This means the statistical errors were underestimated in both cases. However, the fits to the mass differences give a $\chi^2/d.o.f.$ an order of magnitude bigger than the fits to the ratio of correlators. This suggests that the statistical errors are better estimated in the mass difference method.

The mass splittings, being small numbers when compared with the heavy quark mass, are affected by large statistical errors. Nevertheless, apart from spin splittings, our predictions agree well with the experimental numbers, where available. For spin splittings, our data is clearly in disagrement with the experimental numbers. It is known that for heavy-light mesons quenched lattice QCD with $c_{SW} = 1$ underestimates the spin splittings. For baryons, the disagreement seems to be worse, with the numbers having the wrong sign relative to the experimental measurements.

For the Λ-pseudoscalar meson mass splitting we were able to get agreement with experiment. This was not the case in previous lattice simulations performed with Wilson fermions. We believe that this is largely due to the use of the $\mathcal{O}(a)$ improved action to remove lattice spacing effects.

In general, our results agree with the predictions obtained with other non-perturbative

	Exp. $[MeV]$	Mass Difference $[MeV]$
Charm Results		
$M_\Sigma - M_\Lambda$	169(2)	$149\ ^{+61}_{-64}\ ^{+14}_{-13}$
$M_{\Xi'} - M_\Xi$	92	$127\ ^{+47}_{-45}\ ^{+12}_{-11}$
$M_{\Sigma^*} - M_\Sigma$	77(6)	$-1\ ^{+27}_{-42}\ ^{+6}_{-3}$
$M_{\Xi^*} - M_{\Xi'}$	83	$-4\ ^{+18}_{-29}\ ^{+3}_{-4}$
$M_{\Omega^*} - M_\Omega$	–	$-8\ ^{+7}_{-18}\ ^{+2}_{-4}$
b Results		
$M_\Sigma - M_\Lambda$	173(11)	$126\ ^{+83}_{-69}\ ^{+15}_{-15}$
$M_{\Xi'} - M_\Xi$	–	$107\ ^{+56}_{-47}\ ^{+13}_{-12}$
$M_{\Sigma^*} - M_\Sigma$	56(16)	$36\ ^{+46}_{-73}\ ^{+2}_{-1}$
$M_{\Xi^*} - M_{\Xi'}$	–	$22\ ^{+27}_{-45}\ ^{+1}_{-1}$
$M_{\Omega^*} - M_\Omega$	–	$8\ ^{+11}_{-20}\ ^{+1}_{-1}$

Table 4.16: Baryon mass splittings.

methods[11], both for the masses themselves and for the $\Sigma - \Lambda$ splitting.

Our conclusion is that a detailed and precise study of the lowest-lying heavy baryons is feasible on the lattice. In that sense, we consider the study described here a percursor to a high statistics calculation. Also of interest will be the investigation of the behaviour of spin splittings with the coefficient of the clover term. The hope is that the recently suggested large values of c_{SW} will bring the quenched lattice QCD predictions closer to the experimental results. Finally, we would like to emphasise that our data confirms Heavy Quark Effective Theory as a good theoretical tool for investigating heavy baryons.

[11]See chapter 1 for references.

Chapter 5

Semileptonic Decays of Λ_b and Ξ_b Baryons

The decay amplitude for semileptonic decays of hadrons factorizes into the matrix element of a hadronic current and the matrix element of a leptonic current, interacting by the exchange of electroweak gauge bosons. This factorisation makes the semileptonic decays of hadrons an ideal laboratory for studying strong interaction effects and testing the Standard Model. Furthermore, if the transition involves a heavy quark, the theoretical description is simplified considerably by Heavy Quark Effective Theory.

The knowledge of b baryon phenomenology is still quite poor, with only one baryon state, Λ_b, established unambiguously. However, due to the current experimental interest in the subject of heavy baryons, the situation is expected to improve in the next few years.

For Λ_b several experimental groups have measured its mass, life time and studied some of its decays. In particular, the decay $\Lambda_b \to \Lambda_c \, l \, \nu$ was observed but a determination of its characteristic is still to be done.

The Ξ_b particle is not yet discovered. However, according to Heavy Quark Effective Theory, Ξ_b and Λ_b are distinguished only by their strangeness and isospin quantum numbers. Therefore, the theoretical descriptions of their semileptonic decays are similar and they can be studied simultaneously.

The study of the decays $\Lambda_b \to \Lambda_c l\nu$ and $\Xi_b \to \Xi_c l\nu$ is interesting, not only because of current experimental interest, but also as a test to Heavy Quark Effective Theory and QCD. In addition, the decays provide independent measures of V_{cb}.

In the semileptonic decays, the investigation of the couplings between matter fields and electroweak gauge bosons requires computing the matrix elements of both

currents involved. The calculation of the hadronic transition requires evaluating a quark current between hadron states. This requires nonperturbative techniques, and the calculation suits Lattice QCD.

In this chapter, we describe a study of semileptonic decays of heavy baryons using Lattice QCD [112]. Our work focusses on computing the Isgur-Wise function for the decays $\Lambda_b \to \Lambda_c\, l\, \nu$ and $\Xi_b \to \Xi_c\, l\, \nu$. Once the Isgur-Wise function is known, we have a theoretical description of the decays and predictions for the decay rates of both processes may be made.

5.1 Theoretical Background

In this section we review the theoretical framework needed to study the semileptonic decays of Λ_b and Ξ_b baryons - see also section 3.4.

For the decays $\Lambda_b \to \Lambda_c\, l\, \nu$ and $\Xi_b \to \Xi_c\, l\, \nu$ the quark current which is involved has the usual V-A structure, $J_\mu = \bar{c}\gamma_\mu(1-\gamma_5)b$. In the hadronic transition, the nonperturbative strong interaction effects are summarised in six scalar form factors,

$$\begin{aligned}\langle \Lambda_c(v,s)|\, \bar{c}\gamma_\mu(1-\gamma_5)b\, |\Lambda_b(v',s')\rangle \;=\; & \\ \overline{u}_{\Lambda_c}(v,s)\,[\,(\,F_1(\omega)\,\gamma_\mu \,+\, F_2(\omega)\,v'_\mu \,+\, F_3(\omega)\,v_\mu\,) & \\ -\,(\,G_1(\omega)\,\gamma_\mu \,+\, G_2(\omega)\,v'_\mu \,+\, G_3(\omega)\,v_\mu\,)\,\gamma_5\,]\,u_{\Lambda_b}(v',s') & \quad (5.1)\end{aligned}$$

for $\Lambda_b \to \Lambda_c\, l\, \nu$ with a similar set of form factors defined for the decay of Ξ_b. In (5.1) we follow the notation used in (3.20) and (3.21).

In principle, one could measure $F_i(\omega)$ and $G_i(\omega)$ directly from QCD. However, present day simulations cannot use relativistic b quarks. Therefore, to measure the matrix elements relevant to the above semileptonic decays one has to use a set of heavy quark masses around the charm mass and extrapolate the results to the b mass. HQET provides the theoretical framework to perform this extrapolation.

According to HQET, the form factors describing the decay $\Lambda_{Q'} \to \Lambda_Q\, l\, \nu$ are related by a single function, the baryonic Isgur-Wise function $\xi_{QQ'}(\omega)$, and coefficient functions, $N_i(\omega)$, $N_i^5(\omega)$, which can be computed in perturbation theory. The correction factors $N_i(\omega)$ and $N_i^5(\omega)$ are independent of the light degrees of

freedom, but they include perturbative contributions both in $1/m_Q$ and in the strong coupling constant - see (3.22), (3.23) and (3.24)-(3.29) for definitions. The QCD corrections taking into account next-to-leading order effects in the strong constant, $\alpha_s(m_Q)$, and including corrections of type $\alpha_s^2\ (z\,lnz)^n$, $n = 0, 1, 2$ where $z = m_Q/m_{Q'}$, were computed by Neubert in [90].

The dependence on the heavy quark of the form factors and baryon Isgur-Wise function mass, including $1/m_Q$ corrections and next-to-leading order QCD effects, is described in [84].

The heavy quark dependence of the $F_i(\omega)$, $G_i(\omega)$ and $\xi_{QQ'}(\omega)$ is completely determined by the quark mass and the mass of light degrees of freedom[1], $\overline{\Lambda}$. Up to $\mathcal{O}(\Lambda_{QCD}^2/m_Q)$ corrections, the binding energy of the heavy quark is given by

$$\overline{\Lambda}_\Lambda = M_{\Lambda_b} - m_b = M_{\Lambda_c} - m_c\ , \tag{5.2}$$

$$\overline{\Lambda}_\Xi = M_{\Xi_b} - m_b = M_{\Xi_c} - m_c\ . \tag{5.3}$$

The definitions (5.2) and (5.3) involve explicitly the heavy quark mass. Therefore, different choices of quark masses lead to differences in $N_i(\omega)$ and $N_i^5(\omega)$ which are of $\mathcal{O}(\alpha_s^2)$ and $\mathcal{O}(1/m_Q^2)$. This differences are smaller than the statistical precision achieved and, therefore, they are irrelevant for our work. It should be noticed that it is possible to define $\overline{\Lambda}$ without any reference to m_Q - see [84], [114] and references therein. This latter definition is superior in the sense that it avoids the ambiguities associated with having to choose a definition for the heavy quark mass.

5.2 Details of the Simulation

In order to study the semileptonic decays of Λ_b and Ξ_b, we compute the matrix element $\langle \Lambda_Q | \overline{Q} \Gamma_\mu Q' | \Lambda_{Q'} \rangle$ for a number of different quark masses. In the evaluation of the hadronic matrix elements we use the same lattice and β value as in the spectroscopy investigation. Moreover, the 3-point correlation functions were evaluated with the same set of quark masses and gauge configuration used in the study described in the previous chapter. In table 5.1, we report the quark mass

[1] $\overline{\Lambda}$ is also known as the binding energy of the heavy quark.

$(\kappa_{l_1}; \kappa_{l_2})$	$\kappa_{h'} \to \kappa_h$
(0.14144; 0.14144)	All κ_h combinations
(0.14144; 0.14226)	$0.129 \to 0.129$
(0.14226; 0.14226)	$0.129 \to 0.129$

Table 5.1: Quark mass combinations used in the calculation of baryonic three-point functions. For the heavy quark, the following $\kappa_h = 0.121, 0.125, 0.129, 0.133$ values were considered.

combinations for which we evaluate the three-point functions.

In order to reduce discretization errors, the quark propagators were computed using the Sheikholeslami-Wohlert action (2.54) with $r = 1$ and the quark currents evaluated with rotated quark fields,

$$Q(x) \to (1 - \frac{1}{2}\vec{\gamma} \cdot D^{(\to)})\, Q(x) \,, \tag{5.4}$$

$$\overline{Q}(x) \to \overline{Q}(x)\,(1 + \frac{1}{2}\vec{\gamma} \cdot D^{(\leftarrow)}) \,. \tag{5.5}$$

The vector current,

$$V_\mu = \overline{Q}(x)\,(1 + \frac{1}{2}\vec{\gamma} \cdot D^{(\leftarrow)})\,\gamma_\mu\,(1 - \frac{1}{2}\vec{\gamma} \cdot D^{(\to)})\,Q(x) \,, \tag{5.6}$$

and the axial vector current,

$$A_\mu = \overline{Q}(x)\,(1 + \frac{1}{2}\vec{\gamma} \cdot D^{(\leftarrow)})\,\gamma_\mu\gamma_5\,(1 - \frac{1}{2}\vec{\gamma} \cdot D^{(\to)})\,Q(x) \,, \tag{5.7}$$

were computed separately.

In order to improve the overlap with Λ_Q and $\Lambda_{Q'}$ states, we only consider the operator $\mathcal{O}_5$ with all quark fields smeared by the Jacobi method.

$\lvert\vec{q}\rvert$	$\vec{q}$ and $-\vec{q}$
0	$(0,0,0)$
1	$(1,0,0)$, $(0,1,0)$, $(0,0,1)$
$\sqrt{2}$	$(1,1,0)$, $(1,0,1)$, $(0,1,1)$
$\sqrt{3}$	$(1,1,1)$
2	$(2,0,0)$, $(0,2,0)$, $(0,0,2)$

Table 5.2: Momentum combinations used in the calculation of the 3-point function. The momenta $\vec{p}$ takes the values $(0,0,0)$ or $(1,0,0)$. All momenta are in units of $\pi/12$.

5.3 Details of the Analysis

The analysis of the decay $\Lambda_{Q'} \to \Lambda_Q\, l\, \nu$ requires the calculation of the following 3-point correlation function

$$G_\mu^{Q'\to Q}(t_x,\vec{p};t_y,\vec{q}) = \sum_{\vec{x},\vec{y}} e^{-i\vec{p}\cdot\vec{x}}\, e^{-i\vec{q}\cdot\vec{y}}\, \langle \mathcal{O}_5^Q(t_x,\vec{x})\, J_\mu^{Q'\to Q}(t_y,\vec{y})\, \overline{\mathcal{O}}_5^{Q'}(0,\vec{0})\rangle \ . \quad (5.8)$$

This function can be expressed in terms of the quark propagators as

$$G_\mu^{Q'\to Q}(t_x,\vec{p};t_y,\vec{q}) = \sum_{\vec{y}} e^{-i\vec{q}\cdot\vec{y}}\, \mathrm{Tr}\,[\,\Sigma_5(0,y;t_x,\vec{p})_Q\, \Gamma_\mu\, S_{Q'}(y,0)\,] \ , \quad (5.9)$$

where the trace is over colour indices, Γ_μ is the gamma structure of the quark current, $S_q(x,y)$ is the propagator for quark q from point y to x and

$$\Sigma_5^{AB}(0,y;t_x,\vec{p})_Q = \varepsilon_{AFG}\,\varepsilon_{CDE} \sum_{\vec{x}} e^{-i\vec{p}\cdot\vec{x}}\, \mathrm{Tr}\,[(S_{l_1}^{CG}(x,0))^{\mathrm{T}}\, \mathcal{C}\gamma_5\, S_{l_2}^{DF}(x,0)\,\gamma_5\mathcal{C}\,]\, S_Q^{EB}(x,y) \ , \quad (5.10)$$

where A, B, C, D, E, F, G are colour indices and the trace is over spin indices. The extended propagator (5.10) was evaluated by the standard source method [113].

The momenta used in evaluating (5.8) are reported in table 5.2.

In appendix B, the correlation function (5.8) is evaluated for large time separations and including smearing effects. For convenience, we reproduce here the results of appendix B, but only for the particular case used in the numerical simulation,

$t_x = T/2$. If we define $t < T/2$, then[2]

$$G_\mu^{Q'\to Q}(\vec{p};t,\vec{q}) = \mathcal{K}(Q',Q;p',p;t)$$
$$[\tilde{M} + \tilde{E}\,\gamma_4 - i(P_+ + \alpha P_-)\vec{p}\cdot\vec{\gamma}]\,\mathcal{F}_\mu^{Q'\to Q}(p,p')\,[\tilde{M}' + \tilde{E}'\,\gamma_4 - i(P_- + \alpha' P_+)\vec{p}'\cdot\vec{\gamma}]\ , \quad (5.11)$$
$$G_\mu^{Q'\to Q}(\vec{p};T-t,\vec{q}) = -\mathcal{K}(Q',Q;p',p;t)$$
$$[\tilde{M} - \tilde{E}\,\gamma_4 - i(P_- + \alpha P_+)\vec{p}\cdot\vec{\gamma}]\,\mathcal{F}_\mu^{Q'\to Q}(\tilde{p},\tilde{p}')\,[\tilde{M}' - \tilde{E}'\,\gamma_4 - i(P_+ + \alpha' P_-)\vec{p}'\cdot\vec{\gamma}]\ , \quad (5.12)$$

where

$$\mathcal{K}(Q',Q;p',p;t) = \frac{Z_\Lambda(|\vec{p}|)\,Z_{\Lambda'}(|\vec{p}'|)}{4E_\Lambda(\vec{p})E_{\Lambda'}(\vec{p}')}\,e^{-E_\Lambda(\vec{p})(T/2-t)}\,e^{-E_{\Lambda'}(\vec{p}')t}\ . \quad (5.13)$$

Following a similar strategy as in the heavy baryon spectrum study, we look for combinations of correlators components which have a good signal in the Monte Carlo simulation. The identification of these components is more difficult for the 3-point functions than for the 2-point functions, because the former functions have more structure than the later ones. However, the correlation functions

$$\mathcal{P}_\mu(\vec{p};t,\vec{q}) = G_\mu^{Q'\to Q}(\vec{p};t,\vec{q}) + \gamma_4\,\gamma_5\,G_\mu^{Q'\to Q}(\vec{p};T-t,\vec{q})\,\gamma_5\,\gamma_4\ , \quad (5.14)$$
$$\mathcal{M}_\mu(\vec{p};t,\vec{q}) = G_\mu^{Q'\to Q}(\vec{p};t,\vec{q}) - \gamma_4\,\gamma_5\,G_\mu^{Q'\to Q}(\vec{p};T-t,\vec{q})\,\gamma_5\,\gamma_4\ , \quad (5.15)$$

have particular simple relations with $F_i(\omega)$ and $G_i(\omega)$,

Vector Current

$$\mathcal{P}_4 \sim F_1(\omega)\,\gamma_4\ , \quad (5.16)$$
$$\mathcal{P}_j \sim F_2(\omega)\,\frac{p_j'}{M_{\Lambda'}} + F_3(\omega)\frac{p_j}{M_\Lambda}\ , \quad (5.17)$$
$$\mathcal{M}_4 \sim F_2(\omega)\frac{E_{\Lambda'}(\vec{p}')}{M_{\Lambda'}} + F_3(\omega)\frac{E_\Lambda(\vec{p})}{M_\Lambda}\ , \quad (5.18)$$
$$\mathcal{M}_j \sim F_1(\omega)\,\gamma_j\ ; \quad (5.19)$$

Axial Current

$$\mathcal{P}_4 \sim [\,G_2(\omega)\frac{E_{\Lambda'}(\vec{p}')}{M_{\Lambda'}} + G_3(\omega)\frac{E_\Lambda(\vec{p})}{M_\Lambda}\,]\,\gamma_5\ , \quad (5.20)$$

[2] For notation see appendix B. Note that we do not write explicitly the index t_x.

$$\mathcal{P}_j \sim G_1(\omega)\,\gamma_j\,\gamma_5\ , \tag{5.21}$$

$$\mathcal{M}_4 \sim G_1(\omega)\,\gamma_4\,\gamma_5\ , \tag{5.22}$$

$$\mathcal{M}_j \sim [\,G_2(\omega)\frac{p'_j}{M_{\Lambda'}} + G_3(\omega)\frac{p_j}{M_\Lambda}\,]\,\gamma_5\ . \tag{5.23}$$

To choose a combination of components, we classify the matrix elements of (5.14) and (5.15) according to their order of magnitude. For example, some components are suppressed by powers of the baryon momentum and in the Monte Carlo simulation their signal is expected to be noisier when compared with the signal for unsuppressed spin components. To measure the semileptonic decay form factors, we include only contributions from the dominant components.

To illustrate our procedure, let us consider the $G_1(\omega)$ form factor. $G_1(\omega)$ is computed from $\mathcal{M}_4$ and $\mathcal{P}_j$ correlators. If we divide $\mathcal{M}_4$ and $\mathcal{P}_j$ into 2×2 submatrices, and classify their relative importance according to their leading term we arrive at

$$\mathcal{P}_j \sim \begin{pmatrix} (M+E)^2 & \alpha\,p\,(M+E) \\ \alpha\,p\,(M+E) & \alpha^2\,p^2 \end{pmatrix},\ \mathcal{M}_4 \sim \begin{pmatrix} (M+E)\,p & \alpha p^2 \\ \alpha p^2 & \alpha\,p^3/M \end{pmatrix}. \tag{5.24}$$

In both cases, the dominant terms are in the upper left submatrix, with the contributions of the remaining submatrices suppressed by powers of momentum. To compute $G_1(\omega)$, we sum the nonzero matrix elements from the upper left submatrix.

The analysis of the other form factors shows a similar pattern, with the dominant contribution coming from the upper left submatrices of the correlators. Thus, to compute the form factors we sum only the nonzero matrix elements from the upper left 2×2 submatrix of the correlators. In order to improve the signal we average over equivalent momenta[3].

In (5.14) and (5.15), the overall factor $\mathcal{K}(Q',Q;p',p;t)$ as well as the remaining quantities which multiply the form factors can be fully reconstructed from the fits to the finite momentum two-point functions. The study of finite momentum two-point functions is described in section 5.4.

[3]The derivation of the matrix elements combinations used is rather lengthy, however straightforward, and we will not show here details of the derivation or the expressions which were used.

The fits to the 3-point functions were done using the procedure described in section 4.4.2. The statistical errors were evaluated by the bootstrap method, and they correspond to 68% confidence limits of the distribution obtained from 1000 bootstrap samples.

5.4 Two-point Correlation Functions at Finite Momentum

In this section, we discuss the Λ propagator at finite momentum. Here, only the 2-point functions computed using quark propagators smeared at the source and the sink are considered.

The Z^s values and energies which appear in (5.14) and (5.15) can be obtained from the analysis of the 2-point functions

$$G(t,\vec{p}) = \sum_{\vec{x}} e^{-i\vec{p}\cdot\vec{x}} \langle\, \mathcal{O}_5(t,\vec{x})\, \overline{\mathcal{O}}_5(0,\vec{0}) \,\rangle \ . \tag{5.25}$$

In addition, the analysis of (5.25) can test our description of smearing effects. This is an important point in our study of the form factors, since a negative answer would have made our results meaningless. Moreover, from the dispersion relations one can get an idea of the importance of lattice artifacts in the correlation functions and this can help to restrict the range of momenta to be used in the study of 3-point functions.

The 2-point correlation functions, (5.25), were computed using the same set of quark masses as the zero momentum propagator studied in the previous chapter, and for the following momenta[4] : $(0,0,0)$, $(1,0,0)$, $(0,1,0)$, $(0,0,1)$, $(1,1,0)$, $(1,0,1)$, $(0,1,1)$, $(1,1,1)$, $(2,0,0)$, $(0,2,0)$ and $(0,0,2)$.

According to the analysis of smearing effects given in appendix B, the 2-point SS propagator reads

$$\begin{aligned} G_\Lambda^{(ss)}(t,\vec{p}) \ = \ & \tfrac{(Z^s(|\vec{p}|))^2}{2E_\Lambda(\vec{p})}\big[\ (\tilde{M} + \tilde{E}\,\gamma_4 - i\,\alpha(|\vec{p}|)\,\vec{p}\cdot\vec{\gamma})e^{-E_\Lambda(\vec{p})t} - \\ & (\tilde{M} - \tilde{E}\,\gamma_4 - i\,\alpha(|\vec{p}|)\,\vec{p}\cdot\vec{\gamma})e^{-E_\Lambda(\vec{p})(T-t)}\big] \ , \end{aligned} \tag{5.26}$$

[4] All momenta are in lattice units and are multiplied by $\pi/12$.

where

$$\tilde{M} = \frac{1}{2}\left[E_\Lambda(\vec{p}) + M_\Lambda - \alpha^2(|\vec{p}|)\left(E_\Lambda(\vec{p}) - M_\Lambda\right)\right], \tag{5.27}$$

$$\tilde{E} = \frac{1}{2}\left[E_\Lambda(\vec{p}) + M_\Lambda + \alpha^2(|\vec{p}|)\left(E_\Lambda(\vec{p}) - M_\Lambda\right)\right]. \tag{5.28}$$

To test our description of smearing, we define different combinations of correlator components, chosen to be sensitive to the various parameters involved in (5.26), and study how the lattice data fits each of the combinations.

For zero momentum, the correlation function depends only on $Z^s(|\vec{0}|)$ and the exponential of the particle mass. This particular case was investigated in great detail in the previous chapter and we will not repeat the procedure here. When necessary, we quote the results from chapter 4.

For finite momentum, the smearing effects are proportional to the particle momentum. Therefore, to test our description of smearing we study the three different combinations of components,

$$\begin{aligned} G_M(t,\vec{p}) &= \frac{1}{2}\Re\{ [G^{(ss)}(t,\vec{p})]_{11} + [G^{(ss)}(t,\vec{p})]_{22} - \\ &\qquad [G^{(ss)}(T-t,\vec{p})]_{33} - [G^{(ss)}(T-t,\vec{p})]_{44}\} \\ &= (Z^s(|\vec{p}|))^2 \frac{E_\Lambda(\vec{p}) + M_\Lambda}{E_\Lambda(\vec{p})} e^{-E_\Lambda(\vec{p})t}, \end{aligned} \tag{5.29}$$

$$\begin{aligned} G_E(t,\vec{p}) &= -\frac{1}{2}\Re\{ [G^{(ss)}(t,\vec{p})]_{33} + [G^{(ss)}(t,\vec{p})]_{44} - \\ &\qquad [G^{(ss)}(T-t,\vec{p})]_{11} - [G^{(ss)}(T-t,\vec{p})]_{22}\} \\ &= (Z^s(|\vec{p}|))^2\, \alpha^2(|\vec{p}|) \frac{E_\Lambda(\vec{p}) - M_\Lambda}{E_\Lambda(\vec{p})} e^{-E_\Lambda(\vec{p})t}, \end{aligned} \tag{5.30}$$

and a combination of nondiagonal elements [5]

$$G_p(t,\vec{p}) = (Z^s(|\vec{p}|))^2\, \alpha(|\vec{p}|) \frac{|\vec{p}|}{E_\Lambda(\vec{p})} e^{-E_\Lambda(\vec{p})t}. \tag{5.31}$$

The correlators (5.29) - (5.31) are of the type $G_x = Z_x e^{-E_\Lambda t}$. To improve the signal for G_x, $x = M, E, p$ we average over equivalent momenta.

[5] The exact expression depend on the momentum channel.

Correlator	$\|\vec{p}\| = \pi/12$	$\|\vec{p}\| = \sqrt{2}\pi/12$	$\|\vec{p}\| = \sqrt{3}\pi/12$	$\|\vec{p}\| = \pi/6$
G_M	[10, 19]	[8, 19]	[6, 15]	[6, 13]
G_p	[9, 18]	[8, 19]	[6, 15]	[6, 13]
G_E	[11, 18]	[10, 18]	[6, 15]	[6, 13]

Table 5.3: Fitting range for the 2-point correlation function at finite momentum.

Assuming that the continuum dispersion relation holds for the lattice data, one can estimate the relative size of the different Z_x. Expanding the energy factors in powers of momenta and keeping only the leading term $Z_M \sim (Z^s)^2\, 2$, $Z_E \sim (Z^s)^2\, \alpha^2\, p^2/(2M_\Lambda^2)$ and $Z_p \sim (Z^s)^2\, p/M_\Lambda$. This results suggest that G_M should have the cleaner signal, while G_E should have the noisier signal in the Monte Carlo simulation. Besides, from the definitions of the Z_x one expects Z_E to have a sizeable contamination from the parity partner, specially for the lower momentum channels.

From the analysis of the estimates of Z_x we adopt the following procedure. For each κ combination, the energy is computed by fitting $G_M(t, \vec{p})$. The energy obtained in this way, is then used in the fits to $G_E(t, \vec{p})$ and $G_p(t, \vec{p})$ to extract Z_E and Z_p, respectively. The $\alpha(|\vec{p}|)$ function is computed by taking the ratio $Z_p\ (E_\Lambda + M_\Lambda)/[\ Z_M\ p\ ]$. Finally, we compute $Z^s(|\vec{p}|)$ from Z_M, using the masses determined in the spectroscopy study.

The fitting range was chosen from studying the effective mass plots of the combination $(0.14144, 0.14144, 0.121)$ and used in all other κ combinations. In table 5.3 we report on the fitting ranges.

The results of the fittings show reasonable $\chi^2/d.o.f$. For the fits to G_M, the $\chi^2/d.o.f$ are in the range 0.4 and 1.4. For G_p the $\chi^2/d.o.f$ is between 0.8 and 2.0. The fits to G_E have a $\chi^2/d.o.f$ which is typically between 0.9 and 2.0. However, the channel with momentum $|\vec{p}| = \pi/12$ has larger values of the $\chi^2/d.o.f$, reaching a maximum of 5.3. Moreover, the values of Z^s computed using either Z_E or Z_M do not agree for lower momentum - see figure 5.1. We interpret the behaviour observed in G_E as supporting our hypothesis that Z_E has sizeable contributions from the parity partner.

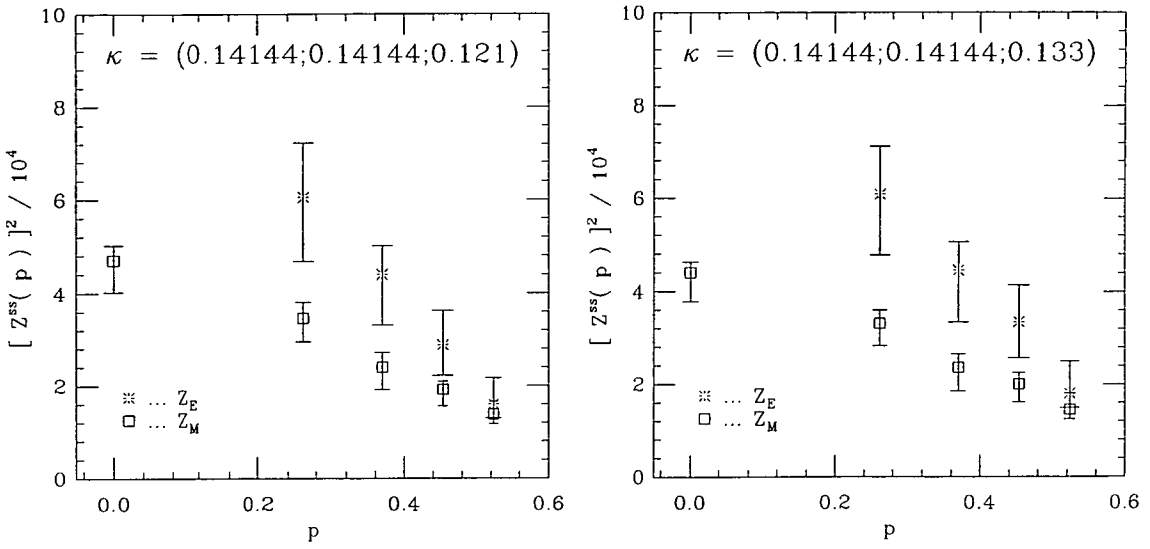

Figure 5.1: $[Z^s(|\vec{p}|)]^2$ computed from G_E and G_M.

In view of the good results of the fits and the understanding of G_E behaviour, our conclusion is that the data is well described by (5.26). This gives us confidence to use our modelling of smearing in the study of the 3-point functions.

Let us now discuss the $\alpha(|\vec{p}|)$ and $Z^s(|\vec{p}|)$ functions. Concerning the $\alpha(|\vec{p}|)$ function, figure 5.2 illustrates its dependence on the quark mass. Within our limited statistics, the data does not show any dependence of $\alpha(|\vec{p}|)$ with either the particle momentum and the light quark mass. However, $\alpha(|\vec{p}|)$ shows a mild dependence on the heavy quark mass, with the largest deviations from $\alpha = 1$ occurring for the heavier quarks. However, within two standard deviations the results are all compatible.

The observed behaviour of Z^s with momentum (see figure 5.1) can be understood in terms of Lorentz contraction, i.e. higher momentum states have lower Z^s. Unfortunately, we have no intuition about how $\alpha(|\vec{p}|)$ should behave with the quark mass and baryon momentum. It would be interesting to perform a high statistics simulation in order to study and try to understand the dependence of $\alpha(|\vec{p}|)$ with the quark mass and the baryon momentum.

Finally, let us have a look at the particle dispersion relations. For all the momenta used in the evaluation of the 2-point correlation function, the values for the fitted

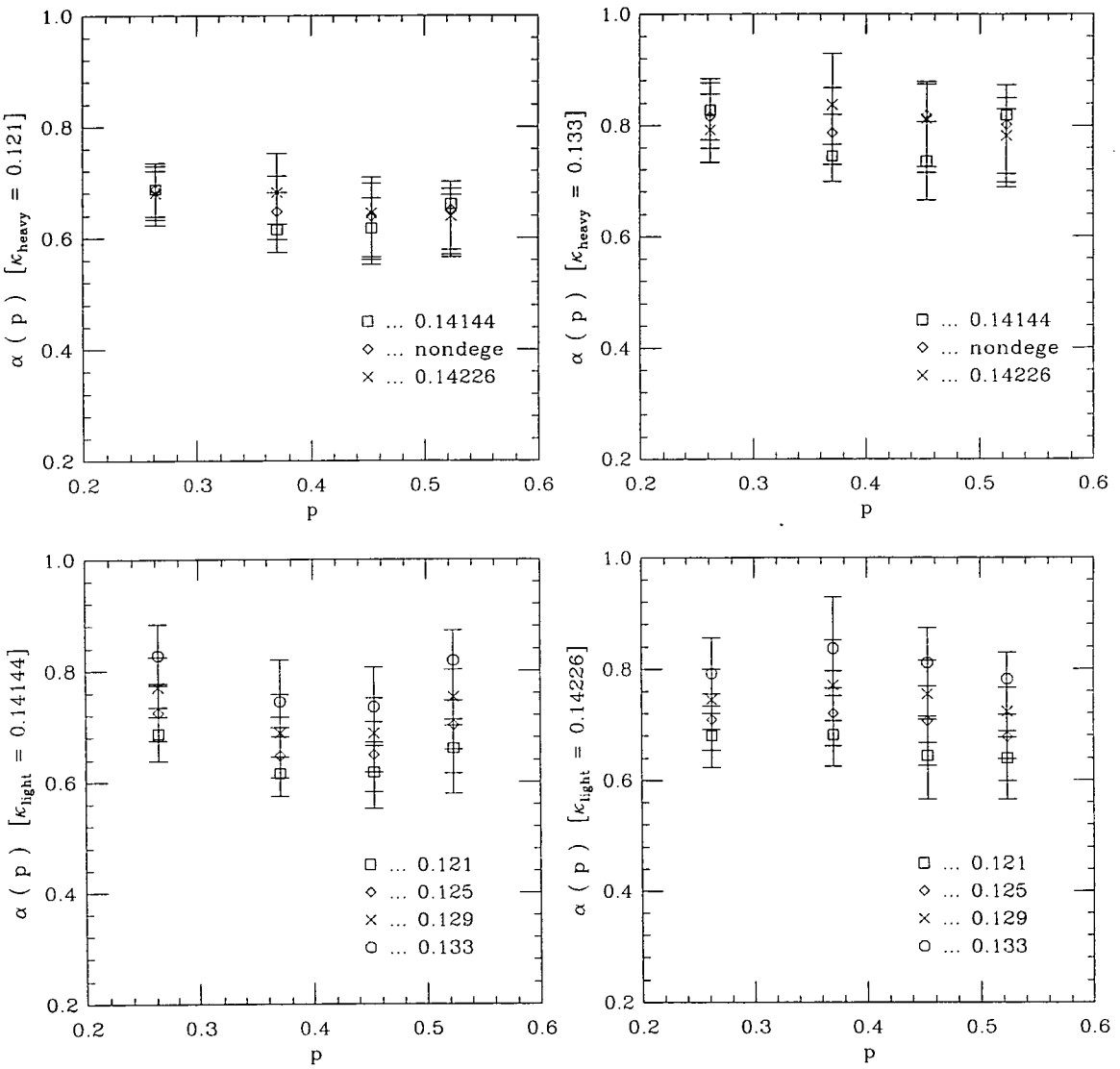

Figure 5.2: Quark mass dependence of $\alpha(|\vec{p}|)$.

energy agree well with the continuum dispersion relation,

$$a^2 E^2 = a^2 m^2 + a^2 p^2 , \tag{5.32}$$

if one uses am from the fit to the zero-momentum correlator. As can be seen in figure 5.3, the agreement between (5.32) and the lattice data is excellent for $|\vec{p}| = \pi/12$ and $\sqrt{2}\,\pi/12$. For higher momenta, the fitted energy and the energy evaluated using equation (5.32) agree within errors. However, for these momenta the statistical errors are significantly larger.

The study of the dispersion relations suggests that lattice artifacts are small for momentum up to $\sqrt{2}\,\pi/12$. Furthermore, since for larger momenta the statistical errors are significantly increased, we will use only $|\vec{p}| \leq \sqrt{2}\pi/12$ in the calculation of the form factor.

In this section we have studied the 2-point correlation function at finite momenta. We found that (5.26) describes the lattice data well. This suggests that our description of the smearing effects can be extended to the 3-point function. In addition, we found good agreement between the fitted energy and the continuum dispersion relation (5.32). This result allows us to recompute Z^s by fitting G_M with the energy constrained by (5.32). In the calculation of the form factors from the 3-point correlation function, we use the Z^s from the constraint fits and, at every stage, assume that (5.32) holds for our data. In table 5.4 we show the values of energies and Z^s used in extracting the form factors.

5.5 Three-point Functions and Lattice Form Factors

According to HQET, it is sufficient to know the Isgur-Wise function in order to describe the semileptonic decays of heavy baryons. This simplifies considerably our task, in the sense that instead of having to compute all the $F_i(\omega)$ and $G_i(\omega)$ one can extract the Isgur-Wise function from a subset of the six form factors needed to described the decay. This is particularly important because, due to our limited statistics, the results of fitting separately F_2, F_3, G_2 and G_3 are often compatible with zero. On the other hand, for G_1 and $F^{(sum)} = F_1 + F_2 + F_3$ the Monte Carlo data has a clear signal. In addition, since G_1 and $F^{(sum)}$ do not have $1/m_Q$ corrections at zero momentum transfer, it is possible to make a

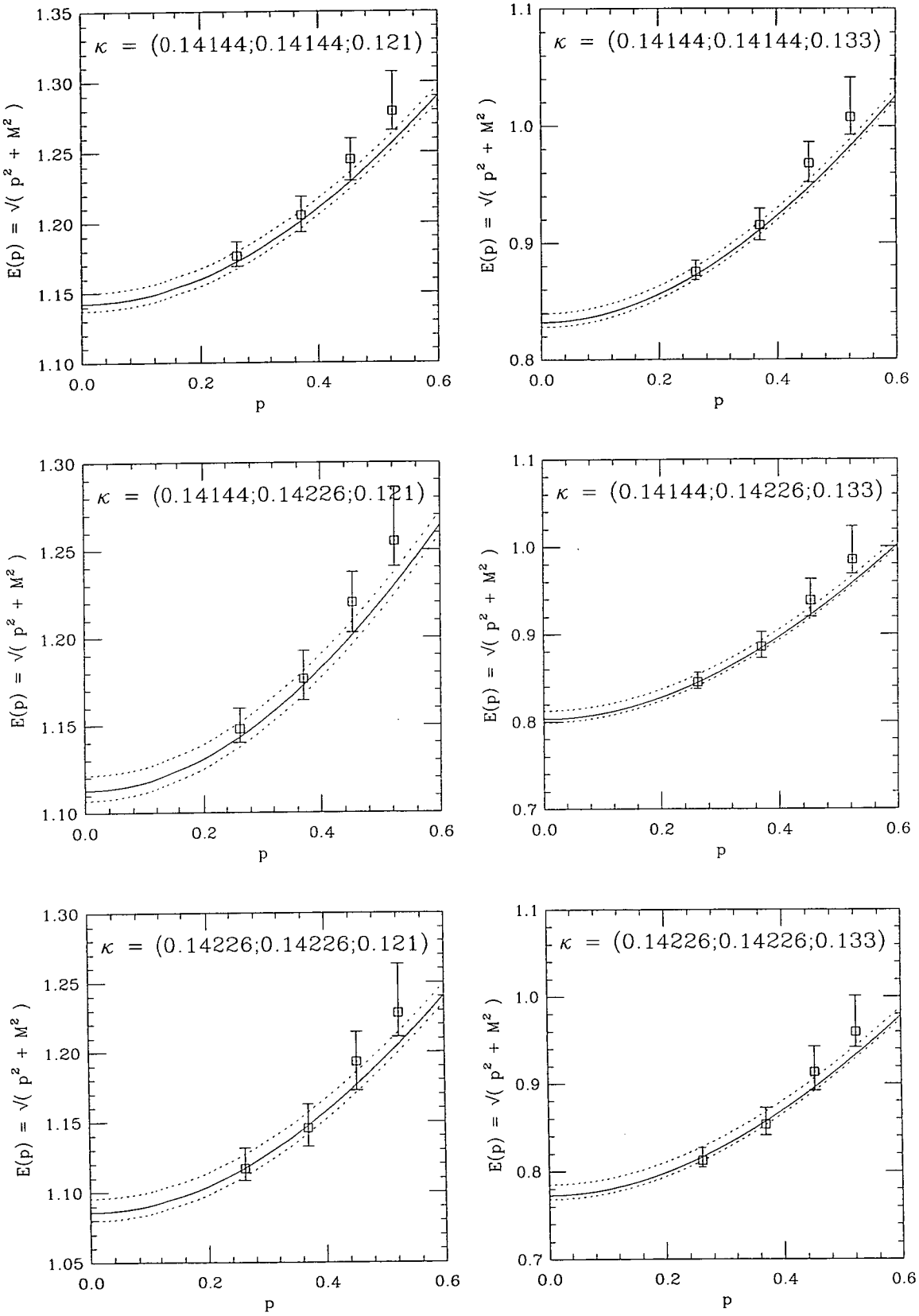

Figure 5.3: Comparisation of fitted energy with the results from the continuum dispersion relation. The values for the mass are from the fits to the zero momentum propagator.

	$\kappa_h = 0.121$	$\kappa_h = 0.125$	$\kappa_h = 0.129$	$\kappa_h = 0.133$
$\kappa_{light} = (0.14144; 0.14144)$				
$[Z^s(0)]^2 \times 10^{-4}$	$4.70 \pm^{32}_{68}$	$4.68 \pm^{29}_{67}$	$4.60 \pm^{25}_{65}$	$4.40 \pm^{22}_{62}$
E_Λ	$1.142 \pm^{8}_{5}$	$1.044 \pm^{8}_{5}$	$0.941 \pm^{8}_{5}$	$0.832 \pm^{7}_{4}$
$[Z^s(\frac{\pi}{12})]^2 \times 10^{-4}$	$3.32 \pm^{23}_{47}$	$3.33 \pm^{22}_{46}$	$3.31 \pm^{20}_{45}$	$3.21 \pm^{19}_{43}$
E_Λ	$1.172 \pm^{7}_{5}$	$1.077 \pm^{8}_{5}$	$0.977 \pm^{7}_{4}$	$0.872 \pm^{7}_{4}$
$[Z^s(\sqrt{2}\frac{\pi}{12})]^2 \times 10^{-4}$	$2.29 \pm^{13}_{37}$	$2.30 \pm^{12}_{35}$	$2.30 \pm^{11}_{34}$	$2.25 \pm^{11}_{33}$
E_Λ	$1.201 \pm^{7}_{5}$	$1.108 \pm^{7}_{5}$	$1.012 \pm^{7}_{4}$	$0.911 \pm^{7}_{4}$
$\kappa_{light} = (0.14144; 0.14226)$				
$[Z^s(0)]^2 \times 10^{-4}$	-	-	$4.69 \pm^{24}_{76}$	-
E_Λ	-	-	$0.916 \pm^{10}_{5}$	-
$[Z^s(\frac{\pi}{12})]^2 \times 10^{-4}$	-	-	$3.18 \pm^{23}_{41}$	-
E_Λ	-	-	$0.952 \pm^{10}_{5}$	-
$[Z^s(\sqrt{2}\frac{\pi}{12})]^2 \times 10^{-4}$	-	-	$2.16 \pm^{14}_{34}$	-
E_Λ	-	-	$0.988 \pm^{10}_{4}$	-
$\kappa_{light} = (0.14226; 0.14226)$				
$[Z^s(0)]^2 \times 10^{-4}$	-	-	$4.46 \pm^{23}_{72}$	-
E_Λ	-	-	$0.884 \pm^{12}_{5}$	-
$[Z^s(\frac{\pi}{12})]^2 \times 10^{-4}$	-	-	$2.97 \pm^{24}_{41}$	-
E_Λ	-	-	$0.922 \pm^{11}_{5}$	-
$[Z^s(\sqrt{2}\frac{\pi}{12})]^2 \times 10^{-4}$	-	-	$1.98 \pm^{13}_{36}$	-
E_Λ	-	-	$0.958 \pm^{11}_{5}$	-

Table 5.4: Amplitude Z^s obtained from constraint fits to the finite momentum 2-point function. The quoted values for the energies were computed from the continuum dispersion relation. All quantities are in lattice units.

nonperturbative measurement of the vector and axial renormalisation constants from $G_1(1)$ and $F^{(sum)}(1)$. Thus, to compute the baryonic Isgur-Wise function, $\xi_{QQ'}(\omega)$, we use only the data from $G_1(\omega)$ and $F^{(sum)}(\omega)$, fitting separately each of the momentum channels.

Let us study the lattice data and the quality of the fits for $G_1(\omega)$ and $F^{(sum)}(\omega)$. In the 3-point correlation functions the time, energy and Z^s dependence is eliminated using the results from the 2-point functions. Once this dependence has been accounted for, we observe long plateaux. In figure 5.4 we show examples of the plateaux, and include the results of the fits to 3 time-slices centred around $t = 12$.

The analysis of the data shows that plateaux for the axial form factor, $G_1(\omega)$, are typically larger and smoother than plateaux for $F^{(sum)}(\omega)$. The $\chi^2/d.o.f.$ for the fits to $F^{(sum)}(\omega)$ are between 0.03 and 4.7. For degenerate heavy quark transitions, $\Lambda_Q \to \Lambda_Q$, the $\chi^2/d.o.f.$ stays in the range 0.1 to 2.2. For the axial form factor, G_1, the $\chi^2/d.o.f.$ for the fits belongs to the interval 0.001 to 2.2, whereas for degenerate transitions the range of values is slightly reduced, 0.003 to 1.9. If for the axial form factor there are no large differences between the degenerate and nondegenerate transitions, for $F^{(sum)}(\omega)$ the plateaux for the degenerate data look smoother and the fits have clearly better values of the $\chi^2/d.o.f.$ We understand this difference as a manifestation of discretization errors, i.e. the vector form factor has sizeable lattice artifacts, whereas for the axial form factor the lattice artifacts are smaller than our statistical precision. The reader should note that this result is not a complete surprise. Actually, the analysis of the semileptonic heavy-light mesons also shows measurable discretization errors only for the vector current [118].

Despite using only three points to fit a constant, the fitting results are not always on top of the lattice data. This is due to the presence of strong correlations between the time-slices. In view of the observed strong time-slice correlations and because the behaviour of some of the plateaux for the vector current (see figure 5.4) we did not attempt to use larger fitting intervals.

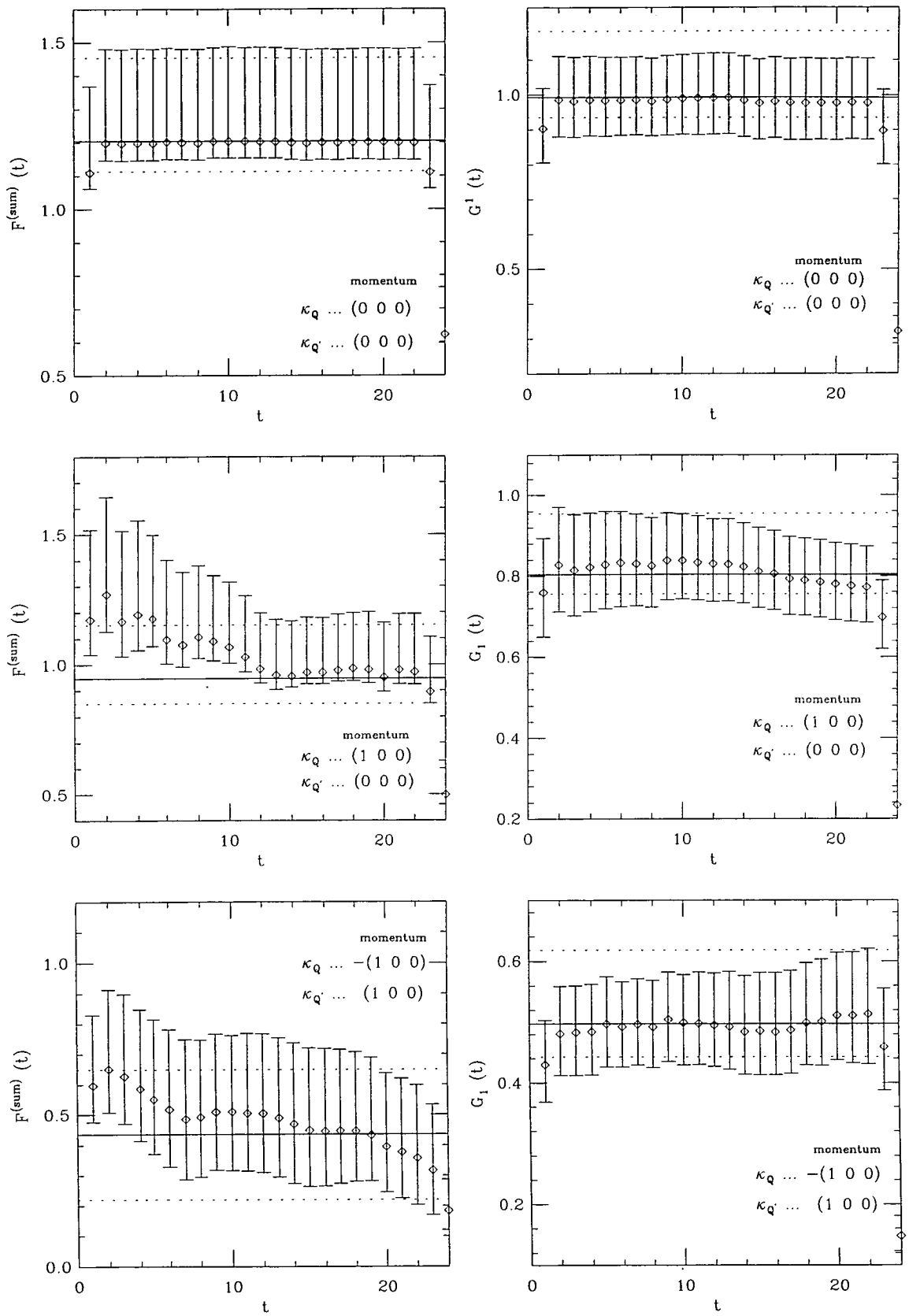

Figure 5.4: Lattice form factor G_1 and $F^{(sum)}$ computed from $\langle \Lambda_Q | J_\mu | \Lambda_{Q'} \rangle$. The data shown refers to the mass combination $\kappa_{l_1} = \kappa_{l_2} = 0.14144$ and $\kappa_h = 0.129$.

5.6 The Isgur-Wise Function

In this section we study the Isgur-Wise as a function of the velocity transfer, ω, and of the quark mass.

In order to compute the baryonic Isgur-Wise function, $\xi_{QQ'}(\omega)$, we use the data from both form factors, $G_1(\omega)$ and $F^{(sum)}(\omega)$. The renormalised form factors are related to $\xi_{QQ'}(\omega)$ by

$$G_1(\omega) = N_1^5(\omega)\,\xi_{QQ'}(\omega)\ , \tag{5.33}$$

$$F^{(sum)}(\omega) = N^{(sum)}(\omega)\,\xi_{QQ'}(\omega)\ , \tag{5.34}$$

where $N_1^5(\omega)$ is defined in (3.27) and

$$N^{(sum)}(\omega) = \hat{C}_1(\overline{\omega})+\hat{C}_2(\overline{\omega})(1+\frac{2(\omega-1)}{\omega+1}\frac{\overline{\Lambda}}{2m_Q})+\hat{C}_3(\overline{\omega})(1+\frac{2(\omega-1)}{\omega+1}\frac{\overline{\Lambda}}{2m_{Q'}}) \tag{5.35}$$

and $\overline{\omega}$ is given in (3.30). At zero recoil, Luke's theorem protects both $G_1(\omega)$ and $F^{(sum)}(\omega)$ from $\mathcal{O}(1/m_Q)$ corrections. Then, if we combine this result with the known normalisation of the Isgur-Wise function at zero recoil, $\xi_{QQ'}(1) = 1$, one can determine both the axial and vector renormalisation constants nonperturbatively. Assuming that the $\mathcal{O}(1/m_Q^2)$ corrections are small, one can use the lattice (bare) form factors and compute

$$Z_V = \frac{N^{(sum)}(1)}{F^{(sum)}(1)}\ , \tag{5.36}$$

$$Z_A = \frac{N_1^5(1)}{G_1(1)}\ . \tag{5.37}$$

These Z factors are absorbed into the form factors in (5.33) and (5.34). Then, the renormalised Isgur-Wise function is given by

$$\xi_{QQ'}(\omega) = \frac{G_1(\omega)}{G_1(1)}\frac{N_1^5(1)}{N_1^5(\omega)} = \frac{F^{(sum)}(\omega)}{F^{(sum)}(1)}\frac{N^{(sum)}(1)}{N^{(sum)}(\omega)}\ ; \tag{5.38}$$

all form factors in (5.38) are bare form factors.

In the evaluation of the renormalised form factors, one could have used the axial and vector renormalisation constants computed from other quantities. However,

there is an advantage in using the definitions (5.36) and (5.37). The lattice form factors have discretization errors which are of $\mathcal{O}(a\, m_Q\, \alpha_s(m_Q))$ and $\mathcal{O}(a^2 m_Q^2)$. In principle, the discretization errors are small, and by computing the Isgur-Wise function from ratios of lattice form factors, one expects to suppress most of the dependence on the lattice spacing. As we saw in the analysis of the lattice form factors, there are differences in the way the axial and vector form factors behave. These differences were interpreted as a manifestation of the discretization errors. We will see that, for the Isgur-Wise function most of the effects from the lattice spacing are cancelled.

The functions $N_1^5(\omega)$ and $N^{(sum)}(\omega)$ are known to order α_s and $1/m_Q$. Their evaluation requires the values of the quark masses, heavy quark binding energy, Λ_{QCD} and the number of light quark flavours, n_f. For the last two quantities we use $\Lambda_{QCD} = 250\, GeV$ and $n_f = 0$ as is appropriate for quenched calculations. The quark masses were computed from the chirally extrapolated Λ_Q mass[6], according to the relation

$$m_Q = a^{-1}\, M_{\Lambda_Q} - \overline{\Lambda}_{baryon}\ , \tag{5.39}$$

using $a^{-1} = 2.9 \pm 0.2\ GeV$ to convert lattice to physical units and $\overline{\Lambda}_{baryon} = 0.57\ GeV$. Our value for the heavy quark binding energy is smaller than what naively one would expect, but the choice of $\overline{\Lambda}_{baryon} = 0.57\ GeV$ was motivated by the recent estimate of the spin-average mesonic binding energy by Crisafulli *et al.* [114].

The quark mass can be computed from the spin average heavy-light meson mass,

$$m_Q = \frac{a^{-1}}{4}\,(3M_{V_Q} + M_{P_Q}) - \overline{\Lambda}_{meson}\ , \tag{5.40}$$

where M_{V_Q} is the chirally extrapolated mass of the vector meson with heavy quark Q, M_{P_Q} is the mass of the pseudoscalar meson with heavy quark Q extrapolated to the chiral limit and $\overline{\Lambda}_{meson}$ is the binding energy of the heavy quark in the heavy-light meson. In (5.40), to compute m_Q one needs to know $\overline{\Lambda}_{meson}$. This can be computed from the pole quark masses $m_b = 4.8\ GeV$ and $m_c = 1.45\ GeV$ combined with the the experimental meson masses $M_B = 5.28\ GeV$ and $M_D =$

[6] In the extrapolation to the chiral limit we assumed a linear dependence on the light quark mass.

κ_Q	$a\,M_{P_Q}$	$a\,M_{V_Q}$	m_Q	m_Q^*	$a\,M_{\Lambda_Q}$	m_Q	m_Q^*
0.121	$0.874\,^{+4}_{-3}$	$0.896\,^{+5}_{-4}$	2.13	2.38	$1.02\,^{+1}_{-1}$	2.12	2.39
0.125	$0.773\,^{+3}_{-3}$	$0.799\,^{+4}_{-3}$	1.85	2.10	$0.92\,^{+2}_{-1}$	1.83	2.10
0.129	$0.665\,^{+3}_{-3}$	$0.696\,^{+4}_{-4}$	1.55	1.80	$0.81\,^{+2}_{-1}$	1.52	1.79
0.133	$0.547\,^{+3}_{-3}$	$0.588\,^{+4}_{-5}$	1.23	1.48	$0.71\,^{+2}_{-1}$	1.22	1.49

Table 5.5: Quark masses from meson and baryon data. The values m_Q are computed using the experimental masses for the mesons, whereas m_Q^* are computed using the estimated quark binding energy. Both m_Q and m_Q^* are given GeV.

1.87 GeV, the result being $\overline{\Lambda}_{meson} = 0.45\ GeV$. For baryons, $\overline{\Lambda}_{baryon}$ can be computed in a similar way. The baryon masses are $M_{\Lambda_b} = 5.64\ GeV$ and $M_{\Lambda_c} = 2.28\ GeV$, therefore $\overline{\Lambda}_{baryon} = 0.84\ GeV$. For the heavy quarks considered in this simulation, the estimates of the quark masses from meson data and baryon data are given in table 5.5. The agreement between the two estimates of the heavy quark mass is excellent. Clearly, the final numbers for the quark mass have a strong dependence on the heavy quark binding energy. For heavy-light mesons, Crisafulli *et al.* [114] have computed nonperturbatively the $\overline{\Lambda}_{meson}$ in the quenched approximation. Demanding agreement between meson and baryon heavy quark mass estimates, one can determined $\overline{\Lambda}_{baryon}$. We found that for baryons, the heavy quark binding energy reproducing the quark masses computed from the meson data and using Crisafulli *et al.* result $\overline{\Lambda}_{meson} = 0.200\ GeV$, is $\overline{\Lambda}_{baryon} = 0.57\ GeV$.

5.6.1 The Vector and Axial Renormalisation Constants

In this subsection, we report the results for the vector renormalisation constant, Z_V, and the axial renormalisation constant, Z_A, computed using the definitions (5.36) and (5.37), respectively. In table 5.6 we reported the values of the vector and axial renormalisation constants.

As can be seen in table 5.6, the renormalisation constants computed from the heavy baryon correlators have large statistical errors. Therefore, it is not possible to draw firm conclusions concerning their dependence on the quark mass and, within the statistical errors, Z_V and Z_A are constant. If we take the central values of the vector and axial renormalisation constants for the heavy quark transition $\kappa_h = 0.121 \rightarrow \kappa_h = 0.121$ as reference, then the central values for Z_V and Z_A

$\kappa_{h'} \to \kappa_h$	Z_V	Z_A
$k_{l_1} = 0.14144$; $k_{l_2} = 0.14144$		
$0.121 \to 0.121$	$0.83 \pm^{8}_{14}$	$0.94 \pm^{7}_{15}$
$0.121 \to 0.125$	$0.84 \pm^{7}_{14}$	$0.95 \pm^{6}_{15}$
$0.121 \to 0.129$	$0.86 \pm^{6}_{14}$	$0.98 \pm^{6}_{16}$
$0.121 \to 0.133$	$0.89 \pm^{6}_{15}$	$1.01 \pm^{6}_{16}$
$0.125 \to 0.121$	$0.84 \pm^{7}_{14}$	$0.96 \pm^{8}_{15}$
$0.125 \to 0.125$	$0.83 \pm^{7}_{14}$	$0.95 \pm^{7}_{15}$
$0.125 \to 0.129$	$0.85 \pm^{6}_{14}$	$0.97 \pm^{6}_{16}$
$0.125 \to 0.133$	$0.87 \pm^{5}_{15}$	$1.00 \pm^{6}_{16}$
$0.129 \to 0.121$	$0.86 \pm^{7}_{14}$	$0.99 \pm^{8}_{15}$
$0.129 \to 0.125$	$0.85 \pm^{7}_{14}$	$0.98 \pm^{7}_{16}$
$0.129 \to 0.129$	$0.83 \pm^{7}_{14}$	$0.96 \pm^{6}_{15}$
$0.129 \to 0.133$	$0.85 \pm^{6}_{14}$	$1.00 \pm^{6}_{16}$
$0.133 \to 0.121$	$0.88 \pm^{8}_{15}$	$1.02 \pm^{8}_{16}$
$0.133 \to 0.125$	$0.87 \pm^{7}_{15}$	$1.01 \pm^{7}_{16}$
$0.133 \to 0.129$	$0.85 \pm^{7}_{15}$	$1.00 \pm^{6}_{16}$
$0.133 \to 0.133$	$0.83 \pm^{6}_{15}$	$0.98 \pm^{5}_{16}$
$k_{l_1} = 0.14144$; $k_{l_2} = 0.14226$		
$0.129 \to 0.129$	$0.82 \pm^{7}_{20}$	$0.95 \pm^{4}_{23}$
$k_{l_1} = 0.14226$; $k_{l_2} = 0.14226$		
$0.129 \to 0.129$	$0.85 \pm^{10}_{23}$	$0.99 \pm^{7}_{27}$

Table 5.6: Vector and Axial Vector Renormalisation Constants from the zero recoil form factors of the matrix element $\langle \Lambda_Q | J_\mu | \Lambda_{Q'} \rangle$.

vary within 8% if we consider all the heavy quark transitions. For degenerate transitions, the numbers for Z_V and Z_A are not so spread, and their central values change by 2% and 5%, respectively. The good agreement between the different estimates of the renormalisation constants seems to indicate that the $\mathcal{O}(1/m_Q^2)$ corrections to the form factors are small.

The renormalisation constants for the vector and axial vector currents have been computed using different methods. In [115] the axial vector current was estimated from chiral Ward identities ($Z_A = 1.04\,^{+1}_{-1}$) and in [118] using heavy-light meson correlators

$$\begin{aligned} Z_A &= 1.07\,^{+2}_{-2} \quad \text{at} \quad \kappa_l = 0.14144, \quad \kappa_h = 0.133\ , \\ Z_A &= 1.08\,^{+2}_{-2} \quad \text{at} \quad \kappa_l = 0.14144, \quad \kappa_h = 0.129\ , \\ Z_A &= 1.10\,^{+2}_{-2} \quad \text{at} \quad \kappa_l = 0.14144, \quad \kappa_h = 0.125\ , \\ Z_A &= 1.12\,^{+3}_{-2} \quad \text{at} \quad \kappa_l = 0.14144, \quad \kappa_h = 0.121\ . \end{aligned} \tag{5.41}$$

Our values for Z_A are slightly lower than both these results, but the numbers agree within two standard deviations. However, our numbers for Z_A are in good agreement with one-loop perturbation theory for the $\mathcal{O}(a)$-improved action [117]

$$Z_A = 1 - 0.02\,g^2 + \mathcal{O}(g^4) \simeq 0.97 \quad \text{at} \quad \beta = 6.2\ , \tag{5.42}$$

using the boosted coupling as defined in [75]. For the vector renormalisation constant, the result of [115] is $Z_V = 0.817 \pm 2 \pm 8$, where the first error is statistical and the second error comes from the quark mass dependence, and the estimates from heavy-light meson data [116, 118] are

$$\begin{aligned} Z_V &= 0.8913\,^{+2}_{-1} \quad \text{at} \quad \kappa_l = 0.14144, \quad \kappa_h = 0.133\ , \\ Z_V &= 0.9177\,^{+3}_{-2} \quad \text{at} \quad \kappa_l = 0.14144, \quad \kappa_h = 0.129\ , \\ Z_V &= 0.9428\,^{+2}_{-1} \quad \text{at} \quad \kappa_l = 0.14144, \quad \kappa_h = 0.125\ , \\ Z_V &= 0.9659\,^{+2}_{-1} \quad \text{at} \quad \kappa_l = 0.14144, \quad \kappa_h = 0.121\ . \end{aligned} \tag{5.43}$$

For the vector current, the renormalisation constant as been computed in pertur-

bation theory [117]. The result from one-loop perturbation theory is

$$Z_V = 1 - 0.10\, g^2 + \mathcal{O}(g^4) \simeq 0.83 \quad \text{at} \quad \beta = 6.2\ , \tag{5.44}$$

when evaluated using the boosted value of the coupling constant, obtained from the mean field resummation of tadpole diagrams. Our values for Z_V are in good agreement with the numbers from perturbation theory and chiral Ward identities. The comparisation with the estimates from the heavy-light meson data is not so good, and agreement is found only within two standard deviations.

The results for the renormalisation constants Z_V and Z_A, obtained using estimates from heavy baryon and mesons states differ by less than 20%. This is an indication of the discretization errors in our calculation, and the order of magnitude of the difference is within the theoretical expectations, $\mathcal{O}(\alpha_s a m_Q)$ and $\mathcal{O}(a^2 m_Q^2)$. The Isgur-Wise function is computed from ratios of form factors, and we expect the error in $\xi_{QQ'}(\omega)$ to be smaller than in the renormalisation constants.

5.6.2 The Isgur-Wise Function - the dependence on the velocity transfer

In this subsection we discuss the results for the Isgur-Wise function obtained using both the axial and the vector current.

In figure 5.5 we show the Isgur-Wise function as computed from the axial and vector form factors. The points from the axial form factor involve momenta $|\vec{p}| \leq \sqrt{2}\,\pi/12$, whereas for the vector form factor data, only momenta $|\vec{p}| \leq \pi/12$ are considered. The numerical results for $\xi_{QQ'}(\omega)$ are collected in appendix D.

We make the following observations on the results for the Isgur-Wise function, $\xi_{QQ'}(\omega)$, obtained from $G_1(\omega)$ and $F^{(sum)}(\omega)$:

- The Isgur-Wise functions computed from the axial and vector form factors are compatible within errors.
- The data from the axial form factor is compatible with an universal curve. The points which are slightly off the general behaviour are from transitions involving one baryon with momentum $|\vec{p}| = \sqrt{2}\,\pi/12$ and, for this momentum, discretization errors are expected to be sizeable.

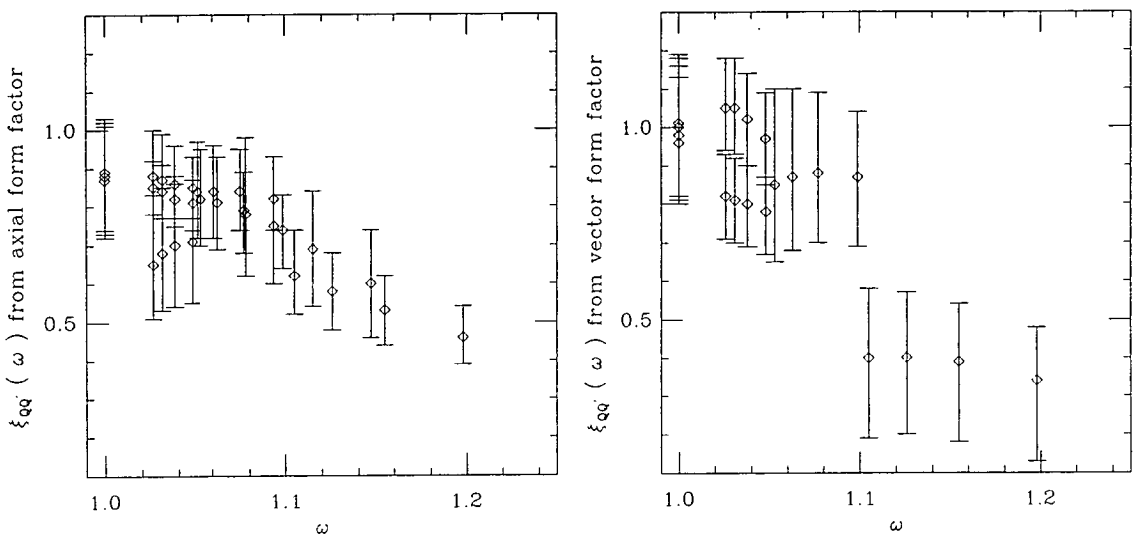

Figure 5.5: Baryonic Isgur-Wise function, $\xi_{QQ'}(\omega)$, as obtained from $G_1(\omega)$ and $F^{(sum)}(\omega)$. The data the from axial form factor include momenta $|\vec{p}| \leq \sqrt{2}\,\pi/12$, whereas in the vector form factor graph only momenta $|\vec{p}| \leq \pi/12$ are considered. Only data from heavy quark degenerate transitions and $\kappa_{l_1} = \kappa_{l_2} = 0.14144$ is used.

- The Isgur-Wise function computed from the axial form factor data involving momentum $|\vec{p}| = \sqrt{2}\pi/12$ is compatible with estimates of the Isgur-Wise function for similar ω and lower momentum. However, the data have larger statistical errors and in the analysis of the mass dependence we will not include states with momentum $|\vec{p}| = \sqrt{2}\pi/12$.

- The statistical errors have a mild dependence on the heavy quark mass and increase for lighter quark masses.

- For the vector form factor data, the statistical errors are always substantially larger than the corresponding axial form factor data.

- As for the axial form factor data, the results from the vector form factor data are compatible with an universal curve. However, because of the large statistical errors no firm conclusion can be made.

- In the case of the vector form factor data, one observes that, for similar ω, estimates of the Isgur-Wise function from different matrix elements do not agree within one standard deviation. This result is not observed in the axial form factor data, and we interpret the discrepancy as a manifestation of discretization errors in $F^{(sum)}$. However, their effects in the Isgur-Wise function are small, as the data always agree within less than 1.5 standard deviations. Suggestions that $F^{(sum)}$ has sizeable discretization errors were found already in the analysis of the fitting plateaux.

The results for the Isgur-Wise function are very encouraging. Even with our limited statistics, we were able to get good signals from both the vector and axial currents. This result demonstrates the feasibility of studying semileptonic decays of baryons with lattice techniques.

5.6.3 $\xi_{QQ'}(\omega)$ as a Function of the Heavy Quark Mass

In order to obtain reliable estimates of phenomenological quantities, we have to extrapolate our data, obtained for initial and final heavy quarks with masses around the charm quark, to the physical $b \to c$ decay. The extrapolation of the Isgur-Wise function requires an understanding of the $1/m_Q$ corrections. The dependence of $\xi_{QQ'}(\omega)$ on the heavy quark masses was studied by Neubert [84] and is reproduced in 3.31.

$\kappa_h = \kappa_{h'}$	vector and axial data ρ^2	$\chi^2/d.o.f.$	axial data ρ^2	$\chi^2/d.o.f.$
0.121	$3.5 \pm^{8}_{10}$	0.68	$3.2 \pm^{8}_{10}$	0.51
0.125	$3.2 \pm^{7}_{7}$	0.65	$3.0 \pm^{7}_{8}$	0.55
0.129	$2.9 \pm^{5}_{5}$	0.60	$2.8 \pm^{5}_{6}$	0.54
0.133	$2.6 \pm^{3}_{4}$	0.51	$2.6 \pm^{3}_{4}$	0.43
all degenerate	$2.2 \pm^{2}_{2}$	0.42	$2.3 \pm^{2}_{2}$	0.28

Table 5.7: Slope of the Isgur-Wise function as function of the heavy quark mass.

For the set of heavy quark masses considered in our simulation, the velocity transfer is in the interval $1 \leq \omega \leq 1.2$. For this range of velocity transfer, the Isgur-Wise function should be well approximated by a linear expansion around $\omega = 1$,

$$\xi_{QQ'}(\omega) = 1 + \rho^2(1-\omega) \; . \tag{5.45}$$

With the aim of studying the heavy quark mass dependence of the Isgur-Wise function, we fit either the vector and axial data to (5.45) or just the axial data and see how the slope, ρ^2, changes with the heavy quark mass. The results for the correlated fits involving only degenerate heavy quark transitions, baryon momenta up to $|\vec{p}| \leq \pi/12$, and the light quark combination $\kappa_{l_1} = \kappa_{l_2} = 0.14144$ are given in table 5.7. The results of the fits suggest a mild dependence of ρ^2 on the heavy quark mass[7]. However, the fits to only the axial current data and the quality of the fits to all degenerate data shows that, within our limited statistics, there is no sign of dependence of the Isgur-Wise function on m_Q - see figure 5.6.

A fit including all vector and axial data, degenerate and nondegenerate heavy quark transitions, yields $\rho^2 = 2.6 \pm^{1}_{1}$ ($2.8 \pm^{1}_{2}$ from axial data) with a $\chi^2/d.o.f. = 1.20$ (1.50 for axial data).

Our conclusion from this analysis is that our data for $\xi_{QQ'}(\omega)$ do not show any evidence of sizeable $1/m_Q$ corrections.

[7] A naive expansion of $\xi_{QQ'}(\omega)$ suggests that ρ^2 should be larger for larger quark masses. It is interesting to note that the central values follow this behaviour with the quark mass.

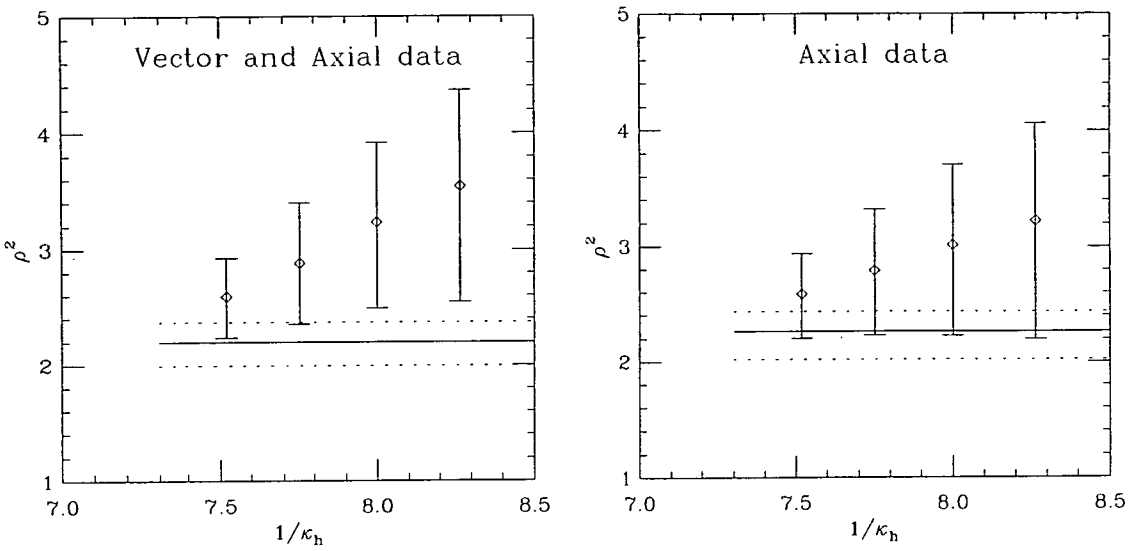

Figure 5.6: Isgur-Wise function slope. The figures include the results of the fits to all degenerate transitions.

5.6.4 $\xi_{QQ'}(\omega)$ as a Function of the Light Quark Mass

The Isgur-Wise function depends both on the heavy quark mass and on the quantum numbers of the light degrees of freedom. Previous studies of the Isgur-Wise function for heavy-light mesons [116], demonstrated that the dependence on the light degrees of freedom is not negligible. Thus, we might expect an even stronger dependence of $\xi_{QQ'}(\omega)$ on the light quark mass.

In order to study how $\xi_{QQ'}(\omega)$ changes with the light quark masses, we consider both the vector and axial data for the degenerate heavy quark transition $\kappa_h = 0.129$ and different light quark combinations. The results of the fits to (5.45) are

$$\begin{aligned}
\rho^2 &= 2.9\,^{+5}_{-5} \quad \text{at} \quad \kappa_{l_1} = 0.14144 \quad \kappa_{l_2} = 0.14144 \quad (\chi^2/d.o.f. = 0.60)\,, \\
\rho^2 &= 2.6\,^{+7}_{-6} \quad \text{at} \quad \kappa_{l_1} = 0.14144 \quad \kappa_{l_2} = 0.14226 \quad (\chi^2/d.o.f. = 0.56)\,, \\
\rho^2 &= 2.4\,^{+9}_{-6} \quad \text{at} \quad \kappa_{l_1} = 0.14226 \quad \kappa_{l_2} = 0.14226 \quad (\chi^2/d.o.f. = 0.54)\,,
\end{aligned} \tag{5.46}$$

and the comparisation between the fits and the data is given in figure 5.7.

In order to obtain the slope of the Isgur-Wise function, ρ^2, for Λ and Ξ particles, we extrapolate ω and $\xi_{QQ'}(\omega)$ assuming a linear dependence on the sum of the

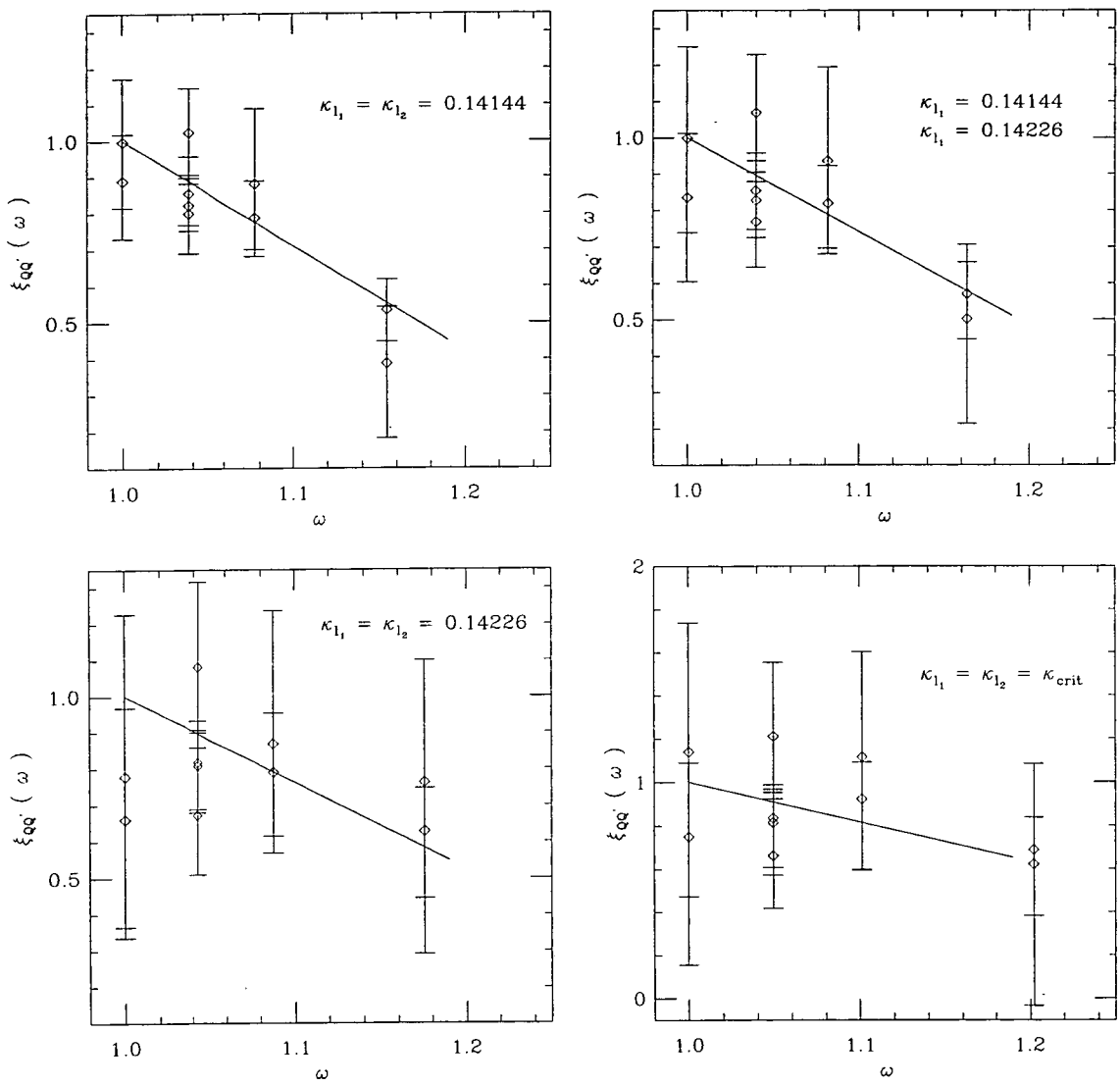

Figure 5.7: Plots of the Isgur-Wise function at fixed heavy quark mass and various light quark masses.

two light quark masses, i.e.

$$\begin{aligned}\omega(\kappa_h,\kappa_{l_1},\kappa_{l_2}) &= \omega(\kappa_h) + C(\frac{1}{2\kappa_{l_1}}+\frac{1}{2\kappa_{l_2}}-\frac{1}{2\kappa_{crit}}) \\ &= \omega(\kappa_h) + C(\frac{1}{\kappa_{eff}}-\frac{1}{2\kappa_{crit}}) \ , \end{aligned} \tag{5.47}$$

with $\kappa_{eff}^{-1} = (\kappa_{l_1}^{-1} + \kappa_{l_2}^{-1})/2$. This assumption is supported by our results for the spectrum presented in the previous chapter. The slope of the Isgur-Wise function is obtained from fits of the extrapolated data to (5.45). Our results for the Λ_b baryon are

$$\rho_\Lambda^2 = 1.8\,^{+1.3}_{-0.7} \ , \tag{5.48}$$

and the fit has a $\chi^2/d.o.f = 0.45$. For the Ξ baryon, we get

$$\rho_\Xi^2 = 2.2\,^{+1.0}_{-0.6} \ , \tag{5.49}$$

with a $\chi^2/d.o.f = 0.52$.

5.7 Phenomenological Implications

In this chapter we computed the Isgur-Wise function relevant for the decays $\Lambda_b \to \Lambda_c\, l\, \overline{\nu}$ and $\Xi_b \to \Xi_c\, l\, \overline{\nu}$ near zero recoil. Up to perturbative corrections, the Isgur-Wise function gives a complete description of the hadronic transition. Therefore, since the perturbative corrections are known, we are in the position of predicting different aspects of both decays.

In this section we discuss the physical form factors for the semileptonic decays of Λ_b and Ξ_b and predict their decay rates.

5.7.1 Physical Form Factors

The physical form factors are related to the Isgur-Wise function through the correction coefficients $N_i(\omega)$ and $N_i^5(\omega)$. Once the form factors are written in terms of $N_i(\omega)$, $N_i^5(\omega)$ and $\xi_{QQ'}(\omega)$ the dependence on the light quark mass is factorized. Whereas the Isgur-Wise function involves both the light and heavy quark masses, the corrections coefficients are functions only of the heavy quark mass. The dependence of the Isgur-Wise function on the light degrees of freedom was studied in section 5.6.4, near zero recoil.

To measure the physical form factors we have to evaluate $N_i(\omega)$ and $N_i^5(\omega)$; see (3.24) - (3.29) for definitions. The short distance coefficients, $\hat{C}_i$ and $\hat{C}_i^5$, were computed with $\Lambda_{QCD} = 0.250\, GeV$ and $n_f = 4$. In the evaluation of $N_i(\omega)$ and $N_i^5(\omega)$ we use the following values for the quark masses,

$$m_b = 4.8\, GeV\ , \qquad m_c = 1.45\, GeV\ . \tag{5.50}$$

The heavy quark binding energies, (5.2) and (5.3), were computed with the quark masses (5.50), using the experimental masses $M_{\Lambda_b} = 5.641 GeV$, $M_{\Lambda_c} = 2.285 GeV$, $M_{\Xi_c} = 2.47\, GeV$ and our prediction $M_{\Xi_b} = 5.77\, GeV$. The averages of the two estimates for each of the decays is

$$\overline{\Lambda}_\Lambda = 0.84\, GeV\ , \qquad \overline{\Lambda}_\Xi = 1.00\, GeV\ . \tag{5.51}$$

In figure 5.8 we show the physical form factors computed using the expansion (5.45), and in appendix D we report the numerical results for the form factors. Apart, from the difference near zero recoil, the form factors for Λ_b and Ξ_b are indistinguishable away from the point $\omega = 1$. The reader should note that the data used to calculate the Isgur-Wise function have $\omega \leq 1.2$. Consequently, and also because we use the expansion (5.45) to describe $\xi_{QQ'}$, the extrapolation of the physical form factors to larger values of the velocity transfer suffers from large statistical errors. These larger errors are a measure of the $(\omega - 1)^2$ effects in the Isgur-Wise function. For $\omega \geq 1.3$ the extrapolated values for form factors become compatible with zero within one standard deviation, and our data is no longer reliable.

5.7.2 Decay Rates

The decay rates can be computed using the helicity formalism. Following reference [85], we define the amplitudes

$$\begin{aligned} H^{V,A}_{\frac{1}{2},0} &= \sqrt{\frac{2M_{\Lambda_b}M_{\Lambda_c}(\omega \mp 1)}{M^2_{\Lambda_b} + M^2_{\Lambda_c} - 2M_{\Lambda_b}M_{\Lambda_c}\omega}} \\ &\quad \left((M_{\Lambda_b} \pm M_{\Lambda_c}) F_1^{V,A} \pm (\omega \pm 1)\left(M_{\Lambda_c} F_2^{V,A} + M_{\Lambda_b} F_3^{V,A} \right) \right)\ , \qquad (5.52) \\ H^{V,A}_{\frac{1}{2},1} &= -2\sqrt{M_{\Lambda_b}M_{\Lambda_c}(\omega \mp 1)}\, F_1^{V,A} \qquad (5.53) \end{aligned}$$

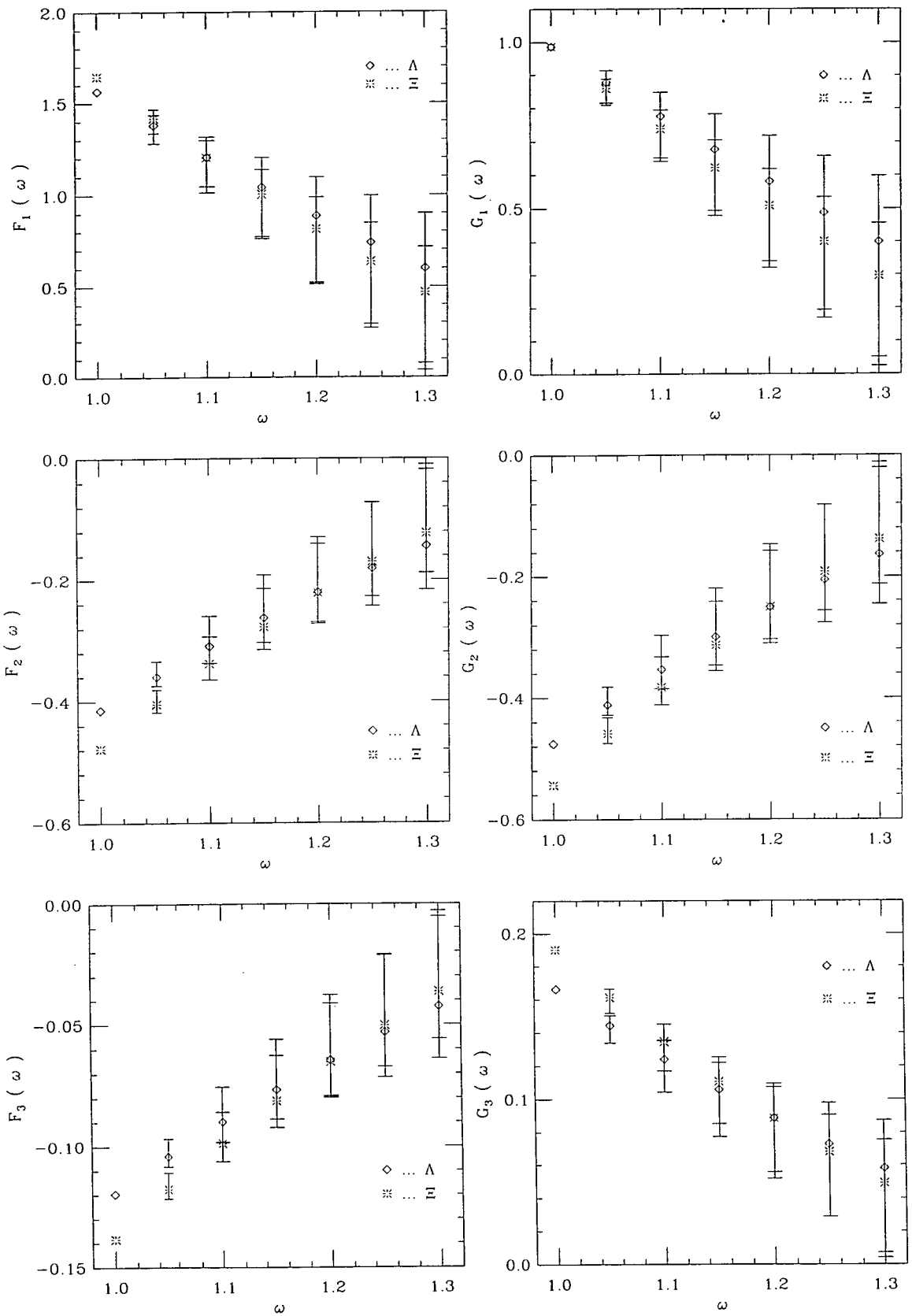

Figure 5.8: Physical form factors for decays $\Lambda_b \to \Lambda_c\, l\, \overline{\nu}$ and $\Xi_b \to \Xi_c\, l\, \overline{\nu}$. The form factors were computed expanding the Isgur-Wise function in $\omega - 1$ up to the linear term.

where $F_i^V = F_i(\omega)$, $F_i^A = G_i(\omega)$, the upper sign holds for the vector current and the lower sign for the axial current. In H_{λ_2,λ_W}, λ_W refers to the helicity of the current ($\lambda_W = 0$ for a longitudinal polarised W and $\lambda_W = \pm 1$ for a transverse polarised W), and λ_2 the helicity of the charm baryon. For convenience, we introduce the notation

$$H_{\lambda_2,\lambda_W} = H^V_{\lambda_2,\lambda_W} + H^A_{\lambda_2,\lambda_W} \ , \tag{5.54}$$

and define the transverse, H_T, and longitudinal, H_L, amplitudes as

$$H_T = |H_{\frac{1}{2},1}|^2 + |H_{-\frac{1}{2},-1}|^2 \ , \tag{5.55}$$

$$H_L = |H_{\frac{1}{2},0}|^2 + |H_{-\frac{1}{2},0}|^2 \ . \tag{5.56}$$

In (5.55) and (5.56), the missing amplitudes can be computed using the following relations

$$H^V_{-\lambda_2,-\lambda_W} = H^V_{\lambda_2,\lambda_W} \ , \qquad H^A_{-\lambda_2,-\lambda_W} = -H^A_{\lambda_2,\lambda_W} \ . \tag{5.57}$$

The partial decay rate for longitudinal and transverse off-shell W boson are given by

$$\frac{d\Gamma_L}{d\omega} = \frac{G_F^2}{(2\pi)^3} |V_{cb}|^2 \frac{q^2 M_{\Lambda_c}^2 \sqrt{(\omega+1)(\omega-1)}}{12 M_{\Lambda_b}} H_L \ , \tag{5.58}$$

$$\frac{d\Gamma_T}{d\omega} = \frac{G_F^2}{(2\pi)^3} |V_{cb}|^2 \frac{q^2 M_{\Lambda_c}^2 \sqrt{(\omega+1)(\omega-1)}}{12 M_{\Lambda_b}} H_T \ , \tag{5.59}$$

where G_F is the Fermi constant, V_{cb} is appropriate element of the Cabibbo-Kobayashi-Maskawa matrix and $q^2 = M_{\Lambda_b}^2 + M_{\Lambda_c}^2 - 2M_{\Lambda_b} M_{\Lambda_c} \omega$. The total decay rate is given by

$$\frac{d\Gamma}{d\omega} = \frac{G_F^2}{(2\pi)^3} |V_{cb}|^2 \frac{q^2 M_{\Lambda_c}^2 \sqrt{(\omega+1)(\omega-1)}}{12 M_{\Lambda_b}} (H_L + H_L) \ . \tag{5.60}$$

The analysis of the decay $\Xi_b \to \Xi_c \, l \, \overline{\nu}$ is similar to b baryon decay, and the above relations have a direct translation for the Ξ_b semileptonic decay.

The decay rates for both b and c baryons can be estimated in a model-independent way, if the form factors $F_i(\omega)$ and $G_i(\omega)$ are known. Our estimates for the form

$\Lambda_b \to \Lambda_c$	ω	1.09	1.11	1.15	1.20	1.24	1.31
	Γ^{part}	$0.44 \pm^{4}_{6}$	$0.59 \pm^{7}_{10}$	$0.9 \pm^{1}_{2}$	$1.1 \pm^{3}_{4}$	$1.4 \pm^{4}_{5}$	$1.6 \pm^{6}_{7}$
$\Xi_b \to \Xi_c$	ω	1.10	1.11	1.15	1.21	1.25	1.31
	Γ^{part}	$0.58 \pm^{4}_{7}$	$0.71 \pm^{7}_{11}$	$1.0 \pm^{1}_{2}$	$1.3 \pm^{3}_{4}$	$1.5 \pm^{4}_{5}$	$1.6 \pm^{5}_{6}$
$\Lambda_b \to \Lambda_c$	ω	1.09	1.11	1.15	1.20	1.24	1.31
	Γ_L^{part}	$0.17 \pm^{2}_{2}$	$0.23 \pm^{3}_{4}$	$0.37 \pm^{6}_{10}$	$10.5 \pm^{1}_{2}$	$0.6 \pm^{2}_{3}$	$0.8 \pm^{4}_{4}$
$\Xi_b \to \Xi_c$	ω	1.10	1.11	1.15	1.21	1.25	1.31
	Γ_L^{part}	$0.23 \pm^{2}_{3}$	$0.30 \pm^{3}_{5}$	$0.43 \pm^{6}_{10}$	$0.6 \pm^{1}_{2}$	$0.7 \pm^{2}_{3}$	$0.8 \pm^{3}_{4}$
$\Lambda_b \to \Lambda_c$	ω	1.09	1.11	1.15	1.20	1.24	1.31
	Γ_T^{part}	$0.27 \pm^{2}_{4}$	$0.35 \pm^{4}_{6}$	$0.50 \pm^{8}_{12}$	$0.6 \pm^{1}_{2}$	$0.7 \pm^{2}_{3}$	$0.8 \pm^{3}_{3}$
$\Xi_b \to \Xi_c$	ω	1.10	1.11	1.15	1.21	1.25	1.31
	Γ_T^{part}	$0.34 \pm^{3}_{4}$	$0.42 \pm^{4}_{6}$	$0.55 \pm^{7}_{11}$	$0.7 \pm^{1}_{2}$	$0.7 \pm^{2}_{2}$	$0.8 \pm^{2}_{3}$

Table 5.8: Partial decay rates for the Λ and Ξ semileptonic decays for various ω. The data shown refers to $\Gamma/|V_{cb}|^2$ and is in units of $10^{13}s^{-1}$.

factors are reliable only up to $\omega \sim 1.2 - 1.3$. However, in the Λ_b decay ω takes values from 1 up to ~ 1.44, whereas for the Ξ_b decay ω is in the range 1 to ~ 1.38. This means that we can not compute exactly the decay rates for both decays. We thus define the partially-integrated decay rate,

$$\Gamma_i^{part}(\omega) = \int_1^{\omega} d\omega \frac{d\Gamma_i}{d\omega} , \tag{5.61}$$

and study its behaviour as a function of ω - see figure 5.9 and table 5.8.

A comparisation of our results with experiment is not yet possible. The semileptonic decay of Λ_b was observed by several experimental groups [119]-[122], but a measurement of the decay rate is not yet available. On the other hand, there have been several theoretical estimates of decay rate. A comparisation of our calculation with the numbers computed with infinite momentum frame wave functions (IMF), a quark model approach with a harmonic oscillator potential (QM), dipole form factors (Dipole) and the free quark model (FQM) (see [85] for references) is given in figure 5.9, where the predictions are quoted for $\omega = \omega_{max}$ of the transition. Despite not being able to compute the decay rate, our predictions seem to be compatible with all other estimates, except the FQM.

Finally, we note that once the form factors are known, a number of interesting

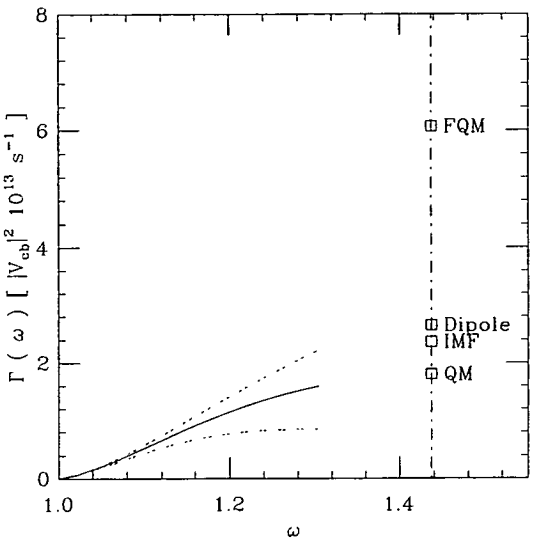

Figure 5.9: Total decay rate for the Λ_b decay. A comparisation with several model estimates is shown at the end-point.

quantities, such us the polarisation of the W-b coupling, asymmetry parameters, ratio of longitudinal to transverse rates, can be computed. However, all these quantities are sensitive to $(\omega - 1)^2$ and they are beyond the precision reached in this study.

5.8 Summary and Conclusions

In this chapter, we computed the Isgur-Wise function for the semileptonic decays $\Lambda_b \to \Lambda_c l\overline{\nu}$ and $\Xi_b \to \Xi_c l\overline{\nu}$. This involves a combined study of two-point and three-point correlation functions. Despite the relatively small number of configurations used in the simulation, the quality of the Monte Carlo data for the dominant form factors allows a determination of the Isgur-Wise function with statistical errors $\mathcal{O}(10-15\%)$. Within our statistical precision, we did not observe $1/m_Q$ effects in the Isgur-Wise function. This suggests that these corrections are small, even at the charm quark mass. Concerning the dependence on the heavy quark mass, a similar conclusion was obtained for the meson Isgur-Wise function [116, 118]. For the heavy-light mesons, the studies of the Isgur-Wise function demonstrate that the dependence on the light quark mass is not negligible, and a similar behaviour for $\xi_{QQ'}(\omega)$ with the light quark mass is expected. To quantify the light quark dependence, we measure the slope of $\xi_{QQ'}(\omega)$ at zero recoil, ρ^2, for the functions

describing the Λ_b and Ξ_b decays. Due to the large statistical errors introduced by the extrapolation, the data does not distinguish in a clear way the two decays.

Finally, using the expansion (5.45), we compute the physical form factors describing the Λ_b and Ξ_b decays and study the partially-integrated decay rates (5.61) as a function of the upper limit of integration.

The main conclusion from the work presented in this chapter is the feasibility of computing the baryonic Isgur-Wise function with lattice methods. Our simulation uses a relatively small number of gauge configurations, 60, and this limits seriously the type of effects which we are able to measure. Thus, we see our calculation as a preliminary study towards a high statistics simulation. A new simulation should also involve larger number of light quark combinations. Eventually, this will allow a proper study of the chiral limit of the form factors.

Chapter 6

Stochastic Gauge Fixing on the Lattice

The generating functional for the Green functions of gauge theories on the lattice is a well-defined mathematical object, and gauge fixing is not required by the quantization procedure. However, in QCD, the fundamental fields are the quark and gluon fields. These fields are gauge dependent and, consequently, the quark and gluon propagators are defined only if a gauge is chosen. Furthermore, without gauge fixing one cannot investigate the Green functions of individual quark and gluon fields. The study of this functions is interesting *per se* as they can bring some light into our understanding of the strong interactions. For example, from the quark and gluon propagators, one expects to achieve a better comprehension of the mechanisms of confinement and chiral symmetry breaking. On the other hand, the study of the quark-gluon vertex can be helpful for understanding the physics of pomeron exchange. In addition, the quark and/or gluon vertex allows a determination of the running QCD coupling from first principles.

The investigation of the Green functions of individual quark and gluon fields requires gauge fixing. However, the interest of gauge fixing goes beyond the above mentioned applications. For example, by choosing a gauge, one can compute, nonperturbatively, renormalisation constants for composite operators, by sandwiching these operators between quark states.

The lattice allows for a study of the nonperturbative aspects of gauge theories. These involve large field amplitudes and, as show by Gribov in [52], for this case the usual local gauge conditions are satisfied more than once in each gauge orbit. Consequently, the traditional continuum gauge conditions, when applied to lattice gauge theories, led to ambiguities which require modifying the generating functional in order to define the quantum theory.

A nonperturbative gauge fixing method was suggested by Zwanziger [55] and,

simultaneously, by Parrinello and Jona-Lasinio [56]. The application of this gauge fixing method to Lattice Gauge Theories was proposed by Fachin and Parrinello [123].

Apart from solving the problem of the Gribov ambiguity, another property of this new method is that it allows a study of the gauge dependence aspects of the correlation functions in a very simple way. The Zwanziger-Parrinello-Jona-Lasinio gauge fixing method introduces a whole family of nonperturbative gauge conditions, distinguishd by one gauge fixing parameter. Therefore, by smoothly varying this parameter, one can observe how the correlation functions change within this family of gauges.

In this chapter we report a numerical study [124] of the gauge fixing algorithm proposed by Fachin and Parrinello. In particular, we study the gluon propagator and its dependence on the gauge fixing parameter.

6.1 Stochastic Gauge Fixing

In this section we introduce the Zwanziger-Parrinello-Jona-Lasinio gauge fixing method. First, we discuss the method in the continuum and then show how it can be implemented for lattice gauge theories.

6.1.1 The Continuum Formulation

According to Singer [53], it is impossible to find a local continuous and unambiguous gauge fixing condition for any $SU(N)$ gauge theory defined on the four-sphere, S_4. Therefore, the nonperturbative definition of a gauge requires adopting a nonlocal gauge condition. Let us describe the gauge fixing method introduced in [55] and [56].

The formal expression for the partition function of QCD is given by

$$Z = \int \mathcal{D}A_\mu \, \mathcal{D}\overline{\psi} \, \mathcal{D}\psi \, e^{-S_{QCD}[A_\mu, \psi, \overline{\psi}]} \, , \tag{6.1}$$

where $A_\mu = \sum_a T^a A^a_\mu$ is the the gluon field and ψ, $\overline{\psi}$ are generic fermion fields.

In order to define a nonperturbative gauge condition, we introduce the following

gauge invariant function

$$I[A] = \int \mathcal{D}g\, e^{-F[A^g]}\,, \tag{6.2}$$

where A^g is the gauge field transformed from A by the gauge transformation $g(x) \in SU(3)$ and F is a functional of the gluon field. The functional $F[A]$ is any function of A such that the integral $I[A]$ exists. Since we are interested in studying gauge dependent correlation functions we also demand $F[A]$ not to be a gauge invariant function of A. Then, gauge invariance of $I[A]$ follows from invariance of the measure under the gauge group.

Following a similar procedure to the Faddeev-Popov quantization method [1], we rewrite (6.1) in the following way

$$Z_{mod} = \int \mathcal{D}A\, e^{-S_{QCD}[A]} \int \mathcal{D}g\, \frac{e^{-F[A^g]}}{I[A]}\,. \tag{6.3}$$

Then, the expectation value of an operator, $O[A]$, is written as

$$\langle O \rangle_{mod} = Z_{mod}^{-1} \int \mathcal{D}A\, e^{-S_{QCD}[A_\mu]} \int \mathcal{D}g\, O[A^g]\, \frac{e^{-F[A^g]}}{I[A]}\,. \tag{6.4}$$

Interchanging the order of integration and making a change of variables from A to A^g one arrives at

$$Z_{mod} = \int \mathcal{D}g \int \mathcal{D}A\, e^{-S_{QCD}[A]}\, \frac{e^{-F[A]}}{I[A]}\,, \tag{6.5}$$

$$\langle O \rangle_{mod} = Z_{mod}^{-1} \int \mathcal{D}g \int \mathcal{D}A\, O[A]\, e^{-S_{QCD}[A]}\, \frac{e^{-F[A]}}{I[A]}\,. \tag{6.6}$$

In (6.5) and (6.6) the integrand is independent of g. Therefore, the integral over the gauge group results in an overall constant which can be absorbed by redefining the normalization of the generating functional. In this way, one obtains

$$Z_{mod} = \int \mathcal{D}A\, e^{-S_{QCD}[A]}\, \frac{e^{-F[A]}}{I[A]}\,, \tag{6.7}$$

$$\langle O \rangle_{mod} = Z_{mod}^{-1} \int \mathcal{D}A\, O[A]\, e^{-S_{QCD}[A]}\, \frac{e^{-F[A]}}{I[A]}\,, \tag{6.8}$$

[1] Fixing a gauge is an operation related only to the gluon fields. For this reason, we omit any reference to the fermionic fields in this section.

for the generating functional of the theory and the expectation value of O, respectively.

The quantum theory defined by (6.7) and (6.8) avoids the problem of the Gribov copies by introducing a normalized probability distribution,

$$\frac{e^{-F[A]}}{I[A]} , \tag{6.9}$$

for each of the gauge orbits. Now, the choice of $F[A]$ is equivalent to the choice of gauge condition in the usual continuum formulation. Thus, (6.8) allows the study of the gluon and quark propagators as well as any other gauge dependent operators.

In principle, the functional which defines the probability distribution over the gauge orbits, $F[A]$, can be any functional which is not gauge invariant and makes the integrals (6.7) and (6.8) well-defined. Among the possible choices, the particular case

$$F[A] = M^2 \|A\|^2 , \tag{6.10}$$

where M^2 is the gauge fixing parameter with dimensions of mass squared, has been studied in some detail [55, 56, 125].

For (6.10) one can prove that F reaches an absolute minimum in each gauge orbit, i.e. the region of these absolute minima of F,

$$\Omega = \{A : F[A^g] \geq F[A], \forall g \in SU(N)\} , \tag{6.11}$$

intersects all gauge orbits [126, 127]. Moreover, if one assumes that the absolute minimum in Ω is unique one can prove that the usual minimal Landau gauge,

$$\partial_\mu A_\mu = 0 \qquad FP[A] > 0 , \tag{6.12}$$

where $FP[A]$ is the Faddeev-Popov determinant for the configuration A_μ, is recovered in the limit $M^2 \to \infty$ [56]. For this reasons, the choice (6.10) turns out to be most convenient.

The perturbative analysis of the theory defined by (6.7), (6.8) and (6.10) was

done by Fachin [125]. He found that the gluon propagator has the following decomposition in terms of longitudinal and transverse components

$$D^{ab}_{\mu\nu}(k) = \delta^{ab}\,[\,\frac{1}{k^2}P^T_{\mu\nu}(k) + \frac{1}{M^2}\,P^L_{\mu\nu}(k)\,]\;, \tag{6.13}$$

and that there are no radiative corrections to the longitudinal part of propagator. The latter result is valid to all orders in perturbation theory. Furthermore, Fachin was able to prove that, at least to second order in the strong coupling constant, the vacuum expectation value of gauge invariant observables does not depend on the gauge fixing parameter, M^2. This result confirms that the global gauge condition as defined by $F[A] = M^2\,\|A\|^2$ leads to a consistent quantization of gauge theories.

6.1.2 The Lattice Formulation

The gauge fixing method discussed in the previous section is easily generalizable to Lattice Gauge Theories. In order to define the procedure used in our numerical simulation, we repeat the formulation of the gauge fixing method applied to lattice theories [123].

Similarly to the continuum formulation, on the lattice we start from the Wilson's lattice gauge model, defined by the gauge invariant partition function (2.33),

$$Z_W = \int \mathcal{D}U\, e^{-S_W}\;; \tag{6.14}$$

for notation see chapter 2. Then, the expectation value of an observable $O[U]$ is given by

$$\langle O\rangle = Z_W^{-1}\int \mathcal{D}U\, O[U]\, e^{-S_W}\;. \tag{6.15}$$

In order to define a nonperturbative lattice gauge-fixing, we modify the partition function (6.14) and (6.15) including an additional integration over the gauge group

$$Z_{mod} = \int \mathcal{D}U\, e^{-S_W}\int \mathcal{D}g\,\frac{e^{-F[U^g]}}{I[U]}\;, \tag{6.16}$$

$$\langle O\rangle_{mod} = Z^{-1}_{mod}\int \mathcal{D}U\, e^{-S_W}\int \mathcal{D}g\, O[U^g]\,\frac{e^{-F[U^g]}}{I[U]}\;, \tag{6.17}$$

where $F[U^g]$ is a generic function of the gauge transformed links,

$$U^g_\mu(x) = g(x)\, U_\mu(x)\, g^\dagger(x+\hat{\mu}) \ , \tag{6.18}$$

and $I[U]$ is defined as

$$I[U] = \int \mathcal{D}g\, e^{-F[U^g]} \ . \tag{6.19}$$

As in the case of the continuum formulation, $I[U]$ is gauge invariant. However, unlike what happens in the continuum, $Z_{mod} = Z_W$ is a finite quantity because the group of gauge transformations on a finite lattice is compact. Thus, one can rewrite the new definition for the expectation value of an observable as

$$\langle O \rangle_{mod} = Z_W^{-1} \int \mathcal{D}U\, e^{-S_W} \int \mathcal{D}g\, O[U^g] \frac{e^{-F[U^g]}}{I[U]} \ . \tag{6.20}$$

Since F is chosen not to be invariant under a gauge transformation, with the definition (6.20), the expectation value of a gauge dependent operator $O[U]$ does not necessarily vanish. If $O[U]$ is gauge invariant the Wilson average (6.15) and (6.20) coincide, so that $\langle O \rangle_{mod}$ defines a consistent, nonperturbative gauge-fixing procedure.

The definition (6.20) suggests a natural way of performing the average in a Monte Carlo simulation. By introducing the gauge invariant average

$$\langle O[U] \rangle_G = \int \mathcal{D}g\, O[U^g] \frac{e^{-F[U^g]}}{I[U]} \ , \tag{6.21}$$

the modified expectation value is written as

$$\langle O \rangle_{mod} = Z_W^{-1} \int \mathcal{D}U\, \langle O[U] \rangle_G\, e^{-S_W} = \langle\, \langle O[U] \rangle_G \,\rangle_W \ , \tag{6.22}$$

where $\langle\,\rangle_W$ denotes the usual Wilson average. The above expression suggests that the average of a gauge dependent observable can be computed in two steps. First, for each configuration U we perform the average over gauge-related configurations, obtaining the gauge invariant function $\langle O[U] \rangle_G$. Then, one takes the average of $\langle O[U] \rangle_G$ *a la* Wilson.

This suggests the following numerical algorithm :

1. generate a set of link configurations $\{U^{(1)}, \cdots, U^{(n)}\}$ weighted by the Wilson action, for some value of β;

2. for each of the Wilson configurations, $U^{(k)}$, generate a set of gauge-related configurations, $\{U^{(k;1)}, \cdots, U^{(k;m)}\}$, by a second Monte Carlo which updates the group elements using $\exp(-F[U^g])$ as weight function. Then, compute the group average $\langle O[U]\rangle_G$.

3. Finally, compute the expectation value of the observable by averaging over the group averages,

$$\langle O\rangle_{mod} = \frac{1}{n}\sum_{i=1}^{n}\langle O[U^{(i)}]\rangle_G \,. \tag{6.23}$$

Of course, the viability of the algorithm depends on the performance of the Monte Carlo defined on step 2.

On the lattice, the analogue of (6.10) is given by

$$F[U^g] = -\beta\, M^2 \sum_{x,\mu} \Re\,\mathrm{Tr}\,[\, g(x)U_\mu(x)g^\dagger(x+\hat{\mu})\,] \,. \tag{6.24}$$

With this choice of the distribution function, the Monte Carlo defined in step 2 of the algorithm simulates the analogue of a $SU(3)$ Higgs model with zero bare mass and zero four-interaction bare coupling. On the other hand, the Monte Carlo for the average over the gauge-related configurations can be understood in the language of Statistical Mechanics, where (6.24) plays the role of an effective Hamiltonian and the parameter $1/\beta M^2$ determines the effective temperature of the system. From this point of view, the system defined by F is a classical 4-dimensional $SU(3)$ spin-glass, where $g(x)$ are to be interpreted as $SU(3)$-valued spins, with nearest-neighbour $SU(3)$ couplings. For small values of β and M^2, i.e. in the high temperature regime of the equivalent statistical system, the numerical results can be compared with analytical ones, derived from strong coupling expansions [123]. For large values of β, the continuum weak coupling expansion performed by Fachin [125] can be useful to investigate the continuum limit of our lattice system.

In the following we refer to the Monte Carlo for the average over the gauge-related configurations as the gauge fixing Monte Carlo (GFMC).

6.2 Performance of the Algorithm and Thermodynamics

The viability of the gauge fixing method described above depends on the performance of the GFMC. In this section we describe a study of GFMC using an 8^4 lattice for the numerical simulations.

Before analysing quenched QCD, we investigated the simpler system described by the effective Hamiltonian (6.24) with all links variables set to the identity. The resulting system has the form of a four-dimensional $SU(3)$ spin model with ferromagnetic couplings. We hope to achieve a first understanding of GFMC from studying the above mentioned "spin-system". Besides, similar three-dimensional models have been discussed previously [128] and a comparisation of results provides another test of our code. Because our goal is to study QCD, we will not give here a detailed description of the results for the "ferromagnetic spin-model".

For the simulation of the above system, the group configurations were generated by Cabibbo-Marinari pseudo-heat-bath updates performed on three $SU(2)$ subgroups. Two observables,

$$\langle E \rangle_G = \frac{\langle \frac{F[1^g]}{\beta M^2} \rangle_G}{N_C N_L} , \tag{6.25}$$

$$C_G = \frac{1}{\beta M^2} \frac{dE}{d(\beta M^2)} = \langle E^2 \rangle_G - \langle E \rangle_G^2 , \tag{6.26}$$

where $N_C = 3$ and N_L is the number of lattice points, were monitored. Figure 6.1 shows the results of the simulation, including a comparison of a strong coupling expansion up to next-to-leading order for $\langle E \rangle_G$,

$$\langle E \rangle_G = \frac{\beta M^2}{2} + \frac{(\beta M^2)^2}{8} , \tag{6.27}$$

with the Monte Carlo data. We observed that $\langle E \rangle_G$ and C_G thermalized typically before the 1000 sweeps and no evidence of metastable states were found for the range of temperatures considered, $0 < \beta M^2 < 2.6$. The small statistical errors for $\langle E \rangle_G$ reported in figure were computed by a jackknife procedure - see [107] for definitions.

From the analysis of figure 6.1 we conclude that the "ferromagnetic spin-system"

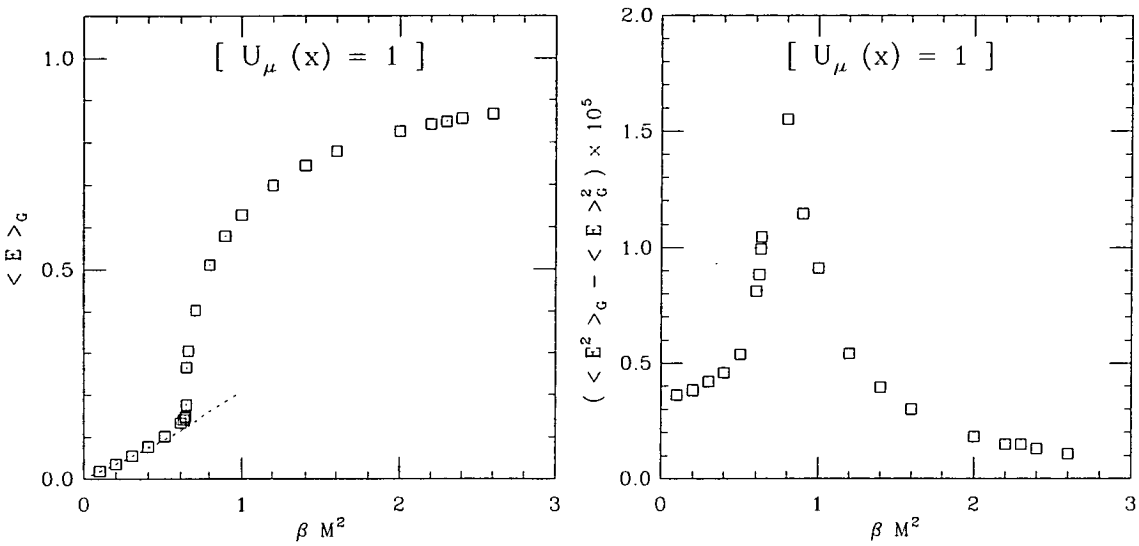

Figure 6.1: $\langle E \rangle_G$ and C_G vs. βM^2. The dotted line are the results of the strong coupling expansion for $\langle E \rangle_G$. The observables were computed using 2000 group configurations.

can be in one of two phases, which seem to be separated by a first-order phase transition. The behaviour of the specific heat, C_G, with βM^2 suggests that the first-order phase transition occurs at $\beta M^2 = 1/T = 0.635$. The equivalent three-dimensional system was investigated by Kogut and collaborators [128]. They found a similar phase-diagram and observed a first-order transition separating the high- and low-temperature phases.

Let us now discuss the simulation for QCD. For this simulation, we first generated 21 gauge configurations, weighted by the Wilson action, using a hybrid-overrelaxed algorithm, where both the Cabibbo-Marinari (CM) pseudo-heat-bath and overrelaxed (OR) updates were performed on three SU(2) subgroups. Next, for each link configuration we produced an ensemble of gauge-related configurations, weighted by the Boltzmann factor $\exp(-F[U^g])$. This was done for many different values of βM^2 and again the GFMC sweep was a combination of CM and OR updates.

In order to study the thermalization in the GFMC, we did a detailed analysis of one gauge configuration. Recalling the analogy with statistical mechanics, one expects the Monte Carlo to perform differently in the low and high temperature

regions. In particular, for low temperatures one expects metastable states to appear. These metastable states are related to local minima of the potential energy function and, in field theory, they can be connected with Gribov copies[2]. From the point of view of the algorithm, one has to make sure that, for a chosen range of values of M^2, the stochastic process can efficiently visit all the states and does not get trapped in a local minimum. To look for these metastable states, we run the GFMC code using at least four different seeds for the random number generator for each βM^2 value, and study the evolution of the average energy of the system,

$$\langle E[U] \rangle_G = \frac{\langle \frac{F[U^g]}{\beta M^2} \rangle_G}{N_C N_L} , \tag{6.28}$$

and the zero-momentum gluon propagator. The definition of the zero-momentum gluon propagator is given on next section. For the chosen configuration, the GFMC shows a pattern which is, in all respects, similar to the behaviour observed in the system described previously, i.e. again the system has two different phases separated by a first-order transition. As far as metastable states are concerned, we found no evidence for them in the average energy. However, for the zero-momentum propagator we saw long-lived metastable states in the low temperature regime. In figure 6.2 we show an example of such metastable states. For the range of gauge fixing parameter considered, $0 \leq \beta M^2 \leq 2.4$, we were able to improve the performance of the algorithm by changing the number of CM and OR updates in each GFMC sweep. For the high temperature region, $\beta M^2 \leq 0.8$, we found that by using a GFMC sweep composed of one CM and two OR updates no metastable were observed in both observables. On the other hand, to have an efficient algorithm in the low temperature region, $\beta M^2 \geq 0.8$, we had to increase the number of OR sweeps vs. CM updates in each GFMC sweep. We observed that by defining a GFMC sweep as one CM update and ten OR sweeps, the metastable states occurred only in the first 1000 to 2000 sweeps of the Monte Carlo simulation.

To gain further confidence in the performance of the GFMC, we measured the integrated autocorrelation time, τ, from the thermalised zero-momentum gluon propagator data. We choose to use the zero-momentum gluon propagator instead

[2]Note that the usual implementation of the Landau Gauge on the lattice is done by minimizing the function $F[U^g]$ - see for example [129, 130].

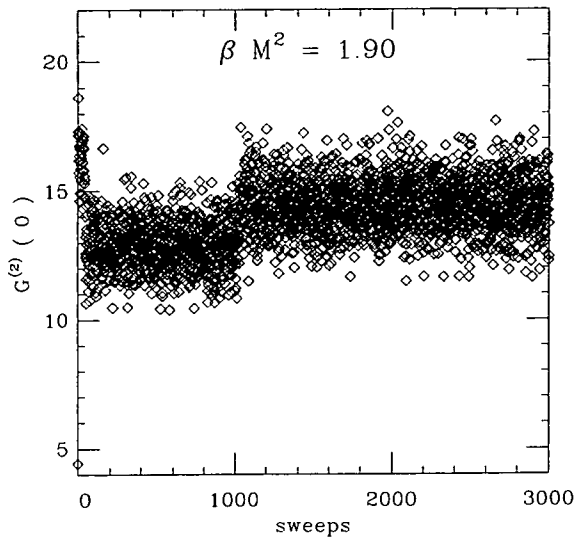

Figure 6.2: Evolution of zero momentum gluon propagator in the GFMC.

of the average energy because the latter quantity, being associated with a local operator, requires less Monte Carlo updates between independent samples and a measure of the autocorrelation time from $\langle E \rangle_G$ would underestimate τ. On the other hand, the dynamics of the zero-momemtum gluon propagator is associated with the long wavelength modes of the system. Therefore, one expects to get a more realistic estimate of the integrated autocorrelation time from the zero-momentum gluon propagator.

To measure τ we follow the procedure given in [72]. Let $G_0(i)$, $i = 1, \cdots, m$ be the thermalized data for the zero momentum gluon propagator. First, we define

$$\hat{G}_0(j) = \frac{1}{m-j} \sum_{i=1}^{m-j} (G_0(i) - \langle G_0 \rangle)(G_0(i+j) - \langle G_0 \rangle) , \tag{6.29}$$

where $\langle G_0 \rangle$ is the propagator mean value. Then, we compute

$$\rho(i) = \frac{\hat{G}_0(i)}{\hat{G}_0(0)} . \tag{6.30}$$

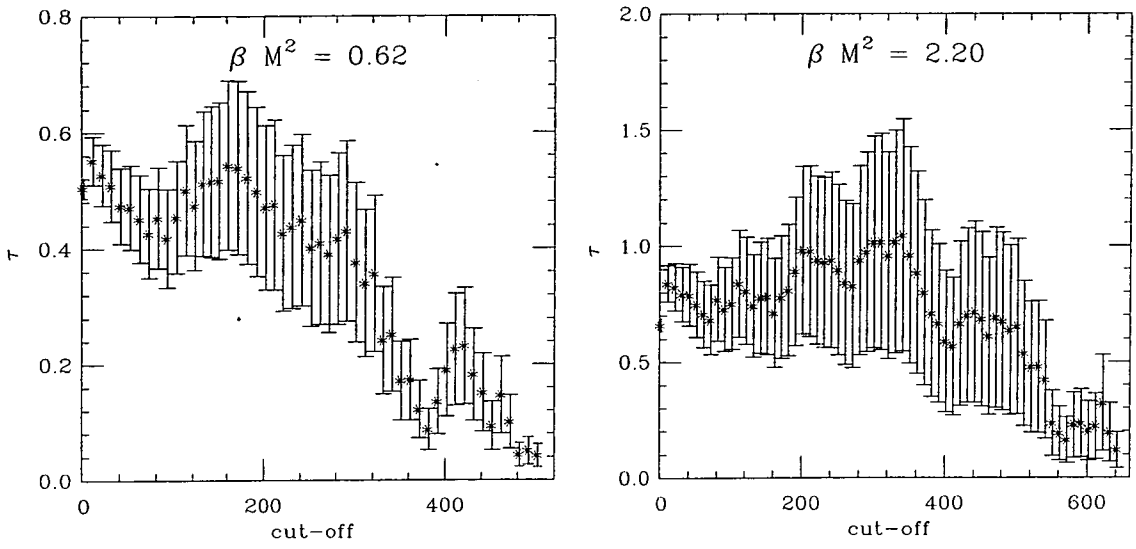

Figure 6.3: Autocorrelation times measured from the zero momemtum gluon propagator.

Finally, we study the integrated autocorrelation,

$$\tau = \frac{1}{2} + \sum_{i=1}^{s} \rho(i) \,, \tag{6.31}$$

as a function of the cut-off s and take its maximum value as the estimate of the integrated autocorrelation time. The errors on τ were computed using

$$\sigma(\tau) = \sqrt{\frac{2(2s+1)}{m}}\,\tau \,, \tag{6.32}$$

which gives the correct answer for $\tau \ll s \ll m$ [72]. Two examples of the autocorrelation time as function of the cut-off are given in figure 6.3.

After studying the GFMC for other link configurations, we quote the following values

$$\tau = \begin{cases} 1 & , \quad \beta M^2 < 0.8 \\ 4 & , \quad \beta M^2 \geq 0.8 \end{cases} \tag{6.33}$$

as a safer upper bound for the autocorrelation time.

βM^2	N_c (E)	N_g (E)	N_c (G(0))	N_g (G(0))
0.20	8	17	8	16
0.40	8	17	8	15
0.60	8	17	8	17
0.62	8	17	8	16
0.66	8	17	8	15
0.70	7	17	7	15
others	21	4000	21	60

Table 6.1: Number of link configurations N_c and gauge-related configurations N_g used in the evaluation of average energy and zero-momentum gluon propagator.

The detailed analysis performed on the first configuration, was later repeated for other link configurations. We found that the general behaviour and the conclusions drawn for the first configuration also apply to the other link configurations.

In summary, we were able to tune the algorithm so as to obtain reasonable evidence that for $\beta M^2 \leq 2.4$ the GFMC process could thermalise correctly.

In table 6.1 we report the statistics used in the calculation of the average energy,

$$\langle E \rangle = \langle \langle E \rangle_G \rangle_W , \tag{6.34}$$

specific heat,

$$C_E = \langle \langle E^2 \rangle_G \rangle_W - \langle \langle E \rangle_G \rangle_W^2 , \tag{6.35}$$

and zero-momentum gluon propagator - see also figures 6.4 and 6.5. Statistical errors, obtained by the jackknife method, were computed for $\langle E \rangle$ and $G^{(2)}(0)$ and are included in the corresponding figures. In figure 6.5, the solid line corresponds to the result of Landau gauge fixing the 21 link configurations by minimizing $F[U^g]$ and the dashed lines are the jackknife estimates of the errors on $G^{(2)}_{Landau}(0)$. We found $G^{(2)}_{Landau}(0) = 29.4 \pm 1.5$. Again, the behaviour observed is similar to the behaviour of the first system analysed. In figures 6.4-6.5 one distinguishes two phases. A strong coupling regime, $\beta M^2 < 0.8$, and a weak coupling one, for $\beta M^2 \geq 0.8$. The data for the specific heat suggest that a phase transition of the first order, at $\beta M^2 = 1/T = 0.8$, separates the two regions. We note the

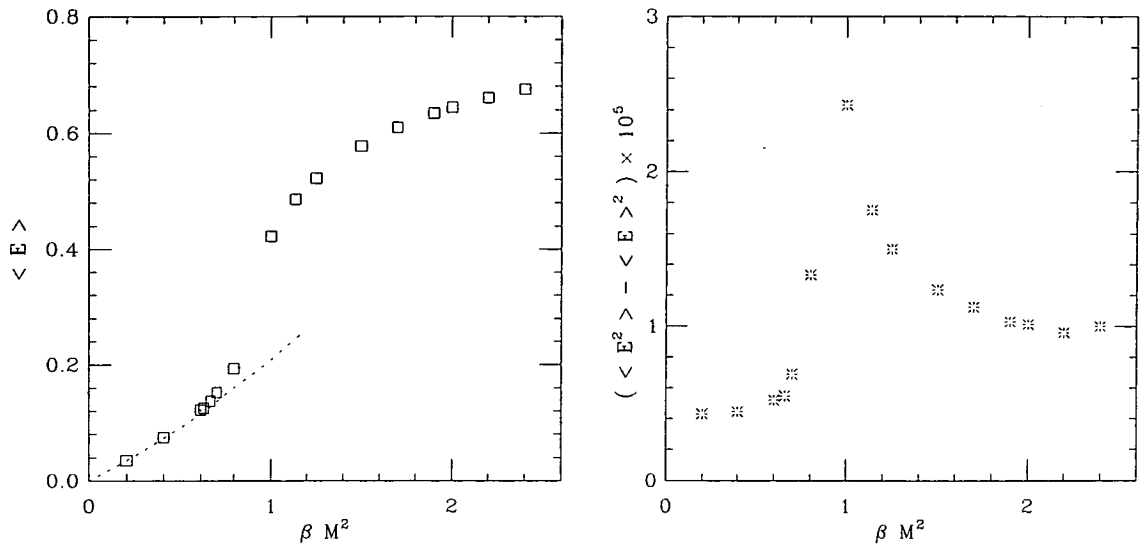

Figure 6.4: Energy and specific heat vs. βM^2. For the energy the dotted line is the result of a next to leading order strong coupling expansion.

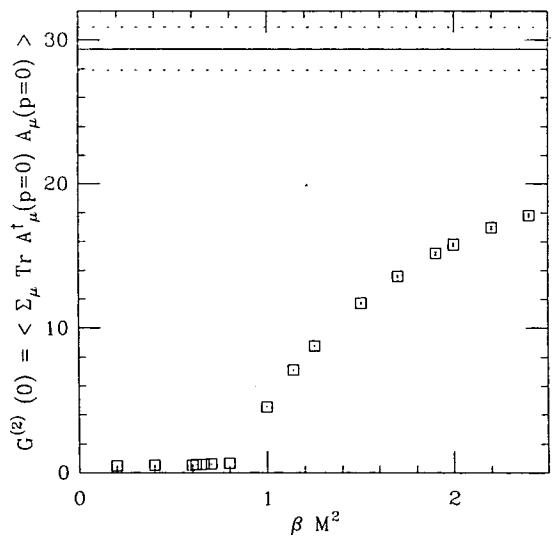

Figure 6.5: Zero momentum gluon propagator vs. βM^2. The figure includes the result for the Landau gauge.

excellent agreement from the strong coupling expansion[3] (6.27) and the numerical simulation up to $\beta M^2 \approx 0.7$.

6.3 Gauge Dependence of the Gluon Propagator

As the first application of the Zwanziger-Parrinello-Jona-Lasinio gauge fixing method us modified to the lattice by Fachin and Parrinello, we study the gluon propagator and its dependence on the gauge fixing parameter, M^2.

The gluon propagator is one of the simplest observables which can be studied by lattice techniques. This quantity has been the object of previous numerical investigations within the minimal Landau gauge (6.12) - see for example [129, 130]. In these studies the gauge fixing procedure involves the minimization of $F[U^g]$ for each gauge link. Since the minimization algorithms which are available only identify local minima, the issue of the contribution of Gribov copies to the gluon propagator has been ignored. However, the existence of Gribov copies on the lattice has been demonstrated by explicit numerical calculations [131] and their influence on some observables have been studied - see for example [132, 133, 134]. Despite not having a systematic way of identifying the different Gribov copies, these studies suggest that their contribution to observables can be of the same order of magnitude as the statistical errors.

Apart the problem of the Gribov copies, also of importance is the identification of the gauge dependent and gauge independent properties of the QCD Green functions. Among these functions, of special relevance is the behaviour of the gluon propagator for momenta $p \approx 0$ in connection with the question of a dynamically generated gluon mass. Lattice studies [129, 130, 135] seem to support a soft behaviour for the gluon propagator at zero-momentum, but one important point is the possible gauge dependence of the gluon mass. In our simulation, we study the gauge dependence of the zero momentum gluon propagator for the family of gauges defined by (6.24) and for a number of different M^2 values at $\beta = 5.7$. However, a complete study of the gluon mass requires an analysis of the continuum limit which is not done here. So, no firm conclusions can be drawn about the gluon mass.

[3]Note that the first terms of the strong coupling expansion are independent of the gauge configuration.

Let us now discuss the details of the simulation. For the gluon field we take the definition [135],

$$A_\mu(x) = \frac{U_\mu(x) - U_\mu^\dagger(x)}{2iag_0} - \frac{1}{3} Tr \left(\frac{U_\mu(x) - U_\mu^\dagger(x)}{2iag_0} \right) , \tag{6.36}$$

where a is the lattice spacing and g_0 is the bare coupling constant. By Fourier transforming the above field, we obtain the gluon field in momentum space,

$$A_\mu(p) = \sum_x e^{-ip\cdot x} A_\mu(x) . \tag{6.37}$$

Then, one can define the bare lattice n-point gluon Green functions in momentum space,

$$G^{(n)}_{\mu_1\mu_2\cdots\mu_n}(p_1, p_2, \cdots, p_n) = \langle A_{\mu_1}(p_1) A_{\mu_2}(p_2) \cdots A_{\mu_n}(p_n) \rangle_{mod} , \tag{6.38}$$

and momentum conservation implies $p_1 + p_2 + \cdots + p_n = 0$. In particular, we study the gluon propagator,

$$G^{(2)}_{\mu\nu}(p) = \langle A_\mu(p) A_\nu(-p) \rangle , \tag{6.39}$$

and the quantity

$$G^{(2)}(p) = \sum_{\mu=1}^{4} \langle A_\mu(p) A_\mu(-p) \rangle . \tag{6.40}$$

For $\beta M^2 \geq 0.8$, the gluon propagators (6.39) and (6.40) were computed using 21 link configurations and, for each link configuration, 60 gauge-related configurations separated by 100 GFMC sweeps were generated. For smaller values of βM^2, (6.40) was computed using the number of configurations reported in table 6.1, and taking gauge-related configurations separated by 1 GFMC update.

As discussed previously, the limit $M^2 \to \infty$ corresponds to the minimal Landau gauge. In order to compare our results at finite M^2 to the minimal Landau gauge, we gauge fixed to the minimal Landau gauge the 21 link configurations by minimizing $F[U^g]$ using the Fourier acceleration techniques described in [136].

In figure 6.6 we plot $G^{(2)}(0)$ vs. p in lattice units, for βM^2 above the phase

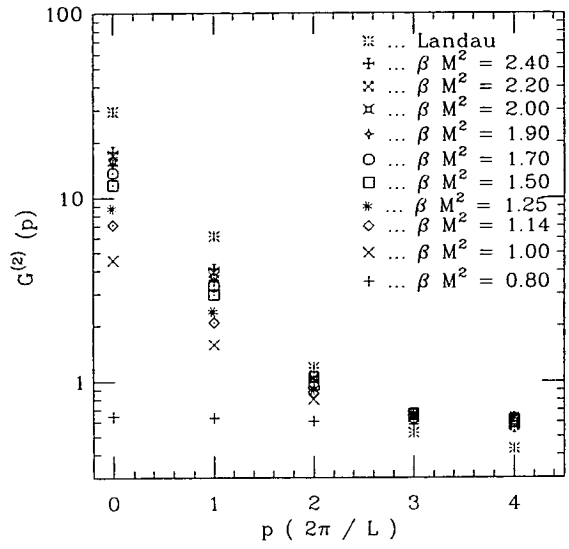

Figure 6.6: Gluon propagator vs. momentum, for various values of βM^2, and in the minimal Landau gauge.

transition and in the minimal Landau gauge. For βM^2 below the phase transition, the probability distribution over the gauge orbits is basically a constant and the gluon propagator should be small, approaching zero with M^2. The data, see figure 6.5, seems to support this behaviour.

The data indicate a strong dependence of the gluon propagator on the gauge fixing parameter, with smaller momentum having the larger M^2-dependence. Also, we observe that for larger values of M^2 our results become closer to the minimal Landau gauge numbers. This behaviour is in agreement with our theoretical expectations.

6.4 Summary and Conclusions

In this chapter, we performed a numerical investigation of the nonperturbative gauge fixing method suggested by Zwanziger, Parrinello, Jona-Lasinio and Fachin. This involves an additional Monte Carlo and we studied its efficiency. We found that, by changing the number of CM updates vs OR sweeps, it was possible to tune the Monte Carlo in order to have an efficient algorithm for the range of M^2 considered.

As a first application, we computed the gluon propagator for different gauges within the class of gauges defined by the M^2 parameter. Figure 6.6 and 6.5 indicates that the numerical study of gauge dependence is feasible. To our knowledge, this is the first time that a systematic investigation of gauge dependence on the lattice is performed. We found a strong M^2-dependence of the propagator, in particular for the zero momentum case. This seems to suggest that a dynamical gluon mass is a gauge dependent quantity and no physical meaning can be given to it. However, any firm conclusions about the gluon mass should involve a study of the continuum limit of the theory. Our preliminary investigation is very encouraging about the possibility of performing a more complete study of the continuum limit.

Appendix A

Euclidean Gamma Matrices

In this thesis we use the following convention for the gamma matrices in Euclidean space

$$\gamma_4 = \begin{pmatrix} 1 & 0 \\ 0 & -1 \end{pmatrix} , \qquad \gamma_j = i \begin{pmatrix} 0 & \sigma_j \\ -\sigma_j & 0 \end{pmatrix} , \quad j = 1,2,3 , \tag{A.41}$$

where σ_j are the usual Pauli matrices

$$\sigma_1 = \begin{pmatrix} 0 & 1 \\ 1 & 0 \end{pmatrix} , \quad \sigma_2 = \begin{pmatrix} 0 & -i \\ i & 0 \end{pmatrix} , \quad \sigma_3 = \begin{pmatrix} 1 & 0 \\ 0 & -1 \end{pmatrix} . \tag{A.42}$$

In addition, we took

$$\gamma_5 = \begin{pmatrix} 0 & 1 \\ 1 & 0 \end{pmatrix} . \tag{A.43}$$

Appendix B

Baryon Correlation Functions

Our investigation of heavy baryons requires the calculation of two types of correlation functions, the two-point functions,

$$G^{(2)}(t,\vec{x}) = \langle 0|\,\mathcal{T}\,(\,O(t,\vec{x})\,\overline{O}(0,\vec{0})\,)\,|0\rangle\ , \tag{B.44}$$

where $O(t,\vec{x})$ is an operator which creates a particle from the vacuum and $\mathcal{T}$ means time ordering, and the three-point functions,

$$G^{(3)}(t_x,\vec{x};t_y,\vec{y}) = \langle 0|\,\mathcal{T}\,(\,O(t_x,\vec{x})\,J(t_y,\vec{y})\,O'(0,\vec{0})\,)\,|0\rangle\ , \tag{B.45}$$

where J is a quark current. In this appendix, we discuss the form of these functions for large Euclidean time and study how the correlation functions are changed by smearing the quark fields [44, 112]

B.1 The 2-point Correlation Function

In this section, we discuss only the two-point correlation function for $\mathcal{O}_5$. However, the results obtained are easily generalised to other operators.

The operator $\mathcal{O}_5(t,\vec{x})$ creates particles with spin parity $J^P = 1/2^+$ from the vacuum. On the lattice and for $t > 0$, the two-point correlation function is given by

$$G^{(2)}_{\Lambda}(t,\vec{x}) = \langle 0|(\,\mathcal{O}_5(t,\vec{x})\,\mathcal{O}_5(0,\vec{0}) - \eta_T\mathcal{O}_5(T,\vec{0})\,\mathcal{O}_5(t,\vec{x})\,)|0\rangle\ , \tag{B.46}$$

where $\eta_T = -1$ takes into account the boundary conditions on the time direction and T is the time lattice extent. In order to compute (B.46), one assumes that $\mathcal{O}_5(t,\vec{x})$ can be expanded in terms of energy-momentum eigenstates of the physical

states it can create from the vacuum, i.e.

$$\mathcal{O}_5(t,\vec{x}) = \sum_i \sum_{\vec{k},s} Z_i(k^2)\,\frac{M_i}{E_i(\vec{k})} \\ [\,b_i(\vec{k},s)u_i(k,s)e^{-E_i(\vec{k})t+i\,\vec{k}\cdot\vec{x}} + d_i^\dagger(\vec{k},s)v_i(k,s)e^{E_i(\vec{k})t-i\,\vec{k}\cdot\vec{x}}\,] \;, \quad \text{(B.47)}$$

where $u_i(k,s)$ and $v_i(k,s)$ are Dirac spinors, $b_i(k,s)$ and $d_i^\dagger(k,s)$ are creation and annihilation operators for the physical state i and $Z_i(k^2)$ measures the overlap of the operator with the physical state describing particle i with four momentum k^μ. The creation and annihilation operators satisfy the following anticommutation relations

$$\{b_i(\vec{k},s), b_j^\dagger(\vec{k}\,',s')\} \;=\; \{d_i(\vec{k},s), d_j^\dagger(\vec{k}\,',s')\} \;=\; \frac{E_i(\vec{k})}{M_i}\,\delta_{\vec{k}\vec{k}'}\,\delta_{ss'}\,\delta_{ij}\;. \quad \text{(B.48)}$$

It should be clear that it only makes sense to compute (B.46) using the expansion (B.47) if the simulation is done close to continuum.

The momentum space correlation function is evaluated inserting the expansion (B.47) in (B.46) and doing the usual Fourier analysis. For large Euclidean time, the momentum correlation function is saturated by the contribution of the lightest particle which the operator $\mathcal{O}_5$ can create from the vacuum state,

$$G_\Lambda^{(2)}(t,\vec{p}) = \sum_{\vec{x}} e^{-i\vec{p}\cdot\vec{x}} G_\Lambda^{(2)}(t,\vec{x}) \;=\; Z_\Lambda(p^2)\frac{M_\Lambda}{E_\Lambda(\vec{p})} \\ \sum_s [u_\Lambda(\vec{p},s)\overline{u}_\Lambda(\vec{p},s)e^{-E_\Lambda(\vec{p})t} + v_\Lambda(-\vec{p},s)\overline{v}_\Lambda(-\vec{p},s)e^{-E_\Lambda(\vec{p})(T-t)}]\;. \quad \text{(B.49)}$$

The explicit form of the spinors $u_\Lambda(\vec{p},s)$ and $v_\Lambda(-\vec{p},s)$ is going to depend on the type of quark operators used. Detailed expressions for the spinors will be given when discussing smearing effects.

B.2 The 3-point Correlation Function

For the 3-point correlation functions, the quark current considered is of type

$$J_\mu \;=\; \overline{Q}\,\Gamma_\mu\,Q'\;, \quad \text{(B.50)}$$

where $\Gamma_\mu = \gamma_\mu, \gamma_\mu\gamma_5$. Defining the momentum space correlator function as

$$G_\mu^{(3)}(t_x, \vec{p}; t_y, \vec{q}) = \sum_{\vec{x},\vec{y}} e^{-i\vec{p}\cdot\vec{x} - i\vec{q}\cdot\vec{y}} G_\mu^{(3)}(t_x, \vec{x}; t_y, \vec{y}) \ , \tag{B.51}$$

and performing the same steps as in the two-point function, one arrives at the following results[4] : *i*) for $t_x > t_y$,

$$G_\mu^{(3)}(t_x, \vec{p}; t_y, \vec{q}) = Z_\Lambda(p^2)\, Z_{\Lambda'}(p'^2) \frac{M_\Lambda M_{\Lambda'}}{E_\Lambda(\vec{p}) E_{\Lambda'}(\vec{p}')} e^{-E_\Lambda(\vec{p})(t_x - t_y) - E_{\Lambda'}(\vec{p}')t_y}$$
$$\sum_{s,s'} [u_\Lambda(\vec{p}, s)\overline{u}_\Lambda(\vec{p}, s)]\, \mathcal{F}_\mu^{Q' \to Q}(p, p')\, [u_{\Lambda'}(\vec{p}', s')\overline{u}_{\Lambda'}(\vec{p}', s')] \ ; \tag{B.52}$$

ii) for $t_y > t_x$

$$G_\mu^{(3)}(t_x, \vec{p}; t_y, \vec{q}) = -Z_\Lambda(p^2)\, Z_{\Lambda'}(p'^2) \frac{M_\Lambda M_{\Lambda'}}{E_\Lambda(-\vec{p}) E_{\Lambda'}(-\vec{p}')} e^{E_\Lambda(\vec{p})(t_x - t_y) + E_{\Lambda'}(\vec{p}')(T - t_y)}$$
$$\sum_{s,s'} [v_\Lambda(-\vec{p}, s)\overline{v}_\Lambda(-\vec{p}, s)]\, \mathcal{F}_\mu^{Q' \to Q}(\tilde{p}, \tilde{p}')\, [v_{\Lambda'}(-\vec{p}', s')\overline{v}_{\Lambda'}(-\vec{p}', s')] \tag{B.53}$$

In the above expressions, we used the notation $\tilde{a}_4 = a_4$, $\vec{\tilde{a}} = -\vec{a}$, $p'_\mu = p_\mu + q_\mu$ and defined the baryon vertex $\mathcal{F}_\mu^{Q' \to Q}(p, p')$ by

$$\langle \Lambda_Q(p, s)|\, J_\mu^{Q' \to Q}\, |\Lambda_{Q'}(p', s')\rangle = \overline{u}_\Lambda(\vec{p}, s) \mathcal{F}_\mu^{Q' \to Q}(p, p') u_{\Lambda'}(\vec{p}', s') \ . \tag{B.54}$$

B.3 Smearing Effects in 2-point and 3-point Correlation Functions

In the heavy baryon simulation, to improve the overlap with the ground state we use Jacobi smeared quark fields. This means replacing the quark fields in the interpolating operators (4.5) by

$$q(t, \vec{x}) = \sum_{\vec{y}} f(\vec{x} - \vec{y}) q(t, \vec{y}) \ , \tag{B.55}$$

where $f(\vec{x})$ is a scalar function. Because the smearing is performed only in the spatial directions, the Lorentz invariance is lost and only spatial translations,

[4] Assuming $|t_x - t_y|$, t_y and/or $T - t_y$ are large enough.

rotations, parity and time reversal survive.

The wave function of the state created with the smeared operator should reflect the breaking of Lorentz invariance. In terms of the Z_i factors, this means they now depend on both the four momentum squared and the modulus of the three momentum, i.e. $Z_i = Z_i^s(p^2; |\vec{p}|)$. The spinors describing the spin-1/2 particles are also modified by the loss of Lorentz invariance. However, their transformation properties under parity, charge conjugation, spatial rotation and time reversal should remain unchanged after the symmetry breaking. In the case where Lorentz symmetry holds, the spinors appearing in the correlation functions are the usual four-component Dirac spinors,

$$u(p,s) = \frac{E(\vec{p})\gamma_4 - i\vec{\gamma}\cdot\vec{p} + M}{\sqrt{2M\,(\,E(\vec{p})+M\,)}}u(0,s)\;; \tag{B.56}$$

$u(0,s)$ describes a particle with zero momentum and spin s. For the situation where Lorentz symmetry is broken, the most general expression for the spinor which fulfils the above requirements is given by

$$u^{(smear)}(p,s) = \frac{E(\vec{p})\gamma_4 - i\,\alpha(|\vec{p}|)\,\vec{\gamma}\cdot\vec{p} + M}{\sqrt{2M\,(\,E(\vec{p})+M\,)}}u(0,s)\;. \tag{B.57}$$

As defined, the function $\alpha(|\vec{p}|)$ measures the breaking of Lorentz invariance, taking the value $\alpha(|\vec{p}|) = 1$ if the Lorentz symmetry is restored and $\alpha(|\vec{p}|) \neq 1$ otherwise. It should be noticed that we have no intuition concerning the values of this new function. The expectations, confirmed by the analysis of the lattice data, are that α should differ from one.

An important point about this description of the smearing effects, is that all changes are resummed in the wave function but without modifying its exponential behaviour. This is expected, since the spatial and time translation properties are not altered by Jacobi smearing the quark fields. Moreover, all effects are proportional to $\vec{p}$ and they disappear for zero momentum.

In this section, we give a description of how smearing affects the particles wave function. Let us now study how the different correlation functions are modified by smearing.

B.3.1 Smearing Effects in the 2-point Functions

In the study of the heavy baryon spectrum, the 2-point correlation functions were computed smearing the quark fields either at the source only (SL) or both at the source and the sink (SS). According to the analysis of the previous section, the nonzero momentum propagators for physical particles have different structures if we consider SL or SS data, and for zero momentum the propagators are the same for both types of correlators.

For the case where the smearing was done both at the source and at the sink, the propagator reads

$$G_\Lambda^{(ss)}(t,\vec{p}) = \frac{(Z^s(|\vec{p}|))^2}{2E_\Lambda(\vec{p})}[\ (\tilde{M} + \tilde{E}\,\gamma_4 - i\,\alpha(|\vec{p}|)\,\vec{p}\cdot\vec{\gamma})e^{-E_\Lambda(\vec{p})t} - (\tilde{M} - \tilde{E}\,\gamma_4 - i\,\alpha(|\vec{p}|)\,\vec{p}\cdot\vec{\gamma})e^{-E_\Lambda(\vec{p})(T-t)}]\ , \quad \text{(B.58)}$$

where

$$\tilde{M} = \frac{1}{2}[\,E_\Lambda(\vec{p}) + M_\Lambda - \alpha^2(|\vec{p}|)\,(E_\Lambda(\vec{p}) - M_\Lambda)\,]\ , \quad \text{(B.59)}$$

$$\tilde{E} = \frac{1}{2}[\,E_\Lambda(\vec{p}) + M_\Lambda + \alpha^2(|\vec{p}|)\,(E_\Lambda(\vec{p}) - M_\Lambda)\,]\ ; \quad \text{(B.60)}$$

note that we did not write the Z^s dependence on the four momentum squared. For the SL correlator, the propagator combines both types of spinors, and the resulting structure is slightly more involved than for the SS case,

$$G_\Lambda^{(sl)}(t,\vec{p}) = \frac{Z^s(|\vec{p}|)Z^l}{2E_\Lambda(\vec{p})}[(\tilde{M} + \tilde{E}\,\gamma_4 - i(1+\alpha)\,\vec{p}\cdot\vec{\gamma} + i(1+\alpha)\,\gamma_4\vec{p}\cdot\vec{\gamma})e^{-E_\Lambda(\vec{p})t} - (\tilde{M} - \tilde{E}\,\gamma_4 - i(1-\alpha)\,\vec{p}\cdot\vec{\gamma} - i(1+\alpha)\,\gamma_4\vec{p}\cdot\vec{\gamma})e^{-E_\Lambda(\vec{p})(T-t)}]\ , \quad \text{(B.61)}$$

where $\alpha = \alpha(|\vec{p}|)$ and now

$$\tilde{M} = \frac{1}{2}[\,E_\Lambda(\vec{p}) + M_\Lambda - \alpha(|\vec{p}|)\,(E_\Lambda(\vec{p}) - M_\Lambda)\,]\ , \quad \text{(B.62)}$$

$$\tilde{E} = \frac{1}{2}[\,E_\Lambda(\vec{p}) + M_\Lambda + \alpha(|\vec{p}|)\,(E_\Lambda(\vec{p}) - M_\Lambda)\,]\ . \quad \text{(B.63)}$$

In chapter 5, we discuss the smearing effects using the lattice data. There, Z^s, α and E_Λ are measured for different momentum and only for SS propagators. The results show that the lattice data is well described by (B.58), that Z^s decreases

when we go to higher momentum and that α seems to be independent of both the momentum and the quark mass[5]. The Z^s behaviour can be understood in terms of Lorentz contraction. However, concerning α, we have no intuition of how it should change with momentum and the quark mass.

B.3.2 Smearing Effects in the 3-point Functions

In the study of the heavy baryon form factors for the semileptonic decays, the 3-point correlation functions which were computed use the operator $\mathcal{O}_5(t,\vec{x})$ with all the quark fields smeared. Then, the correlation function for $t_x > t_y$ is given by

$$G_\mu^{(3)}(t_x,\vec{p};t_y,\vec{q}) = \frac{Z_\Lambda(p^2)Z_{\Lambda'}(p'^2)}{4E_\Lambda(\vec{p})E_{\Lambda'}(\vec{p}')}e^{-E_\Lambda(\vec{p})(t_x-t_y)-E_{\Lambda'}(\vec{p}')t_y}$$
$$[\tilde{M}+\tilde{E}\,\gamma_4 - i(P_+ + \alpha P_-)\vec{p}\cdot\vec{\gamma}]\,\mathcal{F}_\mu^{Q'\to Q}(p,p')\,[\tilde{M}'+\tilde{E}'\,\gamma_4 - i(P_- + \alpha' P_+)\vec{p}'\cdot\vec{\gamma}] \quad \text{(B.64)}$$

and for $t_y > t_x$ by

$$G_\mu^{(3)}(t_x,\vec{p};t_y,\vec{q}) = -\frac{Z_\Lambda(p^2)Z_{\Lambda'}(p'^2)}{4E_\Lambda(-\vec{p})E_{\Lambda'}(-\vec{p}')}e^{E_\Lambda(\vec{p})(t_x-t_y)+E_{\Lambda'}(\vec{p}')(T-t_y)}$$
$$[\tilde{M}-\tilde{E}\,\gamma_4 + i(P_- + \alpha P_+)\vec{p}\cdot\vec{\gamma}]\,\mathcal{F}_\mu^{Q'\to Q}(\tilde{p},\tilde{p}')\,[\tilde{M}'-\tilde{E}'\,\gamma_4 + i(P_+ + \alpha' P_-)\vec{p}'\cdot\vec{\gamma}] \quad \text{(B.65)}$$

In (B.64) and (B.65) the notation is as follows

$$\tilde{M} = \frac{1}{2}[\,E_\Lambda(\vec{p}) + M_\Lambda - \alpha(|\vec{p}|)\,(E_\Lambda(\vec{p}) - M_\Lambda)\,], \quad \text{(B.66)}$$

$$\tilde{E} = \frac{1}{2}[\,E_\Lambda(\vec{p}) + M_\Lambda + \alpha(|\vec{p}|)\,(E_\Lambda(\vec{p}) - M_\Lambda)\,], \quad \text{(B.67)}$$

$$\tilde{M}' = \frac{1}{2}[\,E_{\Lambda'}(\vec{p}') + M_{\Lambda'} - \alpha'(|\vec{p}'|)\,(E_{\Lambda'}(\vec{p}') - M_{\Lambda'})\,], \quad \text{(B.68)}$$

$$\tilde{E}' = \frac{1}{2}[\,E_{\Lambda'}(\vec{p}') + M_{\Lambda'} + \alpha'(|\vec{p}'|)\,(E_{\Lambda'}(\vec{p}') - M_{\Lambda'})\,], \quad \text{(B.69)}$$

$$\alpha = \alpha(|\vec{p}|)\,, \quad \text{(B.70)}$$

$$\alpha' = \alpha'(|\vec{p}'|)\,, \quad \text{(B.71)}$$

$$P_\pm = \frac{1\pm\gamma_4}{2}\,. \quad \text{(B.72)}$$

For the calculation of the Isgur-Wise function, we select appropriate combinations of components of the 3-point correlation function. The choice of these combina-

[5]The values measured for α are always smaller than 1.

tions, together with the discussion of smearing effects for the SS propagator, is investigated in chapter 5.

Appendix C

Hadron Spectrum Results

$(\kappa_{l1}, \kappa_{l2})$	$\kappa_h = 0.121$		$\kappa_h = 0.125$		$\kappa_h = 0.129$		$\kappa_h = 0.133$	
	M_Λ	ν	M_Λ	ν	M_Λ	ν	M_Λ	ν
SS Data								
(0.14144,0.14144)	$1.142 \pm^{8}_{5}$	0.97	$1.044 \pm^{8}_{5}$	0.94	$0.941 \pm^{8}_{5}$	0.92	$0.832 \pm^{7}_{4}$	0.92
(0.14144,0.14226)	$1.113 \pm^{9}_{6}$	0.88	$1.019 \pm^{10}_{5}$	1.11	$0.916 \pm^{10}_{5}$	1.10	$0.803 \pm^{10}_{4}$	1.11
(0.14226,0.14226)	$1.086 \pm^{10}_{6}$	1.00	$0.986 \pm^{10}_{5}$	0.95	$0.884 \pm^{12}_{5}$	0.92	$0.773 \pm^{12}_{4}$	0.94
SL Data								
(0.14144,0.14144)	$1.142 \pm^{8}_{6}$	1.20	$1.043 \pm^{8}_{6}$	1.11	$0.938 \pm^{8}_{5}$	1.09	$0.830 \pm^{8}_{5}$	1.11
(0.14144,0.14226)	$1.108 \pm^{9}_{7}$	1.27	$1.010 \pm^{10}_{7}$	1.12	$0.906 \pm^{10}_{6}$	1.03	$0.797 \pm^{10}_{6}$	1.03
(0.14226,0.14226)	$1.075 \pm^{12}_{9}$	0.98	$0.976 \pm^{12}_{9}$	0.89	$0.873 \pm^{12}_{9}$	0.85	$0.763 \pm^{12}_{9}$	0.90

Table C.2: Λ mass from fitting the correlator; $\nu = \chi^2/d.o.f.$

$(\kappa_{l1}, \kappa_{l2})$	$\kappa_h = 0.121$		$\kappa_h = 0.125$		$\kappa_h = 0.129$		$\kappa_h = 0.133$	
	M_Σ	ν	M_Σ	ν	M_Σ	ν	M_Σ	ν
SS Data								
(0.14144,0.14144)	$1.170 \pm^{12}_{6}$	0.93	$1.072 \pm^{12}_{6}$	0.95	$0.970 \pm^{12}_{7}$	0.97	$0.862 \pm^{11}_{7}$	0.97
(0.14144,0.14226)	$1.150 \pm^{14}_{8}$	1.05	$1.053 \pm^{14}_{8}$	1.06	$0.950 \pm^{15}_{8}$	1.08	$0.842 \pm^{16}_{7}$	1.09
(0.14226,0.14226)	$1.121 \pm^{16}_{9}$	1.03	$1.023 \pm^{16}_{9}$	1.00	$0.920 \pm^{16}_{9}$	0.96	$0.818 \pm^{18}_{9}$	1.06
SL Data								
(0.14144,0.14144)	$1.176 \pm^{9}_{6}$	1.10	$1.080 \pm^{9}_{6}$	1.23	$0.978 \pm^{8}_{6}$	1.31	$0.871 \pm^{8}_{6}$	1.24
(0.14144,0.14226)	$1.149 \pm^{11}_{7}$	0.72	$1.052 \pm^{11}_{7}$	0.83	$0.951 \pm^{11}_{7}$	0.88	$0.843 \pm^{11}_{7}$	0.81
(0.14226,0.14226)	$1.124 \pm^{14}_{9}$	0.52	$1.026 \pm^{14}_{9}$	0.64	$0.924 \pm^{14}_{8}$	0.73	$0.810 \pm^{14}_{8}$	1.23

Table C.3: Σ mass from fitting the correlator; $\nu = \chi^2/d.o.f.$

$(\kappa_{l1}, \kappa_{l2})$	$\kappa_h = 0.121$		$\kappa_h = 0.125$		$\kappa_h = 0.129$		$\kappa_h = 0.133$	
	M_{Σ^*}	ν	M_{Σ^*}	ν	M_{Σ^*}	ν	M_{Σ^*}	ν
SS Data								
(0.14144,0.14144)	$1.170 \pm^{12}_{7}$	1.03	$1.072 \pm^{12}_{7}$	1.03	$0.969 \pm^{11}_{7}$	1.04	$0.860 \pm^{11}_{7}$	1.05
(0.14144,0.14226)	$1.148 \pm^{11}_{8}$	1.02	$1.050 \pm^{11}_{7}$	1.02	$0.947 \pm^{11}_{7}$	1.02	$0.837 \pm^{11}_{7}$	1.03
(0.14226,0.14226)	$1.125 \pm^{12}_{8}$	1.02	$1.026 \pm^{13}_{9}$	1.00	$0.923 \pm^{13}_{9}$	1.00	$0.812 \pm^{13}_{9}$	1.02
SL Data								
(0.14144,0.14144)	$1.170 \pm^{9}_{6}$	1.61	$1.069 \pm^{10}_{6}$	1.73	$0.966 \pm^{10}_{7}$	1.64	$0.856 \pm^{9}_{8}$	1.49
(0.14144,0.14226)	$1.142 \pm^{11}_{8}$	1.19	$1.043 \pm^{11}_{8}$	1.26	$0.939 \pm^{11}_{8}$	1.24	$0.825 \pm^{11}_{8}$	1.09
(0.14226,0.14226)	$1.118 \pm^{16}_{10}$	0.61	$1.009 \pm^{16}_{8}$	1.44	$0.906 \pm^{15}_{8}$	1.11	$0.804 \pm^{15}_{9}$	1.12

Table C.4: Σ^* mass from fitting the correlator; $\nu = \chi^2/d.o.f.$

Appendix D

Isgur-Wise Function Results

The notation used in this appendix is a follows :

- The data refers to the matrix element $\langle \Lambda_Q; \vec{p}|J_\mu|\Lambda_{Q'}; \vec{p}'\rangle$.
- In the tables we refer to the matrix element as $\kappa_h \leftarrow \kappa_{h'}$, where κ_h is the hopping parameter for the heavy quark Q.

$k_{l_1} = 0.14144; k_{l_2} = 0.14144$								
$\vec{p}$	$0.121 \leftarrow 0.121$		$0.121 \leftarrow 0.125$		$0.121 \leftarrow 0.129$		$0.121 \leftarrow 0.133$	
$\vec{p}'$	ω	$\xi_{QQ'}(\omega)$	ω	$\xi_{QQ'}(\omega)$	ω	$\xi_{QQ'}(\omega)$	ω	$\xi_{QQ'}(\omega)$
(0,0,0) (1,0,0)	1.026	$0.88 \pm^{12}_{10}$	1.031	$0.86 \pm^{12}_{10}$	1.038	$0.85 \pm^{11}_{9}$	1.048	$0.83 \pm^{9}_{10}$
(1,0,0) (0,0,0)	1.026	$0.85 \pm^{7}_{7}$	1.026	$0.84 \pm^{7}_{7}$	1.026	$0.84 \pm^{7}_{7}$	1.026	$0.84 \pm^{7}_{6}$
(1,0,0) (1,0,0)	1.000	$0.87 \pm^{14}_{13}$	1.000	$0.87 \pm^{14}_{14}$	1.001	$0.85 \pm^{13}_{14}$	1.003	$0.82 \pm^{15}_{14}$
(1,0,0) (−1,0,0)	1.105	$0.62 \pm^{12}_{10}$	1.115	$0.61 \pm^{11}_{10}$	1.129	$0.59 \pm^{10}_{10}$	1.148	$0.56 \pm^{10}_{9}$
(1,0,0) (0,−1,0)	1.053	$0.82 \pm^{13}_{12}$	1.058	$0.82 \pm^{13}_{12}$	1.065	$0.82 \pm^{12}_{12}$	1.075	$0.80 \pm^{11}_{12}$
(0,0,0) (1,1,0)	1.051	$0.84 \pm^{13}_{12}$	1.061	$0.83 \pm^{12}_{12}$	1.075	$0.83 \pm^{11}_{11}$	1.094	$0.81 \pm^{11}_{10}$
(1,0,0) (1,1,0)	1.026	$0.65 \pm^{18}_{14}$	1.031	$0.63 \pm^{18}_{15}$	1.039	$0.61 \pm^{18}_{15}$	1.051	$0.60 \pm^{19}_{16}$
(1,0,0) (0,−1,−1)	1.078	$0.78 \pm^{20}_{16}$	1.088	$0.77 \pm^{19}_{16}$	1.102	$0.73 \pm^{20}_{16}$	1.123	$0.65 \pm^{21}_{17}$

Table D.5: Isgur-Wise Function from $G_1(\omega)$.

$k_{l_1} = 0.14144; k_{l_2} = 0.14144$								
$\vec{p}$	$0.125 \leftarrow 0.121$		$0.125 \leftarrow 0.125$		$0.125 \leftarrow 0.129$		$0.125 \leftarrow 0.133$	
$\vec{p}'$	ω	$\xi_{QQ'}(\omega)$	ω	$\xi_{QQ'}(\omega)$	ω	$\xi_{QQ'}(\omega)$	ω	$\xi_{QQ'}(\omega)$
(0,0,0) (1,0,0)	1.026	$0.89 \pm^{12}_{9}$	1.031	$0.87 \pm^{12}_{10}$	1.038	$0.85 \pm^{11}_{9}$	1.048	$0.83 \pm^{9}_{9}$
(1,0,0) (0,0,0)	1.031	$0.84 \pm^{7}_{8}$	1.031	$0.84 \pm^{7}_{7}$	1.031	$0.83 \pm^{6}_{7}$	1.031	$0.83 \pm^{7}_{6}$
(1,0,0) (1,0,0)	1.000	$0.88 \pm^{14}_{13}$	1.000	$0.88 \pm^{13}_{14}$	1.000	$0.87 \pm^{14}_{15}$	1.002	$0.84 \pm^{15}_{15}$
(1,0,0) (−1,0,0)	1.115	$0.59 \pm^{11}_{10}$	1.126	$0.58 \pm^{10}_{10}$	1.140	$0.56 \pm^{9}_{9}$	1.160	$0.53 \pm^{9}_{9}$
(1,0,0) (0,−1,0)	1.058	$0.81 \pm^{13}_{11}$	1.063	$0.81 \pm^{12}_{12}$	1.070	$0.80 \pm^{11}_{11}$	1.081	$0.78 \pm^{10}_{11}$
(0,0,0) (1,1,0)	1.051	$0.84 \pm^{13}_{12}$	1.061	$0.84 \pm^{12}_{12}$	1.075	$0.84 \pm^{11}_{11}$	1.094	$0.82 \pm^{11}_{10}$
(1,0,0) (1,1,0)	1.026	$0.69 \pm^{17}_{14}$	1.031	$0.68 \pm^{17}_{15}$	1.038	$0.66 \pm^{17}_{16}$	1.049	$0.64 \pm^{18}_{16}$
(1,0,0) (0,−1,−1)	1.084	$0.76 \pm^{18}_{15}$	1.094	$0.75 \pm^{18}_{15}$	1.108	$0.72 \pm^{18}_{15}$	1.128	$0.64 \pm^{19}_{16}$

Table D.6: Isgur-Wise Function from $G_1(\omega)$.

$k_{l_1} = 0.14144$; $k_{l_2} = 0.14144$								
$\vec{p}$	$0.129 \leftarrow 0.121$		$0.129 \leftarrow 0.125$		$0.129 \leftarrow 0.129$		$0.129 \leftarrow 0.133$	
$\vec{p}'$	ω	$\xi_{QQ'}(\omega)$	ω	$\xi_{QQ'}(\omega)$	ω	$\xi_{QQ'}(\omega)$	ω	$\xi_{QQ'}(\omega)$
(0,0,0) (1,0,0)	1.026	$0.90 \pm^{11}_{9}$	1.031	$0.88 \pm^{11}_{9}$	1.038	$0.86 \pm^{10}_{9}$	1.048	$0.84 \pm^{8}_{8}$
(1,0,0) (0,0,0)	1.038	$0.83 \pm^{7}_{8}$	1.038	$0.83 \pm^{6}_{8}$	1.038	$0.82 \pm^{6}_{7}$	1.038	$0.82 \pm^{6}_{6}$
(1,0,0) (1,0,0)	1.001	$0.90 \pm^{13}_{14}$	1.000	$0.90 \pm^{13}_{15}$	1.000	$0.89 \pm^{13}_{16}$	1.001	$0.87 \pm^{14}_{16}$
(1,0,0) (−1,0,0)	1.129	$0.57 \pm^{11}_{9}$	1.140	$0.55 \pm^{10}_{9}$	1.155	$0.53 \pm^{9}_{9}$	1.176	$0.50 \pm^{8}_{8}$
(1,0,0) (0,−1,0)	1.065	$0.80 \pm^{12}_{11}$	1.070	$0.80 \pm^{11}_{11}$	1.077	$0.79 \pm^{10}_{11}$	1.088	$0.77 \pm^{9}_{11}$
(0,0,0) (1,1,0)	1.051	$0.85 \pm^{13}_{11}$	1.061	$0.84 \pm^{12}_{10}$	1.075	$0.84 \pm^{11}_{10}$	1.094	$0.83 \pm^{10}_{9}$
(1,0,0) (1,1,0)	1.027	$0.73 \pm^{16}_{14}$	1.032	$0.72 \pm^{16}_{15}$	1.038	$0.70 \pm^{16}_{16}$	1.049	$0.68 \pm^{16}_{16}$
(1,0,0) (0,−1,−1)	1.091	$0.73 \pm^{17}_{14}$	1.101	$0.72 \pm^{16}_{14}$	1.115	$0.69 \pm^{15}_{15}$	1.136	$0.63 \pm^{17}_{15}$

Table D.7: Isgur-Wise Function from $G_1(\omega)$.

$k_{l_1} = 0.14144$; $k_{l_2} = 0.14144$								
$\vec{p}$	$0.133 \leftarrow 0.121$		$0.133 \leftarrow 0.125$		$0.133 \leftarrow 0.129$		$0.133 \leftarrow 0.133$	
$\vec{p}'$	ω	$\xi_{QQ'}(\omega)$	ω	$\xi_{QQ'}(\omega)$	ω	$\xi_{QQ'}(\omega)$	ω	$\xi_{QQ'}(\omega)$
(0,0,0) (1,0,0)	1.026	$0.90 \pm^{10}_{9}$	1.031	$0.89 \pm^{10}_{9}$	1.038	$0.87 \pm^{9}_{8}$	1.048	$0.85 \pm^{8}_{8}$
(1,0,0) (0,0,0)	1.048	$0.81 \pm^{7}_{9}$	1.048	$0.81 \pm^{6}_{8}$	1.048	$0.81 \pm^{6}_{8}$	1.048	$0.81 \pm^{6}_{7}$
(1,0,0) (1,0,0)	1.003	$0.90 \pm^{14}_{13}$	1.002	$0.90 \pm^{13}_{14}$	1.001	$0.91 \pm^{14}_{16}$	1.000	$0.89 \pm^{14}_{17}$
(1,0,0) (−1,0,0)	1.148	$0.53 \pm^{10}_{9}$	1.160	$0.52 \pm^{9}_{8}$	1.176	$0.49 \pm^{8}_{8}$	1.198	$0.46 \pm^{8}_{7}$
(1,0,0) (0,−1,0)	1.075	$0.79 \pm^{11}_{11}$	1.081	$0.78 \pm^{10}_{11}$	1.088	$0.77 \pm^{10}_{10}$	1.099	$0.74 \pm^{9}_{10}$
(0,0,0) (1,1,0)	1.051	$0.84 \pm^{13}_{10}$	1.061	$0.83 \pm^{12}_{10}$	1.075	$0.83 \pm^{12}_{9}$	1.094	$0.82 \pm^{11}_{8}$
(1,0,0) (1,1,0)	1.030	$0.75 \pm^{16}_{14}$	1.033	$0.74 \pm^{16}_{15}$	1.039	$0.73 \pm^{17}_{16}$	1.048	$0.71 \pm^{16}_{16}$
(1,0,0) (0,−1,−1)	1.102	$0.69 \pm^{16}_{13}$	1.112	$0.68 \pm^{14}_{13}$	1.126	$0.65 \pm^{14}_{13}$	1.147	$0.60 \pm^{14}_{14}$

Table D.8: Isgur-Wise Function from $G_1(\omega)$.

	$k_{l_1} = 0.14144; k_{l_2} = 0.14226$		$k_{l_1} = 0.14226; k_{l_2} = 0.14226$	
$\vec{p}$ / $\vec{p}'$	$0.129 \leftarrow 0.129$		$0.129 \leftarrow 0.129$	
	ω	$\xi_{QQ'}(\omega)$	ω	$\xi_{QQ'}(\omega)$
(0,0,0) / (1,0,0)	1.040	$0.85 \pm^{10}_{11}$	1.043	$0.81 \pm^{13}_{12}$
(1,0,0) / (0,0,0)	1.040	$0.83 \pm^{5}_{10}$	1.043	$0.82 \pm^{8}_{14}$
(1,0,0) / (1,0,0)	1.000	$0.84 \pm^{18}_{23}$	1.000	$0.66 \pm^{31}_{33}$
(1,0,0) / (−1,0,0)	1.163	$0.57 \pm^{9}_{12}$	1.176	$0.63 \pm^{12}_{18}$
(1,0,0) / (0,−1,0)	1.082	$0.82 \pm^{10}_{14}$	1.088	$0.79 \pm^{16}_{17}$
(0,0,0) / (1,1,0)	1.079	$0.86 \pm^{15}_{13}$	1.084	$0.84 \pm^{27}_{16}$
(1,0,0) / (1,1,0)	1.040	$0.70 \pm^{23}_{29}$	1.043	$0.54 \pm^{44}_{48}$
(1,0,0) / (0,−1,−1)	1.122	$0.73 \pm^{19}_{23}$	1.131	$0.67 \pm^{34}_{37}$

Table D.9: Isgur-Wise Function from $G_1(\omega)$.

$k_{l_1} = 0.14144; k_{l_2} = 0.14144$								
$\vec{p}$ / $\vec{p}'$	$0.121 \leftarrow 0.121$		$0.121 \leftarrow 0.125$		$0.121 \leftarrow 0.129$		$0.121 \leftarrow 0.133$	
	ω	$\xi_{QQ'}(\omega)$	ω	$\xi_{QQ'}(\omega)$	ω	$\xi_{QQ'}(\omega)$	ω	$\xi_{QQ'}(\omega)$
(0,0,0) / (1,0,0)	1.026	$1.05 \pm^{13}_{11}$	1.031	$0.83 \pm^{16}_{13}$	1.038	$0.85 \pm^{13}_{13}$	1.048	$0.88 \pm^{13}_{12}$
(1,0,0) / (0,0,0)	1.026	$0.82 \pm^{11}_{11}$	1.026	$0.81 \pm^{8}_{8}$	1.026	$0.80 \pm^{6}_{8}$	1.026	$0.80 \pm^{6}_{7}$
(1,0,0) / (1,0,0)	1.000	$0.96 \pm^{17}_{16}$	1.000	$1.09 \pm^{19}_{19}$	1.001	$1.10 \pm^{18}_{21}$	1.003	$1.09 \pm^{18}_{21}$
(1,0,0) / (−1,0,0)	1.105	$0.40 \pm^{18}_{21}$	1.115	$0.48 \pm^{12}_{12}$	1.129	$0.47 \pm^{12}_{12}$	1.148	$0.44 \pm^{13}_{12}$
(1,0,0) / (0,−1,0)	1.053	$0.85 \pm^{25}_{20}$	1.058	$0.76 \pm^{12}_{12}$	1.065	$0.76 \pm^{12}_{12}$	1.075	$0.74 \pm^{11}_{11}$

Table D.10: Isgur-Wise Function from $F^{(sum)}(\omega)$.

$k_{l_1} = 0.14144; k_{l_2} = 0.14144$								
$\vec{p}$ / $\vec{p}'$	$0.125 \leftarrow 0.121$		$0.125 \leftarrow 0.125$		$0.125 \leftarrow 0.129$		$0.125 \leftarrow 0.133$	
	ω	$\xi_{QQ'}(\omega)$	ω	$\xi_{QQ'}(\omega)$	ω	$\xi_{QQ'}(\omega)$	ω	$\xi_{QQ'}(\omega)$
(0,0,0) / (1,0,0)	1.026	$0.85 \pm^{17}_{13}$	1.031	$1.05 \pm^{13}_{12}$	1.038	$0.80 \pm^{14}_{11}$	1.048	$0.82 \pm^{13}_{11}$
(1,0,0) / (0,0,0)	1.031	$0.81 \pm^{7}_{8}$	1.031	$0.81 \pm^{11}_{11}$	1.031	$0.80 \pm^{7}_{8}$	1.031	$0.79 \pm^{6}_{8}$
(1,0,0) / (1,0,0)	1.000	$1.03 \pm^{21}_{17}$	1.000	$0.98 \pm^{18}_{17}$	1.000	$1.09 \pm^{19}_{20}$	1.002	$1.09 \pm^{17}_{21}$
(1,0,0) / (−1,0,0)	1.115	$0.50 \pm^{12}_{12}$	1.126	$0.40 \pm^{17}_{20}$	1.140	$0.46 \pm^{12}_{12}$	1.160	$0.43 \pm^{12}_{12}$
(1,0,0) / (0,−1,0)	1.058	$0.75 \pm^{12}_{12}$	1.063	$0.87 \pm^{23}_{19}$	1.070	$0.74 \pm^{11}_{12}$	1.081	$0.72 \pm^{11}_{11}$

Table D.11: Isgur-Wise Function from $F^{(sum)}(\omega)$.

$k_{l_1} = 0.14144; k_{l_2} = 0.14144$								
$\vec{p}$ / $\vec{p}\,'$	$0.129 \leftarrow 0.121$		$0.129 \leftarrow 0.125$		$0.129 \leftarrow 0.129$		$0.129 \leftarrow 0.133$	
	ω	$\xi_{QQ'}(\omega)$	ω	$\xi_{QQ'}(\omega)$	ω	$\xi_{QQ'}(\omega)$	ω	$\xi_{QQ'}(\omega)$
(0,0,0) (1,0,0)	1.026	0.86^{+18}_{-13}	1.031	0.82^{+18}_{-12}	1.038	1.02^{+12}_{-12}	1.048	0.76^{+13}_{-10}
(1,0,0) (0,0,0)	1.038	0.81^{+8}_{-8}	1.038	0.80^{+8}_{-8}	1.038	0.80^{+10}_{-11}	1.038	0.77^{+7}_{-7}
(1,0,0) (1,0,0)	1.001	1.01^{+21}_{-16}	1.000	1.03^{+22}_{-17}	1.000	1.00^{+18}_{-18}	1.001	1.08^{+20}_{-21}
(1,0,0) (−1,0,0)	1.129	0.52^{+11}_{-12}	1.140	0.49^{+11}_{-12}	1.155	0.39^{+15}_{-21}	1.176	0.42^{+11}_{-11}
(1,0,0) (0,−1,0)	1.065	0.75^{+12}_{-12}	1.070	0.74^{+12}_{-11}	1.077	0.88^{+21}_{-18}	1.088	0.70^{+11}_{-12}

Table D.12: Isgur-Wise Function from $F^{(sum)}(\omega)$.

$k_{l_1} = 0.14144; k_{l_2} = 0.14144$								
$\vec{p}$ / $\vec{p}\,'$	$0.133 \leftarrow 0.121$		$0.133 \leftarrow 0.125$		$0.133 \leftarrow 0.129$		$0.133 \leftarrow 0.133$	
	ω	$\xi_{QQ'}(\omega)$	ω	$\xi_{QQ'}(\omega)$	ω	$\xi_{QQ'}(\omega)$	ω	$\xi_{QQ'}(\omega)$
(0,0,0) (1,0,0)	1.026	0.88^{+18}_{-12}	1.031	0.83^{+18}_{-12}	1.038	0.78^{+18}_{-11}	1.048	0.97^{+12}_{-12}
(1,0,0) (0,0,0)	1.048	0.79^{+9}_{-8}	1.048	0.78^{+8}_{-8}	1.048	0.77^{+8}_{-8}	1.048	0.78^{+9}_{-11}
(1,0,0) (1,0,0)	1.003	1.00^{+22}_{-17}	1.002	1.00^{+22}_{-17}	1.001	1.02^{+22}_{-18}	1.000	1.01^{+18}_{-19}
(1,0,0) (−1,0,0)	1.148	0.52^{+11}_{-13}	1.160	0.49^{+11}_{-12}	1.176	0.45^{+10}_{-11}	1.198	0.34^{+14}_{-21}
(1,0,0) (0,−1,0)	1.075	0.75^{+12}_{-12}	1.081	0.73^{+11}_{-11}	1.088	0.71^{+11}_{-11}	1.099	0.87^{+17}_{-18}

Table D.13: Isgur-Wise Function from $F^{(sum)}(\omega)$.

	$k_{l_1} = 0.14144; k_{l_2} = 0.14226$		$k_{l_1} = 0.14226; k_{l_2} = 0.14226$	
$\vec{p}$ / $\vec{p}\,'$	$0.129 \leftarrow 0.129$		$0.129 \leftarrow 0.129$	
	ω	$\xi_{QQ'}(\omega)$	ω	$\xi_{QQ'}(\omega)$
(0,0,0) (1,0,0)	1.040	1.07^{+16}_{-13}	1.043	1.08^{+24}_{-17}
(1,0,0) (0,0,0)	1.040	0.77^{+14}_{-13}	1.043	0.67^{+19}_{-16}
(1,0,0) (1,0,0)	1.000	1.00^{+25}_{-26}	1.000	0.78^{+45}_{-41}
(1,0,0) (−1,0,0)	1.163	0.50^{+21}_{-29}	1.176	0.76^{+34}_{-47}
(1,0,0) (0,−1,0)	1.082	0.94^{+26}_{-24}	1.088	0.87^{+37}_{-30}

Table D.14: Isgur-Wise Function from $F^{(sum)}(\omega)$.

decay	ω	F_1	F_2	F_3	G_1	G_2	G_3
$\Lambda_b \to \Lambda_c$	1.00	1.564	−0.415	−0.120	0.986	−0.476	0.166
	1.05	$1.38 \pm^{6}_{10}$	$-0.36 \pm^{3}_{2}$	$-0.104 \pm^{7}_{4}$	$0.88 \pm^{4}_{6}$	$-0.41 \pm^{3}_{2}$	$0.144 \pm^{6}_{10}$
	1.10	$1.2 \pm^{1}_{2}$	$-0.31 \pm^{5}_{3}$	$-0.090 \pm^{14}_{8}$	$0.78 \pm^{7}_{12}$	$-0.35 \pm^{6}_{3}$	$0.12 \pm^{1}_{2}$
	1.20	$0.9 \pm^{2}_{4}$	$-0.22 \pm^{9}_{5}$	$-0.06 \pm^{3}_{2}$	$0.6 \pm^{1}_{2}$	$-0.25 \pm^{10}_{6}$	$0.09 \pm^{2}_{4}$
	1.30	$0.6 \pm^{3}_{5}$	$-0.14 \pm^{13}_{7}$	$-0.04 \pm^{4}_{2}$	$0.4 \pm^{2}_{3}$	$-0.16 \pm^{14}_{8}$	$0.06 \pm^{3}_{5}$
$\Xi_b \to \Xi_c$	1.00	1.646	−0.478	−0.138	0.986	−0.543	0.190
	1.05	$1.42 \pm^{5}_{8}$	$-0.41 \pm^{2}_{1}$	$-0.118 \pm^{7}_{4}$	$0.86 \pm^{3}_{5}$	$-0.46 \pm^{3}_{2}$	$0.161 \pm^{5}_{9}$
	1.10	$1.20 \pm^{9}_{16}$	$-0.34 \pm^{4}_{3}$	$-0.099 \pm^{13}_{8}$	$0.74 \pm^{6}_{10}$	$-0.38 \pm^{5}_{3}$	$0.13 \pm^{1}_{2}$
	1.20	$0.8 \pm^{2}_{3}$	$-0.22 \pm^{8}_{5}$	$-0.07 \pm^{2}_{1}$	$0.5 \pm^{1}_{2}$	$-0.25 \pm^{9}_{5}$	$0.09 \pm^{2}_{3}$
	1.30	$0.5 \pm^{2}_{4}$	$-0.12 \pm^{11}_{7}$	$-0.04 \pm^{3}_{2}$	$0.3 \pm^{2}_{3}$	$-0.14 \pm^{13}_{7}$	$0.05 \pm^{3}_{5}$

Table D.15: Physical form factors computed expanding the Isgur-Wise function in $(\omega - 1)$ up to first order.

References

[1] C. N. Yang, R. L. Mills, Phys. Rev. **96** (1954) 191.

[2] For general discuss of the SM see, for example, [3] or [4].

[3] I. J. R. Aitchison, A. J. G. Hey; *Gauge Theories in Particle Physics.* Adam Hilger, Bristol and Philadelphia, 1989.

[4] J. F. Donoghue, E. Golowich, B. R. Holstein; *Dynamics of the Standard Model.* Cambridge University Press, 1992.

[5] S. L. Glashow, Nucl. Phys. **22** (1961) 579.

[6] S. Weinberg, Phys. Rev. Lett. **19** (1967) 1264.

[7] A. Salam, in: *Elementary Particle Theory: Relativistic Groups and Analyticity*; ed. N. Svartholm (Almqvist and Wiksell, Stockholm, 1968) p. 367.

[8] H. Fritzsch, M. Gell-Mann, H. Leutwyler, Phys. Lett. **B47** (1973) 365.

[9] For a general discussion of the lattice formulation of field theories or in particular QCD see, for example, [10] [11] [12] [13].

[10] I. Montvay, G. Münster. *Quantum Fields on a Lattice.* Cambridge University Press, 1994.

[11] M. Creutz. *Quarks, Gluons and Lattices.* Cambridge University Press, Cambridge, 1983.

[12] A. Hasenfratz, P. Hasenfratz, Ann. Rev. Nucl. Part. Sci. **35** (1985) 559.

[13] H. J. Rothe. *Lattice Gauge Theories, An Introduction.* World Scientific, 1992.

[14] D. J. Gross, F. Wilczek, Phys. Rev. Lett. **30** (1973) 1343.

[15] H. D. Politzer, Phys. Rev. Lett. **30** (1973) 1346.

[16] S. Coleman, D. J. Gross, Phys. Rev. Lett. **31** (1973) 851.

[17] S. L. Glashow, J. Iliopoulos, L. Maiani, Phys. Rev. **D2** (1970) 1285.

[18] J. J. Aubert *et al.*, Phys. Rev. Lett. **33** (1974) 1404.

[19] J. E. Augustin *et al.*, Phys. Rev. Lett. **33** (1974) 1406.

[20] S. Herb *et al.*, Phys. Rev. Lett. **39** (1977) 252.

[21] E. G. Cazzoli *et al.*, Phys. Rev. Lett. **34** (1975) 1125.

[22] C. Angelini *et al.*, Phys. Lett. **B84** (1979) 151.

[23] M. Basile *et al.*, Lett. Nuovo Cimento **31** (1981) 97.

[24] G. Bari *et al.*, Nuovo Cimento **A104** (1991) 1787.

[25] D. Buskulic *et al.*, Phys. Lett. **B297** (1992) 449.

[26] R. M. Barnett *et al.* (Particle Data Group), Phys. Rev. **D54** (1996) 1.

[27] V. A. Ammosov *et al.*, Pis'ma Zh. Eksp. Teor. Fiz. **58** (1993) 241 [JETP Lett. **58** (1993) 247].

[28] CLEO collaboration, P. Avery *et al.*, Phys. Rev. Lett. **75** (1995) 4364.

[29] CLEO II collaboration, L. Gibbons *et al.*, Phys. Rev. Lett. **77** (1996) 810.

[30] DELPHI collaboration, P. Abreu *et al.*, Z. Phys. **C68** (1995) 541.

[31] D. Bloch, Report at the EPS Conference, Brussels 1995.

[32] J. G. Korner, H. W. Siebert, Annu. Rev. Nucl. Part. Sci. **41** (1991) 511.

[33] A. De Rújula, H. Georgi, S. L. Glashow, Phys. Rev. **D12** (1975) 147.

[34] A. Martin, J. M. Richaud, Phys. Lett. **B185** (1987) 426 and references therein.

[35] R. E. Cutkosky, P. Geiger, Phys. Rev. **D48** (1993) 1315.

[36] W. Kwong, J. L. Rosner, Phys. Rev. **D44** (1991) 212.

[37] R. Roncaglia, D. B. Lichtenberg, E. Predazzi, Phys. Rev. **D52** (1995) 1722.

[38] J. L. Rosner, hep-ph/9508252.

[39] M. J. Savage, Phys. Lett. **B359** (1995) 189.

[40] UKQCD collaboration (N. Stella), Nucl. Phys. **B(Proc. Suppl.)42** (1995) 367.

[41] C. Alexandrou *et al.*, Nucl. Phys. **B(Proc. Suppl.)42** (1995) 297.

[42] C. Alexandrou *et al.*, Phys. Lett. **B337** (1994) 340.

[43] UKQCD collaboration, C. T. H. Davies *et al.*, Nucl. Phys. **B(Proc. Suppl.)34** (1994) 437.

[44] UKQCD collaboration, K. C. Bowler *et al.*, Phys. Rev. **D54** (1996) 3619.

[45] J. D. Richman, P. R. Burchat, Rev. Mod. Phys. **67** (1995) 893.

[46] J. G. Körner, M. Krämer, Phys. Lett. **B275** (1992) 495.

[47] M. Tanaka, Phys. Rev. **D47** (1993) 4969.

[48] O. I. Yakovlev, hep-ph 9608348.

[49] R. P. Feynman, Acta Phys. Pol. **24** (1963) 262.

[50] B. DeWitt, Phys. Rev. **160** (1967) 113; Phys. Rev. **162** (1967) 1195; Phys. Rev. **162** (1967) 1293.

[51] L. D. Faddeev, V. N. Popov, Phys. Lett. **B25** (1967) 30.

[52] V. N. Gribov, Nucl. Phys. **B139** (1978) 1.

[53] I. M. Singer, Communications in Math. Phys. **60** (1978) 7.

[54] T. P. Killingback, Phys. Lett. **B138** (1983) 87.

[55] D. Zwanziger, Nucl. Phys. **345** (1990) 461.

[56] C. Parrinello, G. Jonas-Lasinio, Phys. Lett. **B251** (1990) 175.

[57] B. Alles, D. Henty, H. Panagopoulos, C. Parrinello, C. Pittori, hep-lat 9605033.

[58] J. Skullerud. *Renormalization in Lattice QCD.* Edinburgh, PhD thesis, 1996.

[59] D. Henty, C. Parrinello, D. G. Richards, Phys. Lett. **B369** (1996) 130.

[60] G. Martinelli, C. Pittori, C. T. Sachrajda, M. Testa, A. Vladikas, Nucl. Phys. **B445** (1995) 81.

[61] M. Daniel, C. M. Viallet, Rev. Mod. Phys. **52** (1980) 175.

[62] C. N. Yang, Phys. Rev. Lett. **33** (1974) 445.

[63] T. T. Wu, C. N. Yang, Phys. Rev. **D12** (1975) 3845.

[64] For a discussion of Quantum Field Theory see, for example, D. Bailin, A. Love. *Introduction to Gauge Field Theory.* IOP Publishing, London, 1993.

[65] K. G. Wilson, Phys. Rev. **D10** (1974) 2445.

[66] H. B. Nielsen, M. Ninomiya, Phys. Lett. **B105** (1981) 219; Nucl. Phys. **B185** (1981) 20; Nucl. Phys. **B193** (1981) 173.

[67] T. Banks et al, Phys. Rev. **D15** (1976) 1111; L. Susskind, Phys. Rev. **D16** (1977) 3031.

[68] K. G. Wilson, in *New Phenomena in Subnuclear Physics*, Erice Lectures, ed. A. Zichichi, New York: Plenum Press, 1975.

[69] M. Bochicchio, L. Maiani, G. Martinelli, G. Rossi, M. Testa, Nucl. Phys. **B262** (1985) 331.

[70] T. Bhattacharya, R. Gupta, S. Sharpe, Nucl. Phys. **B(Proc.Suppl.)47** (1996) 549.

[71] UKQCD Collaboration, C.R. Allton *et al.*, Phys. Rev. **D49** (1994) 474.

[72] A descriptions of MC methods and how to use them can be found in A. D. Sokal, in *Quantum Fields On The Computer*, editor M. Creutz, Advanced Series on Directions in High Energy Physics vol. 11, World Scientific, Singapore, 1992.

[73] K. Symanzik, Nucl. Phys. **B226** (1983) 187.

[74] M. Lüscher, S. Sint, R. Sommer, P. Weisz, hep-lat/9605038. M. Lüscher, P. Weisz, hep-lat/9606016.

[75] G. P. Lepage, P. B. Mackenzie, Phys. Rev. **D48** (1993) 2250.

[76] G. Heatlie, C. T. Sachrajda, G. Martinelli, C. Pittori, G. Rossi, Nucl. Phys. **B352** (1991) 266.

[77] B. Sheikholeslami, R. Wohlert, Nucl. Phys. **B259** (1985) 572.

[78] G. Martinelli, C. T. Sachrajda, A. Vladikas, Nucl. Phys. **B358** (1991) 266.

[79] N. Isgur, M. B. Wise, Phys. Lett. **B232** (1989) 113.

[80] N. Isgur, M. B. Wise, Phys. Lett. **B237** (1990) 527.

[81] H. Georgi, Phys. Lett. **B240** (1990) 447.

[82] T. Mannel, W. Roberts, Z. Ryzak, Nucl. Phys. **B368** (1992) 204.

[83] For a review of HQET see [84]. For a review of HQET focusing on the applications to heavy baryons see [85].

[84] M. Neubert, Phys. Rep. **245** (1994) 259.

[85] J. G. Körner, D. Pirjol, M. Krämer, Prog. Part. Nucl. Phys. **33** (1994) 787.

[86] N. Isgur, M. B. Wise, Nucl. Phys. **B348** (1991) 276.

[87] H. Georgi, Nucl. Phys. **B348** (1991) 293.

[88] H. Georgi, B. Grinstein, M. B. Wise, Phys. Lett. **B252** (1990) 456.

[89] T. Mannel, W. Roberts, Z. Ryzak, Nucl. Phys. **B355** (1991) 38.

[90] M. Neubert, Phys. Rev. **D46** (1992) 2212.

[91] M. E. Luke, Phys. Lett. **B252** (1990) 447.

[92] P. Cho, B. Grinstein, Phys. Lett. **B285** (1992) 153.

[93] A. F. Falk, M. Neubert, Phys. Rev. **D47** (1993) 2965; Phys. Rev. **D47** (1993) 2982.

[94] D. B. Lichtenberg. *Unitary Symmetry and Elementary Particles.* 2^{nd} edition, Academic Press, New York, 1978.

[95] J. E. Mandula, G. Zweig, J. Govaerts, Nucl. Phys. **B228** (1983) 91; Nucl. Phys. **B228** (1983) 109.

[96] J. E. Mandula, E. Shpiz, Nucl. Phys. **B232** (1984) 180.

[97] M. Benmerrouche, R. M. Davidson, N. C. Mukhopadhyay, Phys. Rev. **C39** (1989) 2339.

[98] W. Rarita, J, Schwinger, Phys. Rev. **60** (1941) 61.

[99] UKQCD collaboration, C. Allton *et al.*, Nucl. Phys. **B407** (1993) 331.

[100] R. Sommer, Nucl. Phys. **B411** (1994) 839.

[101] UKQCD collaboration (H. Wittig), Nucl. Phys. **B(Proc. Suppl.)42** (1995) 288.

[102] UKQCD collaboration, C. R. Allton *et al.*, Phys. Lett. **B292** (1992) 408.

[103] UKQCD collaboration, R. M. Baxter *et al.*, Phys. Rev. **D49** (1994) 1594.

[104] UKQCD collaboration, C. R. Allton *al.*, Phys. Rev. **D47** (1993) 5128.

[105] R. M. Baxter. *New Approaches to Particle Spectra in Lattice QCD.* Edinburgh, PhD Thesis, 1993.

[106] W. H. Press, S. A. Teukolsky, W. T. Vetterling, B. P. Flannery. *Numerical Recipes. The art of scientific computing.* Cambridge University Press,1996.

[107] B. Efron. *The Jackknife, the Boostrap and Other Resampling Plans.* SIAM, Philadelphia, 1982.

[108] UKQCD collaboration (A. K. Ewing), Nucl. Phys. **B(Proc. Sppl.)42** (1995) 331.

[109] UKQCD collaboration, A. K. Ewing *et al.*, hep-lat/9508030 (to be published in Phys. Rev. D).

[110] M. Bochicchio, G. Martinelli, C. R. Allton, C. T. Sachrajada, D. B. Carpenter, Nucl. Phys. **B372** (1992) 403.

[111] A. A. Khan, C. T. H. Davies, S. Collins, J. Sloan, J. Shigemitsu, hep-lat 9512025.

[112] UKQCD collaboration, K. C. Bowler *et al.*, *First Lattice Study of Semileptonic Decays of* Λ_b *and* Ξ_b *Baryons.* In preparation.

[113] C. Bernard, A. El-Khadra, A. Soni, Nucl. Phys. **B(Proc. Suppl.)9** (1989) 186; Nucl. Phys. **B(Proc.Suppl.)17** (1990) 499.

[114] M. Crisafulli, V. Giménez, G. Martinelli, C. T. Sachrajda, Nucl. Phys. **B457** (1995) 594.

[115] D. S. Henty, R. D. Kenway, B. J. Pendleton, J. I. Skullerud, Phys. Rev. **D51** (1995) 5323.

[116] UKQCD Collaboration, K. C. Bowler, *et al.* Phys. Rev. **D52** (1995) 5067.

[117] A. Borrelli, R. Frezotti, E. Gabrielli, C. Pittori, Nucl. Phys. **B409** (1993) 382.

[118] H. Hoeber.*A Lattice Investigation of Heavy Quark Symmetry in Semileptonic Decays of B Mesons.* Edinburgh, PhD thesis, 1994.

[119] ALEPH Collaboration, D. Decamp *et al.*, Phys. Lett. **B278** (1992) 367.

[120] OPAL Collabaration, P. Acton *et al.*, Phys. Lett. **B281** (1992) 394.

[121] ALEPH Collboration, D. Buskulic *et al.*, Phys. Lett. **B294** (1992) 145.

[122] DELPHI Collaboration, P. Abreu*et al.*, Phys. Lett. **B311** (1993) 311.

[123] S. Fachin, C. Parrinello, Phys. Rev. **D44** (1991) 2558.

[124] D. S. Henty, O. Oliveira, C. Parrinello, S. Ryan, hep-lat 9607014, accepted for publication in Phys. Rev. D.

[125] S. Fachin, Phys. Rev. **D47** (1993) 3487.

[126] M. A. Semenov-Tian-Shansky, V. A. Franke, Zap. Nauchn. Semin. LOMI **120** (1982) 159 [J. Sov. Math. **34** (1986) 1999].

[127] G. Dell'Antonio, D. Zwanziger, Commun. Math. Phys. **138** (1991) 291.

[128] J. Kogut, M. Snow, M. Stone, Nucl. Phys. **B200** (1982) 211.

[129] C. Bernard, C. Parrinello, A. Soni, Phys. Rev. **D49** (1994) 1585.

[130] P. Marenzoni, G. Martinelli, N. Stella, M. Testa, Phys. Lett. **B318** (1993) 511.

[131] E. Marinari, C. Parrinello, R. Ricci, Nucl. Phys. **B362** (1991) 487.

[132] M. L. Paciello, C. Parrinello, S. Petrarca, B. Taglienti, A. Vladikas, Phys. Lett. **B289** (1992) 405.

[133] P. Marenzoni, P. Rossi, Phys. Lett. **B311** (1993) 219.

[134] M. L. Paciello, S. Petrarca, B. Taglienti, A. Vladikas, Phys. Lett. **B341** (1994) 187.

[135] J. E. Mandula, M. Ogilvie, Phys. Lett. **B185** (1987) 127.

[136] C. T. H. Davies, G. G. Batrouni, G. R. Katz, A. S. Kronfeld, G. P. Lepage, K. G. Wilson, P. Rossi, B. Svetitsky, Phys. Rev. **D37** (1998) 1581.